

**Examination of neuroinflammation and impaired neurogenesis
characteristic of the pathology of Alzheimer's Disease, and
mapping of treatment options in the APP/PS1 transgenic mouse
model**

PhD Thesis

Titanilla Zita Szilágyi-Szögi

Szeged,
2023

University of Szeged
Albert Szent-Györgyi Medical School
Doctoral School of Theoretical Medicine

**Examination of neuroinflammation and impaired neurogenesis
characteristic of the pathology of Alzheimer's Disease, and
mapping of treatment options in the APP/PS1 transgenic mouse
model**

PhD Thesis

Titanilla Zita Szilágyi-Szögi

Supervisor:
Dr. Livia Fülöp

Szeged,
2023

Contents

Publications related to the PhD Thesis	1
List of Figures and Tables	2
List of Abbreviations	4
1. Introduction	6
1.1 Alzheimer's Disease	6
1.2. Adult hippocampal neurogenesis	6
1.3. Mouse AD models	8
1.3. Neuroinflammation in AD	10
1.4. The role of Fe65 in AD	11
2. Aims	15
3. Materials and methods	16
3.1 Synthesis of the compounds.....	16
3.2 Purification of the peptides	17
3.3 ITC measurements	17
3.4 Animals	17
3.5 MWM.....	19
3.6 ELISA	19
3.7 WB	20
3.8 Quantification of spine density	21
3.9 Immunohistochemistry	21
3.10 Quantitative analysis of dendritic spines	22
3.11 Quantification of immunohistochemical data	23
3.12 Statistical analysis	23
4. Results	25
4.1 A longitudinal study of neurogenesis, neuroinflammation, and AD pathology on APP/PS1 transgenic mice	25
4.1.1 Hippocampal neurogenesis is impaired by aging in APP/PS1 and WT mice.....	25
4.1.2 Neuroinflammation increases with age in APP/PS1 mice	27
4.1.3. Age-related modulation of APP processing pathways in APP/PS1 mice.....	29

4.2 The effects of P33 on learning and memory, neurogenesis, neuroinflammation, and AD pathology in APP/PS1 mice.....	31
4.2.1 P33 binds to Fe65-WW but not to Pin1-WW <i>in vitro</i>	31
4.2.2 P33 exerts a positive effect on the learning ability and memory functions in an MWM paradigm	32
4.2.3. P33 restores the pathologically reduced spine density and protects the synapses	35
4.2.4. Elongated treatment with pentapeptide P33 improves neurogenesis in APP/PS1 Mice	36
4.2.5. P33 hinders inflammatory processes in the mouse brain.....	37
4.2.6. P33-treatment does not influence key protein levels involved in the Fe65/APP route in the transgenic mice	38
4.2.7. P33 significantly reduces the amounts of both soluble and deposited A β forms in the APP/PS1 animals	39
5. Discussion	41
6. Conclusion.....	48
7. Acknowledgements	49
8. References	50

Publications related to the PhD Thesis

I. Titanilla Szögi, Ildikó Schuster, Emőke Borbély, Andrea Gyebrovski, Zsolt Bozsó, János Gera, Róbert Rajkó, Miklós Sántha, Botond Penke and Livia Fülöp

Effects of the Pentapeptide P33 on Memory and Synaptic Plasticity in APP/PS1 Transgenic Mice: A Novel Mechanism Presenting the Protein Fe65 as a Target

International Journal of Molecular Sciences, 2019 Jun 22; 20(12):3050. DOI:

10.3390/ijms20123050

IF: 4.556

II. Titanilla Szögi^a, Emőke Borbély^a, Ildikó Schuster, Zsolt Bozsó, Miklós Sántha, Melinda E. Tóth, Botond Penke and Livia Fülöp

^a These authors contributed equally to this work

Examination of Longitudinal Alterations in Alzheimer's Disease-Related Neurogenesis in an APP/PS1 Transgenic Mouse Model, and the Effects of P33, a Putative Neuroprotective Agent Thereon

International Journal of Molecular Sciences, 2022 Sep 8; 23(18):10364. DOI:

10.3390/ijms231810364

IF: 6.20

List of Figures and Tables

The connection between neurogenesis and AD.....	7
Neurogenesis in AD mouse models.....	8
Human and mouse domain structures of Fe65.....	11
Sequences of the WW domains.....	13
Chemical structures of P33 and PPPPP.....	15
Experimental protocols of the longitudinal study, and the P33 experiment.....	17
Primary and secondary Abs for WB.....	19
Primary and secondary Abs for immunohistochemical experiments.....	21
Quantitative results of BrdU and DCX stainings in the DG.....	25
Quantitative results of NeuN staining in the DG.....	26
Quantitative results of GFAP and Iba1 stainings in the DG.....	27
Measurement of APP, C99/C83 ratio by WB, soluble A β ₁₋₄₂ by ELISA and plaque density by immunohistochemistry.....	30
ITC measurements.....	32
Statistical analysis of the behavior studies.....	34
Measurement of dendritic spine density, PSD95 and SYN by WB.....	35
Quantitative results of BrdU and DCX stainings in the DG of the animals.....	36
Quantitative results for GFAP and Iba1 stainings.....	37
WB analysis of Fe65, APP, pThr ⁶⁶⁸ -APP levels, and C99/C83 ratio.....	39
Measurement of A β ₁₋₄₂ levels by ELISA, and plaque density by immunohistochemistry.....	40
Age-related pathological changes in APP/PS1 mice.....	42
Table 1.....	9
Figure 2.....	12
Figure 3.....	14
Figure 4.....	16
Figure 5.....	18
Table 2.....	20
Table 3.....	22
Figure 6.....	26
Figure 7.....	27

Figure 8.....	28
Figure 9.....	30
Figure 10.....	32
Figure 11.....	33
Figure 12.....	35
Figure 13.....	36
Figure 14.....	37
Figure 15.....	39
Figure 16.....	40
Table 4.....	42

List of Abbreviations

ACN - acetonitrile	HPLC – high pressure liquid chromatography
AD – Alzheimer’s disease	HRP – horseradish peroxidase
ADAM10 - ADAM metallopeptidase domain 10	i.p. – intraperitoneal(ly)
AICD – APP’s intracellular domain	Iba1 – ionized calcium-binding adapter molecule 1
APOE - apolipoprotein E	ICV – intracerebroventricular
APP – amyloid precursor protein	ITC – isotherm titration calorimetry
A β – β -amyloid	JIP-1 - c-Jun N-terminal kinase-interacting proteins
BACE1 - β -site APP cleaving enzyme 1	KO – knockout
BrdU – 5-bromo-2’-deoxyuridine	LPS – lipopolysaccharide
BSA – bovine serum albumin	LRP1 – LDL receptor-related protein 1
CHO - Chinese hamster ovary	MBHA x HCl - 4-methylbenz-hydryl-amine hydrochloride
CTF α or C83 – cytoplasmic tail fragment α	MCI – mild cognitive impairment
CTF β or C99 – cytoplasmic tail fragment β	MDCK - Madin–Darby canine kidney cells
CTX – cortex	Mena - mammalian-enabled protein
Dab-1 – Disabled-1	mFe65 – mouse Fe65
DCC - N,N’-dicyclohexyl-carbodiimide	MWM – Morris water maze
DCX – doublecortin	NFTs – neurofibrillary tangles
DG – dentate gyrus	NPCs – neural progenitor cells
DIPEA - N,N’-diisopropylethylamine	NSCs – neural stem cells
DPX – dibutyl phthalate xylene	PBS – phosphate-buffered saline
EGFR – epidermal growth factor receptor	PFA – paraformaldehyde
ELISA – enzyme-linked immunoassay	Pin1 - peptidyl-prolyl cis-trans isomerase NIMA-interacting-1
FAD – familial form of Alzheimer’s disease	PPIase - peptidyl-prolyl cis/trans isomerase
GCL – granular cell layer	Prox1 - Prospero homeobox protein 1
GFAP – glial fibrillary acidic protein	PS1/2 – presenilin-1/2
GSK3 β - glycogen synthase kinase 3 β	PSA-NCAM - polysialylated-neural cell adhesion molecule
hAPP – human APP	PSD95 – postsynaptic density protein 95
HATU - 1-[bis(dimethylamino)-methylene]-1H-1,2,3-triazolo[4,5-b]pyridinium-3-oxid	PTB1/2 - phosphotyrosine-binding 1/2
HC – hippocampus	ROI – region of interest
HEK293 - human embryonic kidney cells 293	RT – room temperature
HOBt - 1-hydroxybenzotriazole	

SAD – sporadic form of Alzheimer’s disease

sAPP α/β – soluble amyloid precursor protein α/β

SEM – standard error of the mean

SGZ – subgranular zone

Sox2 - SRY-box transcription factor 2

STZ – streptozotocin

SVZ – subventricular zone

SYN - synaptophysin

TBS – Tris-buffered saline

TFA - trifluoroacetic acid

WB – western blot

WT – wild-type

1. Introduction

1.1 Alzheimer's Disease

Alzheimer's Disease (AD), which is the most common type of dementia, is characterized by cognitive deficits, and memory loss in the elderly. The patients suffer from language disorders, behavioral and physiological symptoms, and memory deficiency [1-3]. The main pathological hallmarks of AD are β -amyloid ($A\beta$) plaques and neurofibrillary tangles (NFTs), consisting of abnormally hyperphosphorylated tau protein [2, 4].

AD is classified into two subtypes: familial AD (FAD) and sporadic AD (SAD) [3]. FAD, which manifests before 65 years of age, is caused by autosomal dominantly inherited mutations in the amyloid- β precursor protein (APP), presenilin-1 (PS1), and presenilin-2 (PS2) genes. PS1 and PS2 genes encode the catalytic core of γ -secretase. This enzyme is responsible for the cleavages of APP, together with other secretases [5]. In the non-amyloidogenic pathway, APP is cleaved by the α -secretase, resulting in the soluble APP (sAPP α) and the cytoplasmic tail fragment α (CTF α or C83). The γ -secretase cleaves the C83 to APP's intracellular domain (AICD) and p3 [6]. SAPP α is assumed to have neuroprotective effects: it presumably protects neurons, and it promotes neurogenesis and neurite outgrowth [7-10]. In the amyloidogenic pathway, APP is cleaved by the β -secretase resulting in sAPP β and CTF β (C99). Enzymatic digestion of C99 by the γ -secretase produces AICD and $A\beta$ [6]. The mutations typical of SAD shift the synthesis and processing of APP to the amyloidogenic pathway, leading to enhanced $A\beta$ production [3, 11].

SAD appears in individuals commonly after 65 years [3]. Its principal risk factor is increasing age, but by having a multifactorial character, other risk factors of SAD, such as female sex, brain injury, depression, physical activity, and specific genetic mutations can also be identified [3]. The apolipoprotein E (APOE) gene has a crucial effect on the development of SAD [12, 13]. APOE binds to $A\beta$ receptors on glial cells, therefore it can block $A\beta$ uptake and inhibit its clearance. Furthermore, it enhances the fibrillization of $A\beta$ and the formation of aggregate depositions [3, 14].

1.2. Adult hippocampal neurogenesis

In mammals, including humans, neurogenesis occurs throughout life. In adulthood, neuronal cell formation is present in the subventricular zone (SVZ) of the lateral ventricles and in the subgranular zone (SGZ) of the dentate gyrus (DG) within the hippocampus (HC)

[15]. Adult hippocampal neurogenesis consists of the following stages: precursor, expansion, early survival and postmitotic maturation, late survival and maturation [16]. In the precursor phase, new cells (type-1) are formed via mitosis from neural stem cells (NSCs). NSCs have radial glia-like and astrocytic properties, and they express the following markers: glial fibrillary acidic protein (GFAP), nestin, and SRY-box transcription factor 2 (Sox2) [16-18]. The NSCs generate highly proliferative neural progenitor cells (NPCs) (type-2) in the expansion stage [16, 17, 19-21]. Some of the NPCs can migrate, proliferate and differentiate into neurons or glial cells, and these new cells can integrate into the circuitry of the olfactory bulb and the granular cell layer (GCL) of the DG, but a large proportion of these cells die by apoptosis early in their life cycle. Furthermore, both intrinsic modulators (signal transduction pathways, metabolic factors, hormonal stage, epigenetic factors, immune and vascular systems) and extrinsic factors (stress, drug and alcohol abuse, aging, physical activity, learning, and environmental enrichments) affect the proliferation, differentiation, as well as the morphological and physiological maturation, fate determination and the survival of these new cells [8, 21-28]. Type-2 cells undergo rapid proliferation and express specific markers, like nestin, neuroD, and doublecortin (DCX) [16-18]. These cells produce neuroblasts (type-3), which enter the early survival and postmitotic maturation phase, and express neuroD, DCX, and polysialylated-neural cell adhesion molecule (PSA-NCAM). During the maturation process, neuroblast cells develop into immature neurons. These immature neurons, after leaving the cell cycle, express neuronal nuclear protein (NeuN), calretinin, and DCX. Finally, in the late survival and maturation stage, the new neuron expresses calbindin, NeuN, and Prospero homeobox protein 1 (Prox1) [16-18].

The neurons, formed during adult hippocampal neurogenesis, are essential for spatial and episodic memory, learning processes, and other cognitive functions [29]. The extent of neurogenesis declines with age, and it may be altered in neurodegenerative disorders such as AD [7, 24, 26, 28, 30, 31]. The connection between adult hippocampal neurogenesis and AD is examined in humans as well as in many different mouse models of AD.

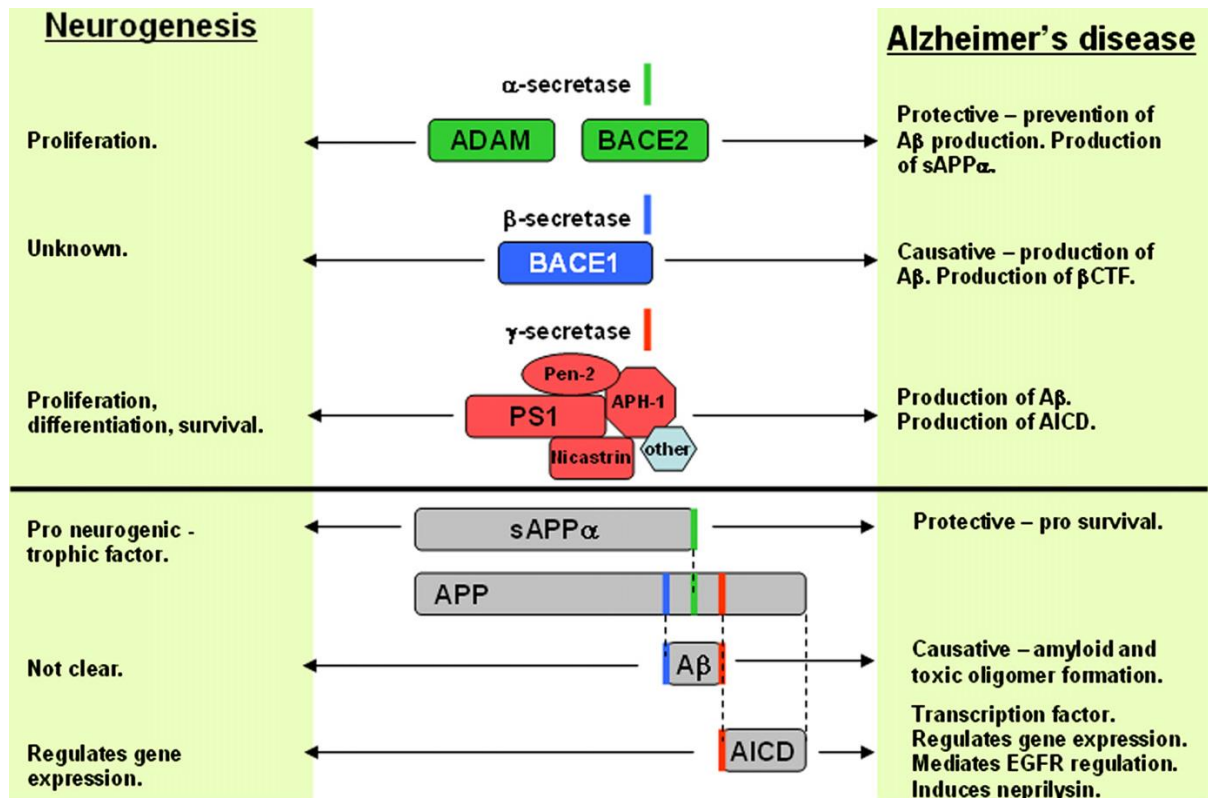


Figure 1: The connection between neurogenesis and AD [7]

It is experimentally proven, that PS1 regulates the differentiation of NPCs (Figure 1) [28, 32, 33] by the Wnt/β-catenin pathway, through which proliferation can be controlled [34, 35]. Products of APP processing can also influence neurogenesis (Figure 1). sAPPα is able to positively modulate the proliferation and survival of NPCs. In contrast, AICD has a negative effect on these processes [7-10]. The sAPPα and the AICD can bind to the epidermal growth factor receptor (EGFR), which is expressed by neural stem cells and is important in the process of proliferation [36, 37]. Zhang *et. al* detected that the overexpression of AICD reduces the level of EGFR in APP/APLP2 double knockout cells, whereas the overexpression of sAPPα did not have such an effect [36]. Aβ may influence adult neurogenesis negatively, as it was proven both in *in vitro* experiments with human cell lines [38, 39] and in mouse models [39-43], suggesting a strong correlation between amyloidosis, Aβ deposition, and impaired neurogenesis [41, 43, 44].

1.3. Mouse AD models

Several transgenic mouse strains were generated to model FAD and investigate the development of AD pathology [23, 26, 31, 45]. Many of them have already been also used to prove the connection between AD and impaired neurogenesis. Table 1 summarizes the most common transgenic strains and the ages of the animals, in which alterations in the two

phenomena could be detected. For our experiments, the APP_{Swe}/PS1_{dE9} (APP/PS1, Tg) transgenic model was used [46]. The APP_{Swe}/PS1_{dE9} line harbors two mutations, whereby these animals overexpress chimeric mouse/human amyloid precursor protein (Mo/HuAPP695_{Swe}) with a Swedish mutation (K595N/M596L), and a human presenilin-1 with a deletion of exon 9 (PS1_{dE9}) [47, 48]. Although several papers discuss the alteration of neurogenesis in the APP_{Swe}/PS1_{dE9} strain [43, 45, 49], to the best of our knowledge, none of these studies have examined the progression of neurogenesis and gliosis throughout the lifespan of these transgenic animals. Results of other research groups regarding neurogenesis in the APP/PS1 strain will be summarized together with ours in the ‘Discussion’ section.

Strain	Genetic modification	AD pathology	Neurogenesis
PDAPP	APP Indian mut. (V717F) [50]	6 to 9 months [51]	2 months: increased proliferation 12 months: decreased proliferation and survival [52]
Tg2576	APP Swedish mut. (KM670/671NL) [53]	11 to 13 months [54]	3 months: increased proliferation, decreased survival [55]
APP23	APP Swedish mut. (KM670/671NL) [56]	6 months [57]	5 months: decreased proliferation, and survival 25 months: increased proliferation, and survival [58]
J20	APP Swedish mut. (KM670/671NL), Indian mut. (V717F) [59]	5 to 7 months [60]	3 months: increased proliferation, 5 months: decreased proliferation [61] 3 and 12 months: increased proliferation, and survival [62]
3xFAD	APP Swedish mut. (KM670/671NL) MAPT mut. P310L, Psen1 mut. M146V [63]	6 months [63]	2, 4, months: decreased proliferation, and survival [64, 65]
5xFAD	APP Swedish (KM670/671NL), Florida (I716V), London (V717I) mut., PSen1 M146L, L286V mut. [66]	2 months [67]	2, 3, 4, 7 months: decreased proliferation [67] 4 months: increased proliferation, survival, 8 months: decreased proliferation, survival [68]

Table 1: Neurogenesis in AD mouse models

Although the impairment of neurogenesis in animal AD models is undoubtedly proven, the results cannot be translated to human AD cases easily. Several studies attempted to prove that neurogenesis is altered in AD patients. However, the results of the human studies seem to be contradictory and confusing. Early experiments with *post-mortem* human tissue detected signs of an increased neurogenesis in the HC of AD patients [69, 70]. Later, methodical inventions were introduced to preserve the activity and structure of the cellular components that play key roles in the detection of neurogenetic processes, by which researchers could

successfully prove that adult hippocampal neurogenesis is constantly declining throughout the entire lifespan in healthy individuals [71, 72]. Moreover, they found that, compared to healthy controls, neurogenesis is further decreased in patients diagnosed not only with AD but with mild cognitive impairment (MCI), as well. The discrepancies between the former and latter experiments point out the importance of careful methodical planning, and the consideration of *post-mortem* delays, fixation procedures, immunohistochemistry markers, and cell count methods, as critical experimental parameters [73, 74]. Based on these findings we can accept the existing connection between impaired adult neurogenesis and AD, however, it is also debated whether impaired neurogenesis is a contributing factor or a consequence of AD [25, 26]. Mapping the molecular processes involved in altered neurogenesis can help to clarify this issue [28, 44, 75].

1.3. Neuroinflammation in AD

A β depositions and plaques are associated with neuroinflammation in AD [5] since A β is proven to provoke inflammatory responses [76]. Microglia and astrocytes, which are the main cell types of immune cells of the neurogenic niche, play a crucial role in AD pathology [77-79]. Neuroinflammation is caused by the alteration of the balance between anti-inflammatory and proinflammatory signaling [80]. In the early phase of the disease, microglia are activated by A β , whereby their morphology, and biological function (such as phagocytic capacity, and cytokine expression) will also be changed [81-83]. These cells cluster around the plaques to promote A β clearance, thus slowing the progression of AD [28, 44, 82-85]. The secretion of proinflammatory cytokines (IL-1 β , IL-6, TNF- α) results in a consequent secondary microglia activation and neurodegeneration [80]. Astrocytes play an important role in synaptogenesis, neurogenesis, maintaining homeostasis, modulation of oxidative stress, signal transmission, and neurotransmitter secretion [86, 87]. In AD, A β also provokes the activation of astrocytes. The reactive astrocytes may promote the activity of β -site APP cleaving enzyme 1 (BACE1) and γ -secretase, thus increasing the level of A β [88, 89]. They also release inflammatory mediators, induce oxidative stress, and failure of the A β clearance through LDL-related receptor protein 1 (LRP1) [90, 91]. LRP1 is a multifunctional, capillary transport protein, which interacts with APP, BACE1 and A β [91]. The activity of the LRP1 is reduced at the blood-brain-barrier in AD patients [92]. The chronic activation of microglia and astrocytes turns disadvantageous and harmful, as it leads to constant overproduction of inflammatory mediators, resulting in prolonged neuroinflammation [28]. Because of their early activation, microglia and astrocytes may serve as biomarkers of AD, whereas the

elements of the inflammatory system might serve as potential therapeutic targets against the disease [28, 42, 84, 85, 93].

In animal models, the bacterial lipopolysaccharide (LPS) is an effective activator of the inflammatory system, and it is able to induce a neuroinflammatory state [94]. LPS triggers a cascade in microglia, whereby cognitive functions and neurogenesis will be strongly affected [65]. Studies showed that the induction of inflammation processes by LPS reduced the amount of BrdU⁺ and DCX⁺ cells and increased the number of microglia in DG [65, 95, 96].

Besides LPS, the intracerebroventricular (ICV) administration of another compound, streptozotocin (STZ), produces neuroinflammation, oxidative stress, and learning and memory impairments [97]. Therefore, although STZ is a type I diabetes inducer, it can also be used to establish models of SAD. STZ negatively regulated the rate of cell proliferation, synaptic plasticity, and learning [98], and it significantly decreased the number of BrdU⁺ and DCX⁺ cells and increased neuroinflammation in DG [97, 99]. These findings support the connection between neuroinflammation and decreased neurogenesis in both LPS- and STZ-induced animal AD models.

1.4. The role of Fe65 in AD

During the last decade, proteolytic products of the APP different from A β became the targets of AD research, as A β could not be proven to possess a decisive role in AD pathomechanism. AICD is produced both in the amyloidogenic and non-amyloidogenic pathways, but the transcriptionally active form is produced during the amyloidogenic pathway only [100, 101]. Its interactome is wide and complex (e.g., the X11 protein family [102-105], Disabled-1 (Dab-1) [105, 106], Shc-transforming protein [107, 108], c-Jun N-terminal kinase-interacting proteins (JIP-1) [105], the Fe65 protein family [109-111], and peptidyl-prolyl cis-trans isomerase NIMA-interacting-1 (Pin1) [110, 112]). Interaction between AICD and these proteins can modulate A β levels, tau phosphorylation, and transcriptional activity [110]. Therefore, AICD is hypothesized to be strongly involved in the development of AD. The internalization of APP from the plasma membrane and its intracellular trafficking regulates A β production [113].

The Fe65 family (Fe65, Fe65L1, and Fe65L2) plays a principal role in APP processing and trafficking, as well as in actin cytoskeleton remodeling, cell motility, neuronal growth cone formation, synapse formation, synaptic plasticity, and consequently in the learning process [114-116]. The protein Fe65 contains three domains: two C-terminal phosphotyrosine-binding

(PTB1 and PTB2) regions and an N-terminal WW domain [114, 117]; all of them are highly conserved. The mouse Fe65 WW domain is identical with that of human Fe65, while the PTB2 domains differ only in one amino acid in the two species (Figure 2).

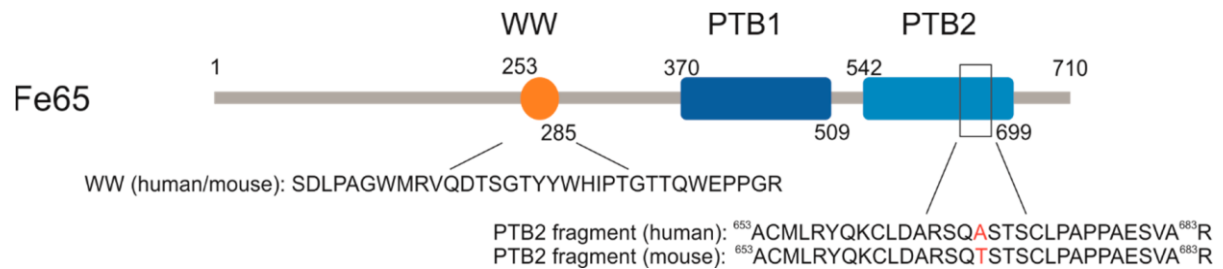


Figure 2: Human (Uniprot: O00213) and mouse (Uniprot: Q9QXJ1) domain structures of Fe65. WW (tryptophan, tryptophan) protein interaction domains are the same in human and mouse Fe65; PTB2 (phosphotyrosine-binding) domains differ only in one amino acid at position 668.

Fe65 binds through its PTB2 domain to APP, and they form a protein complex with Tip60 [110, 114, 118]. The complex translocates to the nucleus, where it regulates the expression of various genes (glycogen synthase kinase 3 (GSK3 β), BACE1, ADAM metalloproteinase domain 10 (ADAM10), APP), thus modulates the proteolytic processing and trafficking of APP, and consequently, A β production [10, 110, 114, 118-123]. However, literary data are contradictory on whether Fe65 decreases or increases the level of A β , with results seeming to vary based on the applied experimental model [110, 118].

In Fe65 transfected cells (human embryonic kidney cells 293 (HEK293), human H4 neuroglioma cells (H4), and Madin–Darby canine kidney cells (MDCK), overexpression of Fe65 increased the production of A β [124-127]. Coincidentally, silencing the Fe65-encoding gene (*APBB1*) caused reduced levels of A β secretion in an H4 cell culture [128]. Suh *et al.* [129] obtained identical results in a primary cortical neuron culture. Furthermore, in two Fe65/Fe65L1 knockout (KO) mouse strains (Tg2576 and 129SvEv Bradley), the lack of Fe65 resulted in reduced A β levels [130, 131]. In contrast, Ando and colleagues [112] found that Fe65 overexpression decreases the production of A β ₁₋₄₀ and A β ₁₋₄₂ in an HEK293 cell line transiently transfected with APP695, compared to the controls. Adjacently, it was found that a Glu⁶⁶⁸-APP mutation causes a significant increase in the levels of A β ₁₋₄₀ and A β ₁₋₄₂, presumably due to the decreased formation of pThr⁶⁶⁸-APP. APP has eight phosphorylation positions in the cytoplasmic region, among which phosphorylation at pThr⁶⁶⁸ is held responsible for the binding of APP to Fe65, and for the consequent nuclear translocation of APP, thus playing a key role in its metabolism [124, 132]. This result was confirmed by experiments in double hFe65/APP (751 isoform carrying the Swedish and London mutation) and single APP

transgenic mouse strains. Resulting from Fe65 overproduction, total A β and A β ₁₋₄₂ concentrations, as well as the number of A β plaques were reduced in double transgenic mice in comparison with single APP transgenic animals [118].

Fe65 can modulate neurogenesis due to its binding to AICD. This connection might alter the proliferation negatively [10]. In a FeC γ 25 mouse strain, which co-expresses AICD and human Fe65, the numbers of BrdU⁺ and DCX⁺ cells were significantly reduced [133]. Another study demonstrated that the axonal glycoprotein TAG1, which is assumed to be the functional ligand of APP as well, supports AICD release, and that neurogenesis is negatively regulated by Fe65 via the TAG1-APP pathway [134].

The WW domain, which is represented in Fe65 together with the PTB1 and PTB2 domains, possesses a compact, antiparallel, three-stranded β -sheet structure providing an interface for binding linear peptide motifs [135, 136]. WW domains are known to interact with special protein structures, the so-called proline-rich sequences [137, 138]. The K_d of this binding typically falls in the low μ M range [135, 139]. This was also proven for the WW domain of Fe65, which anchors several proteins equipped with a common PXP motif [109, 114, 140-142], many of them having key roles in Fe65-mediated transcription mechanisms (SET [143]), kinase activation, actin polymerization (mammalian-enabled protein (Mena [144])), and A β production (GSK3 β , c-Abl kinase [145]). As Fe65 activity bears great influence on APP processing and A β formation, the stereochemical regulation of Fe65 activity through its WW domain using proline-rich sequences might pioneer new therapeutic ways to suppress or modulate AD development.

Another WW domain-containing protein with a relevancy in AD is the prolyl isomerase Pin1 which besides its N-terminal WW domain, contains a C-terminal peptidyl-prolyl cis/trans isomerase (PPIase) domain [146]. The Pin1 WW domain has a sequence different from that can be found in Fe65 (Figure 3) [142]. Pin1 can bind to AICD through the pThr⁶⁶⁸-Pro motif [146]. Pin1, which is expressed in neurons, has a neuroprotective effect in healthy cells, as it plays an important role in cell cycle regulation, and it regulates proteins responsible for neuronal function, and survival [146, 147]. Under oxidative stress or in AD, decreased Pin1 levels shift APP processing toward the amyloidogenic pathway. Pastorino *et al.* [147] found decreased levels of A β in Pin1 overexpressing Chinese hamster ovarian (CHO) cells. Pin1 also modulates tau phosphorylation [110, 148]. Pin1 deficit causes tau hyperphosphorylation [149], after which the hyperphosphorylated tau aggregates into NFTs instead of undergoing microtubule polymerization.

Fe65-WW: Acetyl-SDLPAGWMRVQDTSGTYYWHIPTGTTQWEPPGR-amide

Pin1-WW: Acetyl-EKLPPGWEKRMSRSSGRVYYFNHITNASQWERPSG-amide

Figure 3: Sequences of the WW domains (Fe65-WW domain, Pin1-WW domain).

2. Aims

Since the connection between AD and neurogenesis still raises many questions, our research group aimed to further examine their relationship on an elongated timescale. We investigated the long-term connection of neurogenesis to the neuroinflammation, and to the AD pathology in APP_{Swe}/PS1_{ΔE9} transgenic and C57BL/6J wild-type (WT) mice from 1 to 12 months and at 18 months of age. We detected the temporal changes in hippocampal neurogenesis with immunohistological methods. By measuring the alteration in proliferation and differentiation we could decide whether these modifications contribute to the development of the disease, or they are rather a consequence of AD pathology. Moreover, we wanted to reveal the extent of neuroinflammation related to the production of toxic A β aggregates in the transgenic mouse strain, with immunohistological methods. As the balance between the non-amyloidogenic and amyloidogenic pathways is generally disturbed in AD, we assumed similar phenomena in the transgenic model, therefore we examined the changes in APP processing by Western blot (WB) and enzyme-linked immunosorbent assay (ELISA).

Fe65 alters APP degradation and A β formation. In order to modulate this process, we sought to design a molecule with a specific PXP motif. The pentapeptide P33, which is composed of D-amino acids representing the binding sequence, was examined in isothermal titration calorimetry (ITC) studies, in order to determine its binding affinity to the WW domain of Fe65. To address selectivity, we also used the WW domain of Pin1 in control ITC experiments. Effects of a long-term (6-month) treatment with P33 on spatial learning and memory were tested with Morris water maze (MWM), and on hippocampal neurogenesis with immunohistochemical methods in the aforementioned FAD mouse model. We assumed that P33 would alter the level of synaptic markers, and the amounts of products formed in the amyloidogenic pathway, and it would also influence neuroinflammation which was triggered by A β . We examined these processes with the methods described above.

3. Materials and methods

3.1 Synthesis of the compounds

N-terminally protected amino acids were purchased from Orpegen (Heidelberg, Germany), Bachem (Bubendorf, Switzerland), and GL Biochem (Shanghai, China). N,N'-dicyclohexyl-carbodiimide (DCC), 1-hydroxybenzotriazole (HOBt), 1 [bis(dimethylamino)-methylene]-1H-1,2,3-triazolo[4,5-b]pyridinium-3-oxid hexafluorophosphate (HATU), and 4-methylbenzhydrylamine hydrochloride (MBHA x HCl) resin were purchased from GL Biochem (Shanghai, China), and Rink Amide resin was obtained from Bachem (Bubendorf, Switzerland). Solvents and N,N'-diisopropylethylamine (DIPEA) were obtained from Sigma-Aldrich (St. Louis, MO, USA). High pressure liquid chromatography (HPLC)-grade trifluoroacetic acid (TFA) was ordered from Pierce (Rockford, IL, USA).

For the synthesis of P33 (for structure see Figure 3), standard *t*-butyloxycarbonyl chemistry was used on an MBHA x HCl (1.9 mmol·g⁻¹) resin, with DCC/HOBt activation. The peptide was cleaved from the resin with a cleavage cocktail containing 10 mL of HF, 0.8 mL of dimethyl-sulfide, and 0.2 mL of anisole for 1 g of peptide-resin, at 0 °C, for 45 min. The crude peptide was precipitated with diethyl-ether, dissolved in 50% acetonitrile (ACN)/H₂O, and lyophilized.

Synthesis of acetyl-Fe65-WW, acetyl-Pin1-WW, and the control P33 (structures are represented in Figure 3 and 4) was carried out on a Rink Amide AM (0.3 mmol·g⁻¹) resin using fluorenylmethyloxycarbonyl chemistry and activation with HATU in the presence of DIPEA. Cleavage was achieved by a treatment with TFA/H₂O/triisopropylsilane/1,4-dithio-DL-threitol/phenol (90:5:3:1:1) at room temperature (RT). TFA was removed *in vacuo*, the peptides were then precipitated using cold, dry diethyl-ether, dissolved in ACN/H₂O, and lyophilized.

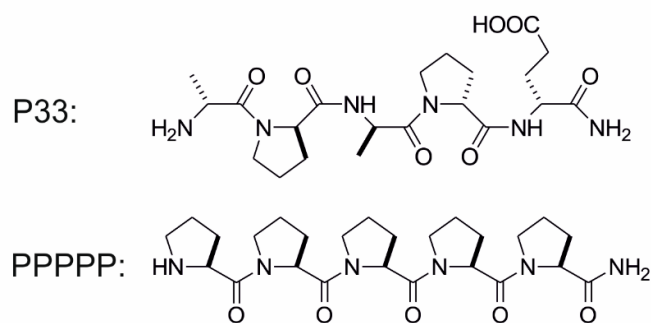


Figure 4: Chemical structures of P33 and P33PPPP.

3.2 Purification of the peptides

Peptides were analyzed and purified using reverse phase HPLC. 0.1% TFA in deionized (d.i.) water and 80% ACN, 0.1% TFA in d.i. water were used as eluent A and eluent B, respectively. Analytical HPLC experiments were performed on a Hewlett-Packard Agilent 1100 Series HPLC apparatus using a Luna C18 column (100 Å, 5 µm, 250 x 4.60 mm, Phenomenex, Aschaffenburg, Germany), at a flow rate of 1.2 mL·min⁻¹

Preparative chromatography was carried out on a Shimadzu HPLC instrument equipped with a Luna C18 column (100 Å, 10 µm, 250 x 21.2 mm, Phenomenex, Aschaffenburg, Germany), applying the same solvent system as for analytical HPLC, at a flow rate of 4 mL·min⁻¹.

3.3 ITC measurements

Isothermal titrations were performed using a Microcal VP-ITC instrument (Malvern Instruments, Malvern, UK). Binding experiments were carried out in degassed phosphate-buffered saline (PBS) at pH 7.4. The concentrations of Fe65-WW and Pin1-WW were normalized for the peptide contents. In one titration experiment, 10 µL portions of the ligand-containing solution (P33 or PPPPP) were injected from a computer-controlled 300 µL microsyringe at intervals of 300 s into the solution of the WW domain (Fe65-WW or Pin1-WW), dissolved in the same buffer as for the ligand. Measurements were repeated twice at 310 K. The starting concentrations of Fe65-WW and Pin1-WW in the cell were 83.5 and 81.4 µM, respectively, and the concentrations of the stock solutions containing P33 or PPPPP in the syringe were 1.006 and 1.056 mM, respectively. Control experiments were performed by injecting P33 or PPPPP into the cell containing plain buffer without the WW domain, with results achieved via subtracting the dilution heat from those measured in the presence of the WW domain.

3.4 Animals

For the longitudinal study, 1- to 12- and 18-month-old male and female WT and APP/PS1 mice were used. Thirteen groups of 5 were established (male n = 2, female n = 3). To detect stem cells, 5 animals per group were injected intraperitoneally (i.p.) with 5-bromo-2'-deoxyuridine (BrdU; 100 mg·kg⁻¹) once a day on 6 consecutive days. Mice were terminated two weeks after the last BrdU injection (Figure 5A).

For the P33 experiment, 3-month-old male and female WT and APP/PS1 mice were divided into four groups: WT vehicle-treated (physiological saline) (male n = 4; female n =

6), WT P33-treated (male n = 6; female n = 5), APP/PS1 vehicle-treated (male n = 3; female n = 5), and APP/PS1 P33-treated (male n = 6; female n = 2). Animals were injected with P33 i.p. with a dose of 5 mg·kg⁻¹ for five days per week, over the course of six months (Figure 5B).

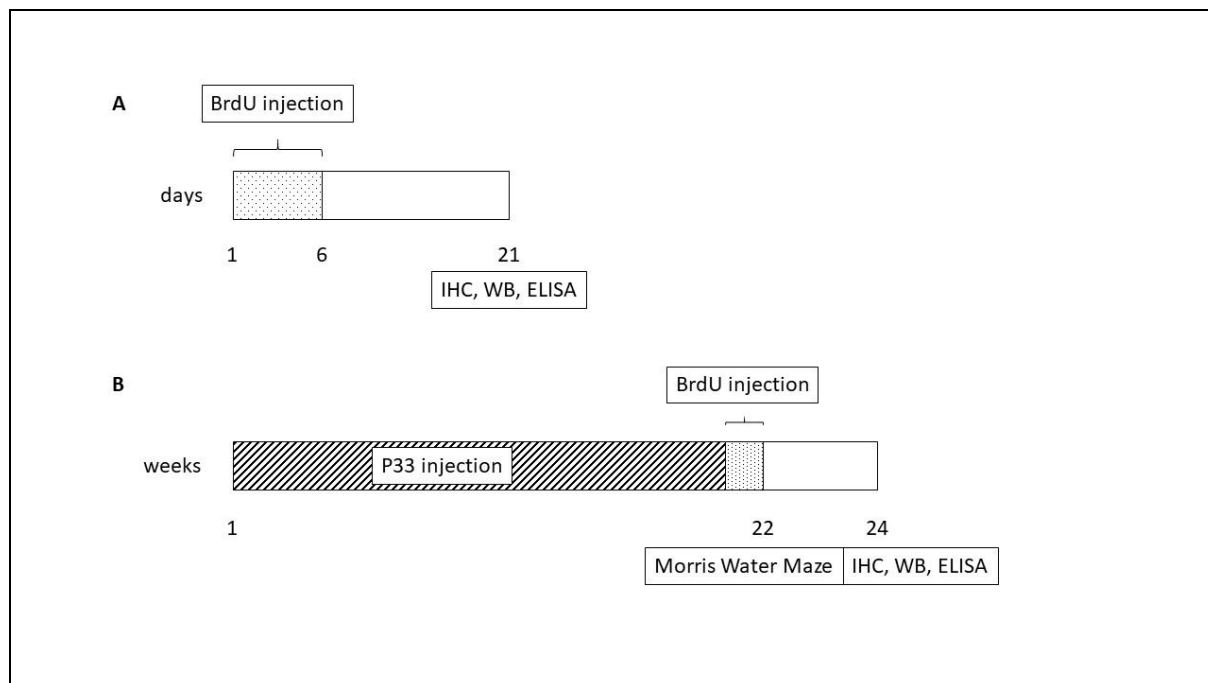


Figure 5: Experimental protocols: (A) Longitudinal study, (B) P33 experiment.

For both experiments, APP/PS1 double transgenic mice were obtained from The Jackson Laboratory (USA), from a colony housed at the Biological Research Centre of the Hungarian Academy of Sciences, by breeding APP/PS1 males with WT females (license number: XVI./1248/2017). Animals were kept in groups under constant temperature (23 ± 0.5 °C), lighting (12–12 h light–dark cycle, lights on at 7 a.m.), and humidity (~50%). Standard mouse chow and tap water were supplied *ad libitum*. All behavioral experiments were performed in the light period. Handling was done daily at the same time.

All experiments were performed in accordance with Directive 2010/63/EU of the European Parliament and of the Council of 22 September 2010 on the protection of animals used for scientific purposes and were approved by the regional Station for Animal Health and Food Control (Csongrad County, Hungary; project identification code: I-74-16/2017, 04.07.2017). The experimental protocols were approved by the National Food Chain Safety and Animal Health Directorate of Csongrad County, Hungary (project licenses: XXVI./3642/2017, XXVI./3643/2017). Formal approval to conduct the experiments was obtained from the Animal Welfare Committee of the University of Szeged.

3.5 MWM

Spatial learning and memory were studied in an MWM paradigm. A circular pool ($d = 130$, $h = 60$ cm), filled with water (23 ± 1 °C), served as the maze bound by a black curtain with some high-contrasted distal paper cues. Additionally, some other spatial objects were visible from the pool (e.g., lamps, video camera). The water was opalized with milk. The maze was segmented into four virtual quadrants with the platform ($d = 10$ cm) positioned in the middle of one of them (target quadrant), set 0.5 cm below the water surface. The room was illuminated by three lamps diffusely lighting all points of the maze with approximately equal intensity. The experiment lasted for five days. Mice were tested twice every day so that they were allowed to swim until they found the platform. If the animal failed to find the platform within 90 s, it was guided to it or placed manually on top of it for 15 s. Four different starting points were used during the experiment; starting points were changed randomly during the tests. Trajectories of the mice were recorded with a video camera fixed on the ceiling, equipped with the software EthoVision XT8 (Noldus Information Technology, The Netherlands, 2011). The tracking system calculated the time to reach the platform, swimming speed, length of the swimming path (distance), and percentage time spent in each of the four virtual quadrants during the trials.

3.6 ELISA

Three animals per group were euthanized via cervical dislocation. Their brains were removed, and the tissue containing the HC and the CTX was quickly dissected and stored at -80 °C until further use. The tissue was homogenized on ice, in a buffer containing 50 mM Tris-HCl, pH 7.4; 150 mM NaCl, and 1 mM EDTA, in the presence of a protease inhibitor cocktail (1:100 dilution, Sigma-Aldrich, Saint Louis, MO, USA). The homogenate was then centrifuged at $10,000\times g$ for 15 min at a temperature of 4 °C, and the supernatant was collected. The pellet was suspended in a lysis buffer supplemented with the protease inhibitor cocktail and was centrifuged again. The supernatants were pooled and centrifuged at $15,000\times g$ for 30 min at 4 °C. The final supernatants were stored at 4 °C for 1–2 h until use. To quantify the level of A β in the mice, we used a sandwich ELISA Kit (Innotest Amyloid- β_{1-42}) from Innogenetics (Gent, Belgium), following the instructions of the manufacturer. The absorbance values were measured at 450 nm on a 96-well plate reader (NOVOstar OPTIMA, BMG Labtech, Offenburg, Germany).

3.7 WB

Protein samples, identically prepared as for ELISA, (20 µg/lane) were separated on a 15% SDS-polyacrylamide gel (80 V, 20 min at RT; then 130 V, 60 min at RT) or on a 4–12% NuPAGE® Bis-Tris Gel (Thermo Fischer Scientific, Waltham, MA, USA, 200V, 30 min at RT) and transferred to a nitrocellulose membrane (Whatman, Maidstone, UK, 450 mA, 90 min at 4 °C). The membranes were washed twice with blocking solution (Tris-buffered saline (TBS) containing 0.1% Tween-20 and 5% bovine serum albumin (BSA)); then, they were incubated overnight at 4 °C with the primary antibodies (Abs) diluted in the blocking solution (Table 2). Subsequently, membranes were washed three times with washing buffer (TBS containing 0.1% Tween-20), and they were incubated with the corresponding secondary Abs for 2 h at RT (Table 2). The visualization was performed with the WesternBright ECL detection kit (Sycamore, Houston, TX, USA). Membranes were scanned with a Bio-Rad Molecular Imager® ChemiDoc XRS+Imaging System (Bio-Rad Laboratories, Hercules, CA, USA) and evaluated with the Image Lab 4.0 software.

Primary Ab	Dilution	Company
rabbit anti-Fe65	1:5000	Thermo Fisher Scientific, Waltham, MA, USA
mouse anti-A β (6E10)	1:1000	BioLegend, San Diego, CA, USA
rabbit anti-pT668-APP	1:2000	GeneTex, Irvine, CA, USA
mouse anti- β -actin	1:20,000	Sigma-Aldrich, St. Louis, MO, USA
rabbit anti-AICD	1:2000	Sigma-Aldrich, St. Louis, MO, USA
mouse anti-PSD95	1:20,000	Invitrogen, Carlsbad, CA, USA
mouse anti-synaptophysin	1:50,000	Invitrogen, Carlsbad, CA, USA
rabbit anti-GAPDH	1:200,000	Cell Signaling, Leiden, Netherlands

Secondary Ab	Dilution	Company
goat anti-rabbit	1:5000	Immuno Reagents, Raleigh, NC, USA
rabbit anti-mouse	1:5000	Immuno Reagents, Raleigh, NC, USA

Table 2: Primary and secondary Abs for WB

3.8 Quantification of spine density

Golgi impregnation was carried out with an FD Rapid GolgiStain™ Kit (FD NeuroTechnologies, Consulting & Services, Inc., USA), according to the manufacturer's instructions. The brains (n=12, 3 per group) were quickly removed and tissue blocks including HC (approximately 0.7-0.8 cm) were cut from the brain. The tissues were placed in Golgi-Cox solutions for a two-phase impregnation. 100 µm coronal sections were cut with a vibration microtome (Zeiss Microm HM 650V) and were mounted on gelatin-coated glass slides. The slides were coverslipped with dibutyl phthalate xylene (DPX) mountant for histology (Sigma-Aldrich, Saint Louis, MO, USA) [150].

3.9 Immunohistochemistry

All chemicals, except the Abs, were purchased from Sigma-Aldrich (St. Louis, MO, USA).

To detect stem cells, 5 animals per group were injected i.p. with BrdU as described previously (Figure 4A). Mice were anesthetized with chloral hydrate (1 mg·kg⁻¹) and were perfused transcardially with phosphate-buffered saline (PBS), followed by ice-cold 4% paraformaldehyde (PFA). The brains were removed, post-fixed in the same fixative, and immersed in a 30% sucrose solution containing 0.01% sodium-azide. They were sliced up from the dorsal to the ventral part of the HC, on a freezing microtome, into 20 µm-thick coronal sections (12 sections/animal/staining). In the free-floating sections, endogenous peroxidases were quenched with 0.3% H₂O₂ in PBS. The acquired sections were then subjected to further immunohistochemical experiments.

For BrdU staining, the sections were incubated in 2 M HCl for 2 h at room temperature (RT) to denature DNA. For BrdU, GFAP, and NeuN, sections were blocked in a mixture of 8% normal goat serum, 0.3% BSA and 0.3% Triton X-100 in PBS for 1 h. For DCX and Iba1 labeling, sections were blocked in 0.1% BSA and 0.3% Triton X-100 in PBS for 1 h. For 4G8 staining, the sections were incubated in 100% formic acid for 1 min at RT to aid in the immunohistochemical detection of amyloid plaques. The sections were subsequently rinsed four times in PBS, following the pretreatments. Sections were incubated overnight at 4 °C with primary antibodies (Table 3). The next day, the sections were rinsed three times in PBS. For BrdU, NeuN, and GFAP stainings, the sections were treated with a polymer-based horseradish peroxidase (HRP)-amplifying system (Super Sensitive™ One-Step Polymer-HRP IHC Detection System, BioGenex, Fremont, CA, USA). The assay was used in accordance with the manufacturer's instructions. For DCX, Iba1, and Aβ stainings,

the sections were incubated with the corresponding secondary antibodies (Table 3). The sections were then rinsed in PBS 3 times, and were incubated with an avidin–biotin complex (VECTASTAIN® Elite ABC-Peroxidase Kit; Vector Laboratories, Burlingame, CA, USA), at RT, for DCX staining in 1:800 for 90 min, for and A β staining in 1:500 for 90 min, and for Iba1 staining in 1:400, for 60 min. Peroxidase immunolabeling was developed for 30 min in 0.5 M Tris-HCl buffer (pH 7.7) with 3,3'-diaminobenzidine (10 mM,) at RT. Sections were mounted with DPX onto slides and coverslipped.

Primary Ab	Dilution	Company
mouse anti-BrdU	1:800	Santa Cruz Biotechnology, Inc., Dallas, TX, USA
goat anti-DCX	1:4000	Santa Cruz Biotechnology, Inc., Dallas, TX, USA
mouse anti-NeuN	1:500	Merck Millipore, Darmstadt, Germany
rabbit anti-Iba1	1:3600	Code No.: 019-19741, Wako Chemicals GmbH, Neuss, Germany
mouse anti-GFAP	1:1500	Santa Cruz Biotechnology, Inc., Dallas, TX, USA
mouse anti- β -amyloid (4G8)	1:10,000	BioLegend, San Diego, CA, USA

Secondary Ab	Dilution	Company
donkey anti-goat	1:1500	Jackson ImmunoResearch, West Grove, PA, USA
goat anti-rabbit	1:400	Jackson ImmunoResearch, West Grove, PA, USA
goat anti-mouse	1:400	Thermo Fisher Scientific, Waltham, MA, USA

Table 3: Primary and secondary Abs for immunohistochemical experiments

3.10 Quantitative analysis of dendritic spines

We examined the Golgi-impregnated sections with inverse light microscopy (Zeiss Observer Z1, with 10x ocular magnification). Pyramidal neurons (n=25/animal) from the dorsoventral hippocampal CA1 (stratum radiatum) region were selected from 12 mice. We measured the spine density of the proximal apical dendrite area, which is located in a distance of 100 μ m from the soma. For spine density quantification, we selected one 100 μ m-long segment of a second or third-order dendrite. Oil-immersion objectives (100x lens) were applied, and the images were captured with a camera (AxioCam MRC V5, program: AxioVision 40 V. 4.8.1.0 Carl Zeiss Imaging Solutions GmbH). Multiple images taken from

the dendrite were stacked into one file, then the spine density was analyzed by ImageJ 1.44 software (National Institute of Health, Bethesda, USA).

3.11 Quantification of immunohistochemical data

Slides were scanned by a digital slide scanner (Mirax Midi, 3DHistech Ltd., Budapest, Hungary), equipped with a Pannoramic Viewer 1.15.4, a CaseViewer 2.1 program, and a QuantCenter, HistoQuant module (3DHistech Ltd., Budapest, Hungary). For quantifications, all sections derived from each animal were analyzed (12 slices per animal). In CTX, DG, and HC, the regions of interest (ROIs) were manually outlined. Antibody-positive cell types for all ROIs were counted and quantified. The number of stem cells (BrdU+) and neuroblasts (DCX+) were assessed at the border between GCL and the hilus, and divided by the size of the DG/HC area (cells/mm²). The percentual densities (%) of neurons (NeuN+), microglia (Iba1+), astrocytes (GFAP+), and A β plaques were calculated by the quantification software.

3.12 Statistical analysis

Behavioral data were analyzed by mixed ANOVA, followed by Fisher's LSD *post hoc* tests for multiple comparisons. The classical and modified ANOVA data evaluation methods applied for the raw measurements could detect only some significant effects without explaining their positions. Convenient *post hoc* analysis methods, like Student's t-statistics, need a Gaussian distribution of the analysis data. Additionally, only the probability of the false positive decision error can be set up, and the probability of the false negative decision error remains unknown. Therefore, we developed and used nonparametric statistics. The one-response variable data (swimming times) were used to generate a two-variable model: (1) the reciprocal of the slope of the fitted straight line between the swimming time and the days (its negative value close to zero indicates an improvement in the memory and learning functions of the mice from day to day); (2) swimming time data of the last day (closeness to zero indicates an effective learning process). The two variables were combined and evaluating them together gave more reliable multiple statistical results. For the correct estimation and use of the probability of the false positive decision error, a permutation test was applied, while, for the correct estimation and use of the probability of the false negative decision error, we used bootstrap resampling. In the case of both resampling methods, 50,000 resamples were generated independently, using an in-house developed Matlab script.

In the P33 study, the results of spine density and immunohistochemistry experiments were calculated with one-way ANOVA followed by Fisher's LSD *post hoc* tests. In the

longitudinal experiment, the data obtained from the immunohistochemistry analyses were evaluated with Student's t-test for independent samples. For both experiments, WB and ELISA data did not follow normal (Gaussian) distribution; they were, therefore, analyzed with Kruskal-Wallis nonparametric tests, followed by Mann-Whitney U tests for multiple comparisons. Data analysis was carried out with the SPSS software (IBM SPSS Statistics 24), and the results were expressed as mean \pm standard error of the mean (SEM). Statistical significance was set at $p \leq 0.05$.

4. Results

4.1 A longitudinal study of neurogenesis, neuroinflammation, and AD pathology on APP/PS1 transgenic mice

In our longitudinal study, APP_{Swe}/PS1_{dE9} transgenic and C57BL/6J control mice were compared by using histological methods from 1 to 12 months and at 18 months of age. Temporal changes in hippocampal neurogenesis and their relation to neuroinflammatory markers as well as to A β pathology were assessed.

4.1.1 Hippocampal neurogenesis is impaired by aging in APP/PS1 and WT mice

To characterize the first stage of neurogenesis, we stained dividing stem cells with BrdU [151]. In the first month of life, the number of BrdU+ cells increased in both the Tg and WT groups, while between months 2 and 7 no significant between-group differences in cell proliferation were detected. From months 8 to 12, significant reductions in the number of BrdU+ cells were revealed in APP/PS1 mice compared to age-matched WT controls (Figure 6A, C, independent sample *t*-test: **8th month:** $p=0.039$, **9th month:** $p=0.018$, **10th month:** $p=0.048$, **11th month:** $p=0.022$, **12th month:** $p=0.044$). At 18 months of age, no significant differences in BrdU+ cell density were detected between the groups ($p=0.601$). Along with aging, the number of BrdU+ cells continuously declined both in APP/PS1 and WT mice. A remarkably low density of stem cells (<5 number/mm²) was detected from the eighth month of life in all age groups.

To examine the process of differentiation during adult neurogenesis, we labelled immature neurons with doublecortin (DCX) antibody [151]. The same pattern as the one observed in the longitudinal examination of stem cells was detected: a continuous decrease in differentiating cells was evident along with aging. In the first month of life, a prominent cell density was detected in both groups. Moreover, at 1 month of age, a significant difference in the densities of immature neurons was detected between transgenic and control mice (Figure 6B, D, independent sample *t*-test: $p=0.048$). However, from months 2 to 8, no significant differences were observed between the groups. In the 9- to 11-month-old age groups, a significant reduction in the densities of immature neurons was evident in transgenic mice compared to WT animals (independent sample *t*-test: **9th month:** $p=0.021$, **10th month:** $p=0.014$, **11th month:** $p=0.022$). Exceptionally low densities (<3 number/mm²) were detected in 12- and 18-month-old animals, but at these ages cell densities did not differ considerably

between the transgenic and WT groups (independent sample *t*-test: **12th month:** $p=0.610$, **18th month:** $p=0.623$).

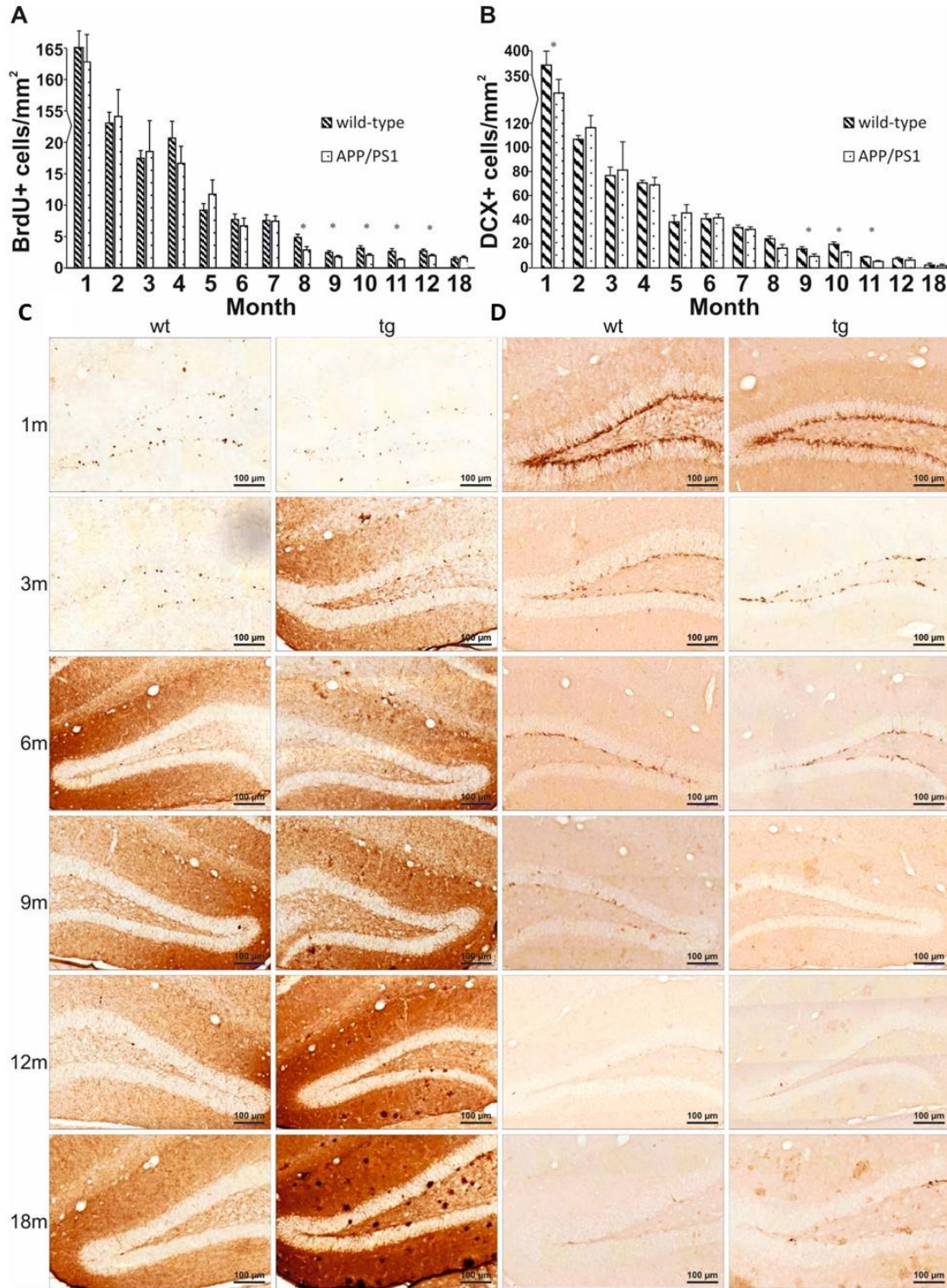


Figure 6: Quantitative results of BrdU and DCX stainings in the DG. (A) Significant differences were observed among the groups from 8 to 12 months of age: transgenic mice had significantly fewer BrdU+ stem cells than controls. (B) Regarding DCX, independent *t*-tests revealed significant differences in the 9-, 10-, and 11-month-old age groups. Data represent mean \pm S.E.M. Representative images of BrdU (C) and DCX (D) stainings. Scale bars represent 100 μ m.

The immunohistochemical analysis of NeuN did not confirm any significant differences in cell densities between Tg and WT mice at any age (Figure 7).

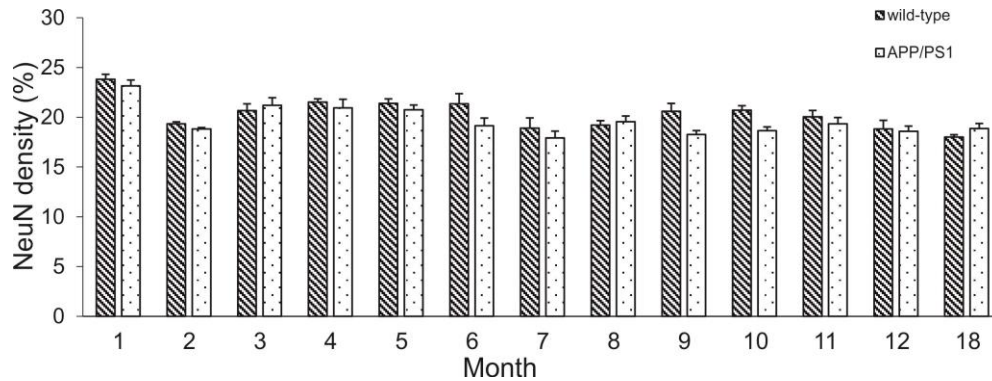


Figure 7: Quantitative results of NeuN staining in the DG.

4.1.2 Neuroinflammation increases with age in APP/PS1 mice

To investigate reactive astrocytes which contribute to the neuroinflammatory processes, we employed GFAP staining. During the first five months of life, there were no differences between the groups. In contrast, 6- to 12-month-old APP/PS1 mice were characterized by significantly higher GFAP+ cell densities compared to controls (Figure 8A, C, independent sample *t*-test: **6th month:** $p=0.026$, **7th month:** $p<0.001$, **8th month:** $p=0.003$, **9th month:** $p=0.010$, **10th month:** $p=0.006$, **11th month:** $p=0.040$, **12th month:** $p=0.039$). However, once again, the densities of GFAP+ cells were similar in the 18-month-old Tg and WT groups (independent sample *t*-test: $p=0.605$).

To detect activated microglia involved in A β clearance and the restoration of a normal brain environment, Iba1 antibody was used. From 1 to 6 months of age, no differences were observed between the WT and Tg groups. However, the densities of Iba1+ cells increased drastically from 7 to 12 months and at 18 months of age in transgenic mice compared to the WT control (Figure 8B, D, independent sample *t*-test: **7th month:** $p<0.001$, **8th month:** $p<0.001$, **9th month:** $p=0.002$, **10th month:** $p<0.001$, **11th month:** $p=0.008$, **12th month:** $p=0.012$, **18th month:** $p=0.013$).

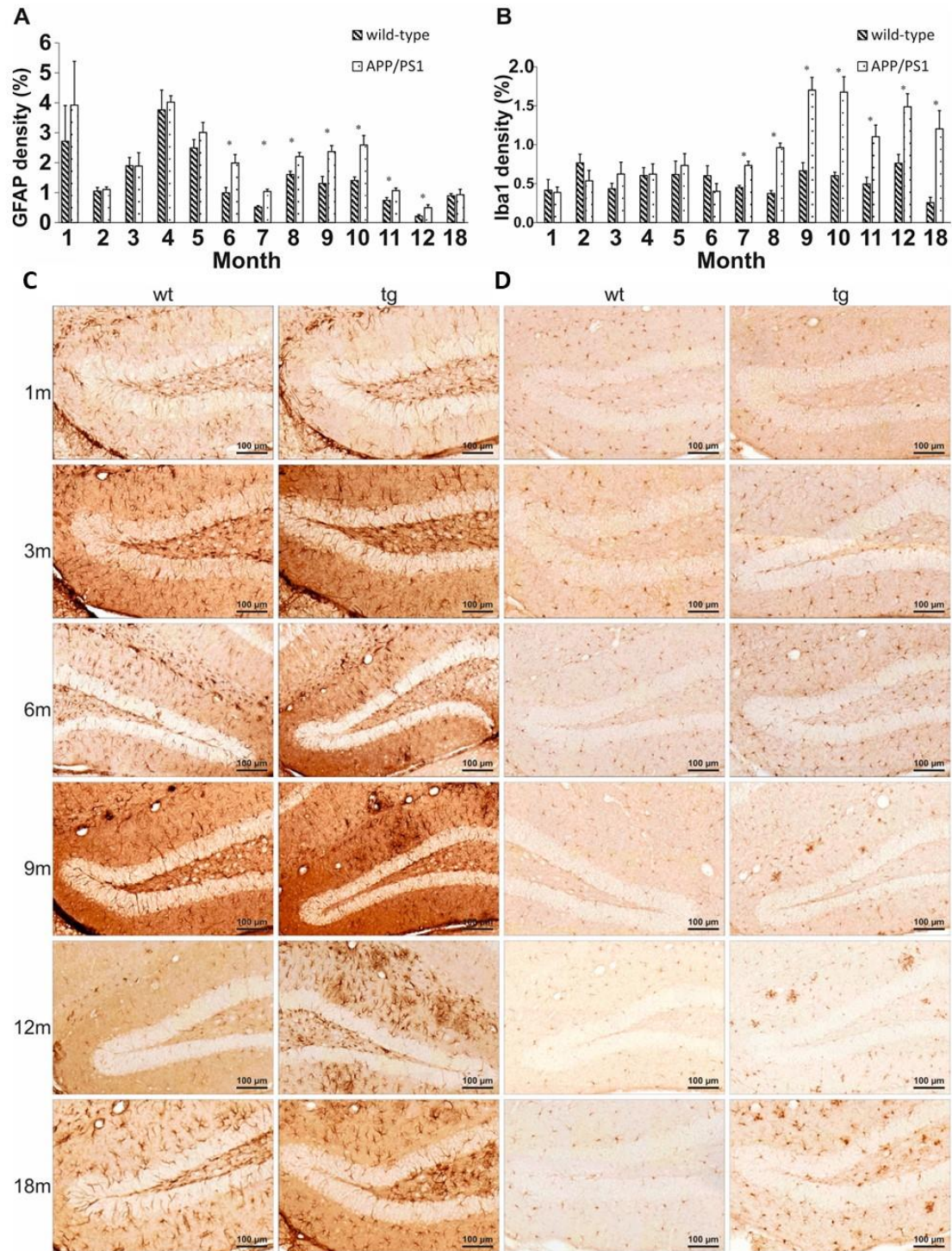


Figure 8: Quantitative results of GFAP and Iba1 stainings in the DG. **(A)** Significant differences in the activation of reactive astrocytes were detected between APP/PS1 mice 5- to 11-month-old and age-matched controls. **(B)** Longitudinal alternations of microglial activation in the DG. The densities of activated microglia of 7- to 18-month-old Tg mice were significantly higher compared to controls. Data represent mean \pm S.E.M. Representative images of GFAP **(C)** and Iba1 **(D)** stainings. Scale bars represent 100 μ m.

4.1.3. Age-related modulation of APP processing pathways in APP/PS1 mice

To assess the association between neurogenesis and the development of AD, we examined the changes in APP processing pathways by analyzing the level of APP, the C99/C83 ratio by WB, the quantity of soluble A β ₁₋₄₂, by ELISA and A β plaque density by immunohistochemical analyses.

The amount of APP may be an early biomarker of AD [9, 152-154]. APP level was elevated in Tg mice from 1 to 4 months of age, while it decreased between months 5 and 18 (Figure 9A, one-way ANOVA $F=18.279$, $p<0.001$; Fisher's LSD *post hoc* tests: **1st month:** $p_4=0.008$; $p_5<0.001$; $p_6<0.001$; $p_7<0.001$; $p_8=0.002$; $p_9<0.001$; $p_{12}<0.001$; $p_{18}<0.001$; **2nd month:** $p_5<0.001$; $p_6<0.001$; $p_7<0.001$; $p_8<0.001$; $p_9<0.001$; $p_{12}<0.001$; $p_{18}<0.001$; **3rd month:** $p_5<0.001$; $p_6<0.001$; $p_7<0.001$; $p_8<0.001$; $p_9<0.001$; $p_{12}<0.001$; $p_{18}<0.001$; **4th month:** $p_1=0.008$; $p_5<0.001$; $p_6<0.001$; $p_7<0.001$; $p_8<0.001$; $p_9<0.001$; $p_{12}<0.001$; $p_{18}<0.001$).

C83 is produced during the non-amyloidogenic processing of APP, while C99 is formed along the amyloidogenic pathway. Thus, the C99/C83 ratio represents the enzymatically regulated balance between these two pathways. During the first five months of age, no difference in the C99/C83 ratio was detected between the groups. From months 6 to 18, an appreciable difference in the C99/C83 ratio became evident for the APP/PS1 group, suggesting an incipient predominance of the amyloidogenic pathway from the sixth month (Figure 9B, one-way ANOVA $F=11.499$, $p<0.001$; Fisher's LSD *post hoc* tests: **1st month:** $p_6<0.001$; $p_7<0.001$; $p_8=0.013$; $p_9<0.001$; $p_{12}<0.001$; $p_{18}<0.001$; **2nd month:** $p_6<0.001$; $p_7=0.004$; $p_8=0.040$; $p_9<0.001$; $p_{12}<0.001$; $p_{18}<0.001$; **3rd month:** $p_6<0.001$; $p_7=0.003$; $p_8=0.033$; $p_9<0.001$; $p_{12}<0.001$; $p_{18}<0.001$; **4th month:** $p_6<0.001$; $p_7<0.001$; $p_8<0.001$; $p_9<0.001$; $p_{12}<0.001$; $p_{18}<0.001$; **5th month:** $p_6<0.001$; $p_7<0.001$; $p_8=0.003$; $p_9<0.001$; $p_{12}<0.001$; $p_{18}<0.001$).

The density of A β plaques may correlate with the development of AD in Tg mice. In our experiment, the plaques appeared in the cortical and hippocampal regions in 4-month-old APP/PS1 mice. The amount of A β plaques progressively increased with age (Figure 9C, E, one-way ANOVA $F=7.336$, $p<0.001$; Fisher's LSD *post hoc* tests: **1st month:** $p_9=0.015$; $p_{12}=0.019$; $p_{18}<0.001$; **2nd month:** $p_9=0.015$; $p_{12}=0.019$; $p_{18}<0.001$; **3rd month:** $p_9=0.015$; $p_{12}=0.019$; $p_{18}<0.001$; **4th month:** $p_9=0.016$; $p_{12}=0.020$; $p_{18}<0.001$; **5th month:** $p_9=0.017$; $p_{12}=0.021$; $p_{18}<0.001$; **6th month:** $p_9=0.020$; $p_{12}=0.025$; $p_{18}<0.001$; **7th month:** $p_9=0.022$; $p_{12}=0.026$; $p_{18}<0.001$; **8th month:** $p_9=0.032$; $p_{12}=0.038$; $p_{18}<0.001$).

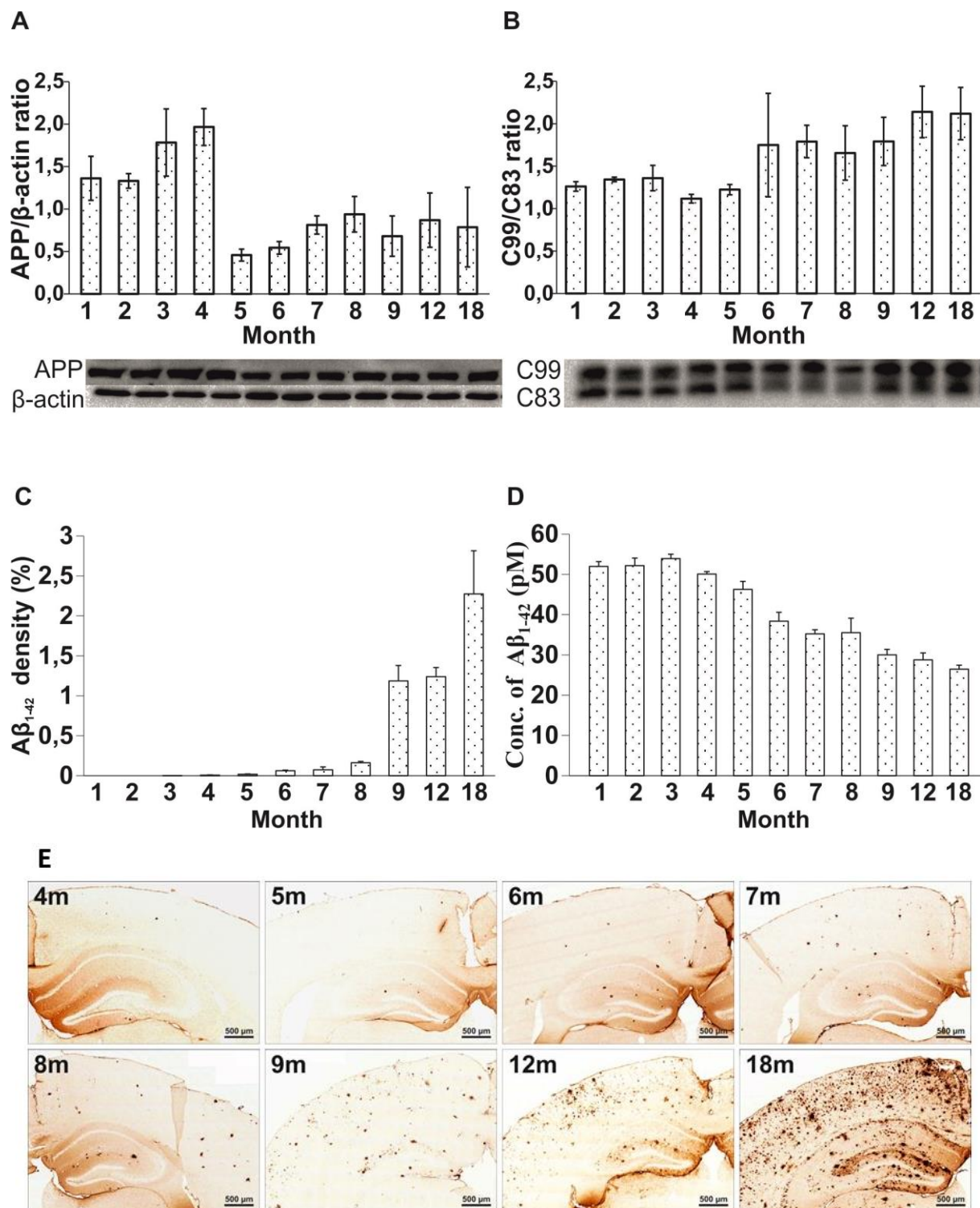


Figure 9: Measurement of APP, C99/C83 ratio by WB, plaque density by immunohistochemistry, and soluble Aβ₁₋₄₂ by ELISA. **(A)** APP level was elevated in APP/PS1 animals from months 1 to 4, then decreased in 5- to 18-month-old mice. **(B)** C99/C83 ratio was elevated in Tg animals, starting from 5 months of age. **(C)** Aβ plaques appeared in APP/PS1 mice at 4 months of age. **(D)** The concentration of soluble Aβ₁₋₄₂ decreased in APP/PS1 mice in the 5- to 18-month-old age groups. Data represent mean ± SEM. **(E)** Representative images of 4G8 staining. Scale bars represent 100 μm.

The age-related changes in the amount of soluble A β_{1-42} were measured along with the plaque density providing information on the development of AD in APP/PS1 mice. The soluble fraction of A β_{1-42} was isolated from the HC and CTX regions of the brains of animals, by following the method of Shankar *et al.* [155] and quantitatively measured with a commercially available ELISA test, which selectively recognizes human A β_{1-42} [156] and is proven to show no cross-reaction with the full-length APP. Elevated levels of soluble A β_{1-42} were detected in the first 4 months of life, whereas the amount of soluble A β_{1-42} strongly decreased in 5- to 18-month-old mice (Figure 9D, one-way ANOVA $F=318.481$, $p<0.001$; Fisher's LSD *post hoc* tests: **1st month**: $p_3=0.002$; $p_5<0.001$; $p_6<0.001$; $p_7<0.001$; $p_8<0.001$; $p_9<0.001$; $p_{12}<0.001$; $p_{18}<0.001$; **2nd month**: $p_4=0.002$; $p_5<0.001$; $p_6<0.001$; $p_7<0.001$; $p_8<0.001$; $p_9<0.001$; $p_{12}<0.001$; $p_{18}<0.001$; **3rd month**: $p_1=0.002$; $p_4<0.001$; $p_5<0.001$; $p_6<0.001$; $p_7<0.001$; $p_8<0.001$; $p_9<0.001$; $p_{12}<0.001$; $p_{18}<0.001$; **4th month**: $p_2<0.001$; $p_3<0.001$; $p_4<0.001$; $p_5<0.001$; $p_6<0.001$; $p_7<0.001$; $p_8<0.001$; $p_9<0.001$; $p_{12}<0.001$; $p_{18}<0.001$).

4.2 The effects of P33 on learning and memory, neurogenesis, neuroinflammation, and AD pathology in APP/PS1 mice

In the P33 experiment, the pentapeptide was examined *in vitro*, regarding its specific capability to bind to the WW domain of Fe65. We also intended to test its effect on spatial learning, memory, and dendritic spine density of transgenic mice, in an elongated experiment. Alterations in synaptic functions, in adult hippocampal neurogenesis, and in neuroinflammation, which are associated with A β pathology, were studied with immunochemical as well as immunohistological methods.

4.2.1 P33 binds to Fe65-WW but not to Pin1-WW *in vitro*

Binding studies were conducted applying ITC measurements. The thermodynamical parameters of the binding interactions between P33 and the WW domain of Fe65 and Pin1 were determined in order to reveal the difference in the two WW domains in question regarding their binding with the pentapeptide. The titration of the Fe65-WW domain with P33 at 310 K resulted in the dissociation constant $K_d = 4.68 \pm 0.04 \mu\text{M}$ ($N = 1.14 \pm 0.01$, $\Delta H = 0.082 \pm 0.001 \text{ kcal}\cdot\text{mol}^{-1}$), calculated from the binding isotherm (Figure 10A). The stoichiometric factor $N = 1.14$ indicates an equimolar interaction and, thus, the formation of a [P33]/[Fe65-WW] complex in a 1:1 ratio. In a control experiment with PPPPP, no binding between the Fe65-WW and the pentapeptide could be observed at 310 K (Figure

10B), thereby proving that the unique structure of P33 is necessary for the binding interaction.

On the other hand, the titration of Pin1-WW with P33 at 310 K showed no considerable binding (Figure 10C) either. These results suggest that P33 can bind selectively to the Fe65-WW domain, which verifies the decisive role of a possible P33/Fe65-WW interaction in APP processing, instead of a Pin1-WW-involved mechanism.

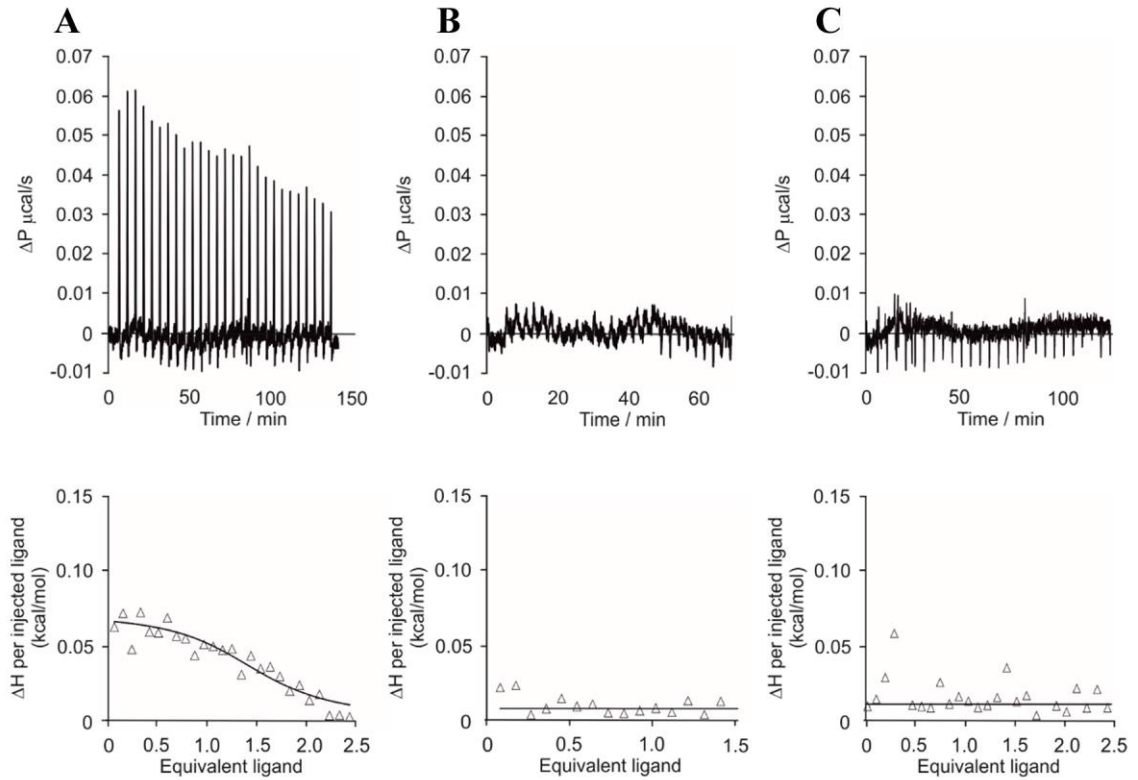


Figure 10: ITC measurements. Raw ITC data (top) and the integrated heat data relative to the molar ratio (bottom) in the interaction of P33 and Fe65-WW (A), PPPPP and Fe65 (B), and P33 and Pin1 (C) in PBS (pH 7.4). (A) $N = 1.14 \pm 0.01$, $\Delta H = 0.082 \pm 0.001 \text{ kcal} \cdot \text{mol}^{-1}$, $K_D = 4.68 \pm 0.04 \mu\text{M}$; (B) no binding observed; (C) no binding observed.

4.2.2 P33 exerts a positive effect on the learning ability and memory functions in an MWM paradigm

To elucidate the effects of P33 on spatial learning and memory, an MWM test was conducted for five days following the administration. Upon evaluation, we performed a mixed ANOVA in which significant differences were found between the parameters (mixed ANOVA, $F_{3,181} = 3.365$, $p = 0.030$). The *post hoc* analysis of the results yielded that the APP/PS1-vehicle group had a significantly bigger latency to find the platform in comparison with the other groups (Figure 11A, WT-vehicle, $p = 0.033$; WT-P33, $p = 0.015$; APP/PS1-P33, $p = 0.006$), which confirms a learning and memory deficit in untreated transgenic mice, whereas P33 seemed to have a positive effect on their learning abilities.

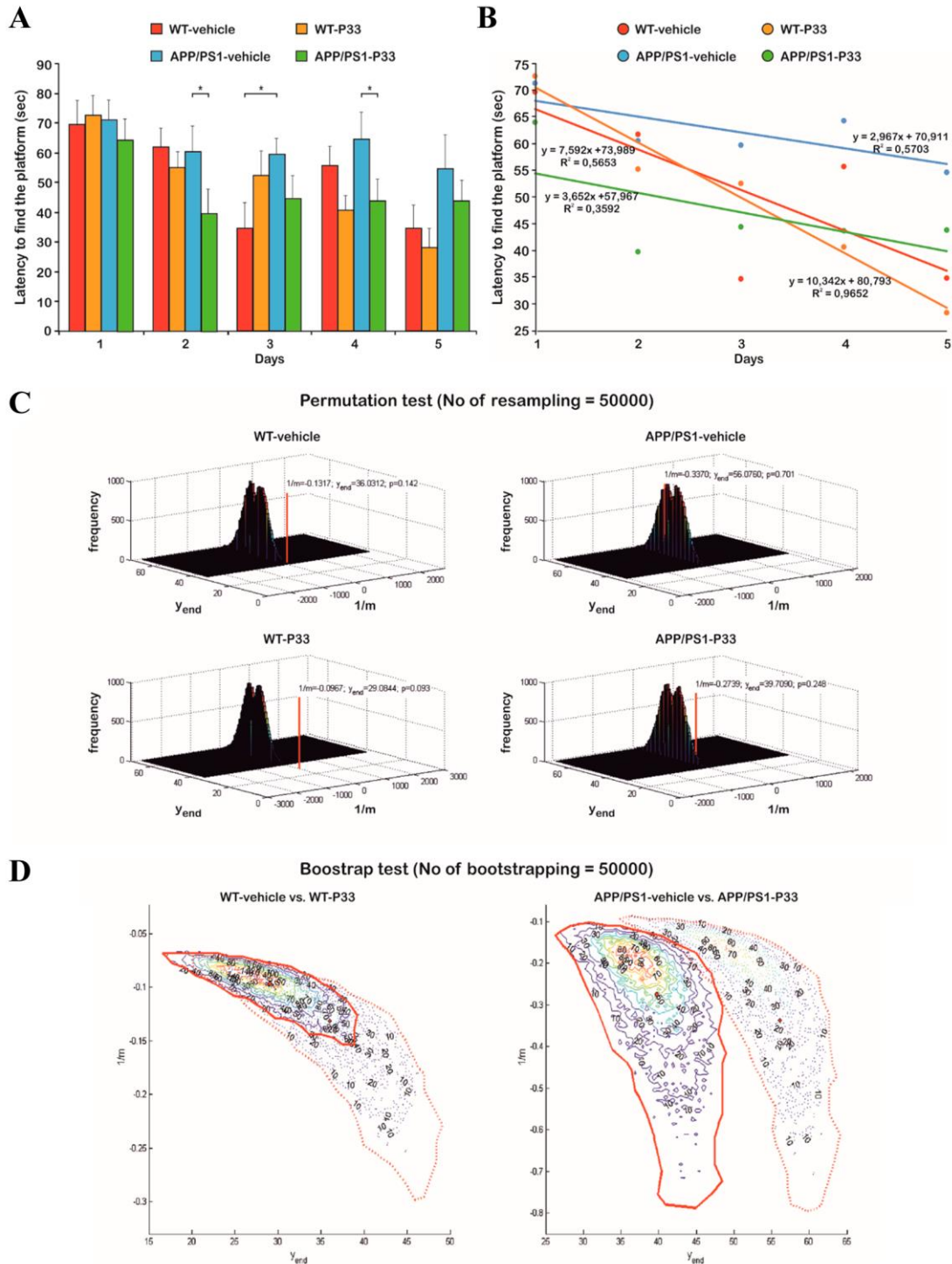


Figure 11: Statistical analysis of the behavior studies. **(A)** The uncertainty and the trend of every latency data versus days on a bar chart. **(B)** Former latency data to find the platform in seconds against days. For each case, trend lines were fitted onto the average swimming times. The fitted equations and the determination coefficient (R^2) values are also shown. **(C)** 3D distribution results of the permutation tests. WT mice results are significantly different from randomness, while the APP/PS1-vehicle treated mice measurements can be considered as a random event generation. P33-treatment led to a significant improvement, as the randomness of the measurements was drastically decreased. **(D)** 2D contour diagrams of WT and transgenic group data distributions based on bootstrapping. The left panel depicts that the WT groups have a high intersection area, indicating that there is no significant difference in the two descriptive parameters between the groups. On the right panel, in the case of the APP/PS1 groups, the intersection area is small, which indicates a significant difference in the parameters between the groups, emphasizing the difference in the learning abilities of the P33-treated vs. non-treated groups.

Since the measured times did not have a Gaussian distribution and because of the problems in the correct interpretation and/or determination of the probabilities of the false positive and negative decisions in cases of multiple testing, an investigation was needed to determine the differences between the groups. Figure 11A depicts the average swimming times on a bar plot. For each case, trend lines were fitted onto the average swimming times, and R^2 values of the fitted points were also calculated (Figure 11B). For the correct determination of the probability of the false positive decision error, a permutation test was applied, in which 50,000 resamples were generated by independently mixing all data related to both the mice and the days. The reciprocals of the slopes ($1/m$) of the fitted straight lines between the swimming times and the days, and swimming time data of the last days (y_{end}) were calculated and plotted onto three-dimensional (3D) distribution maps. The empirical resampled probabilities were generated for all four measured datasets (two different mice with two different treatments; calculated using the average swimming times for each) in the two-dimensional (2D) data space for getting the estimations of the probabilities of the false positive decision error; farther from the bulk of the resampled values of two variables (and closer to the origin) means a more pronounced difference from the randomness (Figure 11C). It can be concluded that WT mice results are significantly different from randomness (position of the red lines fall far from distribution of the randomly generated data), while the APP/PS1-vehicle treated mice measurements can be practically considered as a random event generation (position of the red line falls in the distribution of the randomly generated data). P33-treatment led to a significant improvement, as the randomness of the measurements was drastically decreased.

Secondly, bootstrap resampling with 50,000 iteration steps was used to generate a new dataset independently from that used for the permutation test to reveal the differences between the swimming times of the WT and transgenic groups. Again, the reciprocal of the slopes of the fitted straight lines ($1/m$) and swimming time data of the last day (y_{end}) were calculated and plotted onto 2D contour maps in this case. Red diamond and red dotted contour lines represent the vehicle treatments, while red circle and red continuous contour lines show the P33 treatments. The bolded continuous and dotted lines depict 90% of the generated data. Thus, the conclusion can be drawn with a probability level of 0.9. In Figure 10D (left panel), the WT groups have a high intersection area (32% and 89% of the total areas in case of vehicle and P33-treatments, respectively), which indicates that there is no significant difference in the two descriptive parameters between the groups; both were able to learn the

task similarly. In the case of the APP/PS1 groups (Figure 11D, right panel), the intersection area is small (approximately 2% of the total areas of both vehicle and P33-treatments), which indicates a significant difference in the parameters between the groups, emphasizing the difference in the learning abilities of the P33-treated vs. non-treated groups.

4.2.3. P33 restores the pathologically reduced spine density and protects the synapses

Golgi staining was used to assess the hippocampal apical dendritic spine density of CA1 pyramidal neurons after P33 or vehicle treatment, in WT and APP/PS1 animals. During this procedure, all types of spine were analyzed. At nine months of age, there was a significant difference between the groups (one-way ANOVA; $F_{3,18} = 4.732$, $p = 0.015$). A significant reduction in the spine density could be detected in the APP/PS1-vehicle group (Figure 12A, B), compared to WT-vehicle ($p = 0.002$), and WT-P33 ($p = 0.019$) animals, while treating the APP/PS1 mice with P33 was able to normalize the diminished spine density (APP/PS1-vehicle vs. APP/PS1-P33 $p = 0.041$).

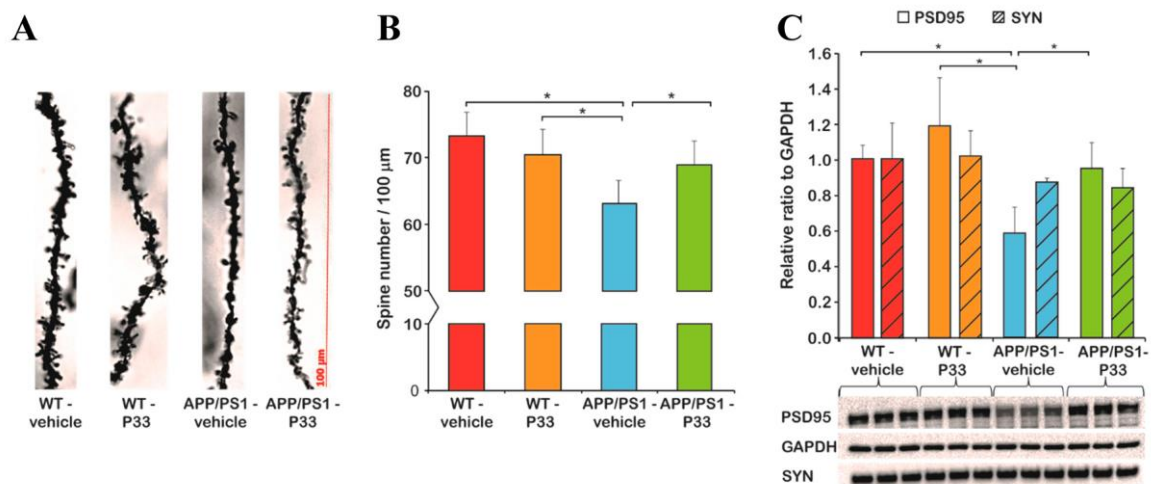


Figure 12: Measurement of dendritic spine density, PSD95, and SYN by WB. **(A)** The apical dendritic spine density in the CA1 region of the HC was monitored. Representative photomicrographs of oblique dendritic segments stemming from WT-vehicle, WT-P33, APP/PS1-vehicle, and APP/PS1-P33 mice (100× magnification; scale bar: 100 μm). **(B)** Golgi staining revealed changes in the spine density after P33-treatment. Quantitative analysis of the apical dendritic spine density proved that P33 protected the synaptic terminals. An impaired density was measured in APP/PS1-vehicle mice compared to WT-vehicle, WT-P33, and APP/PS1-P33 animals. **(C)** A significantly decreased PSD95 level was observed in APP/PS1-vehicle cohort compared to WT-vehicle, WT-P33, and APP/PS1-P33 animals APP/PS1-vehicle vs. WT-vehicle, WT-P33, APP/PS1-P33. P33-treatment resulted in a significantly higher PSD95 level in APP/PS1-P33 mice compared to the APP/PS1-vehicle ones. Regarding SYN level, there is no difference between the four experimental groups.

To further explore the mechanism of P33 on synapses in our AD animal model, we examined the expression of synapse associated proteins PSD95 and SYN. In SYN level, significant differences were not found between the groups (Figure 12C, $H_{3,8} = 1.573$, $p = 0.270$). The expression of PSD95 was significantly decreased in APP/PS1 vehicle-treated

mice compared to the other three, which could be restored by applying P33, demonstrating the positive effect of the P33 on synapse groups (Figure 12C, $H_{3,8} = 5.473$, $p = 0.024$, APP/PS1-vehicle vs. WT-vehicle, WT-P33, APP/PS1-P33 $p = 0.026$, 0.004, 0.036, respectively).

4.2.4. Elongated treatment with pentapeptide P33 improves neurogenesis in APP/PS1 Mice

We have assessed the effect of elongated P33-treatment on the formation of dividing stem cells and immature neurons in APP/PS1 mice, between 3 and 9 month of age. The effects of 6 months of P33 treatment on neurogenesis was examined by monitoring two key markers, BrdU, and DCX. BrdU+ cell density was found to be significantly lower in vehicle-treated APP/PS1 mice compared to the WT-vehicle and WT-P33 groups (Figure 13A, C), one-way ANOVA $F=3.845$, $p=0.026$; Fisher's LSD *post hoc* tests: APP/PS1-vehicle vs. WT-vehicle $p=0.030$, vs. WT-P33 $p=0.008$). In contrast, the density of BrdU+ cells increased in the APP/PS1-P33 group compared to the APP/PS1-vehicle control ($p=0.009$).

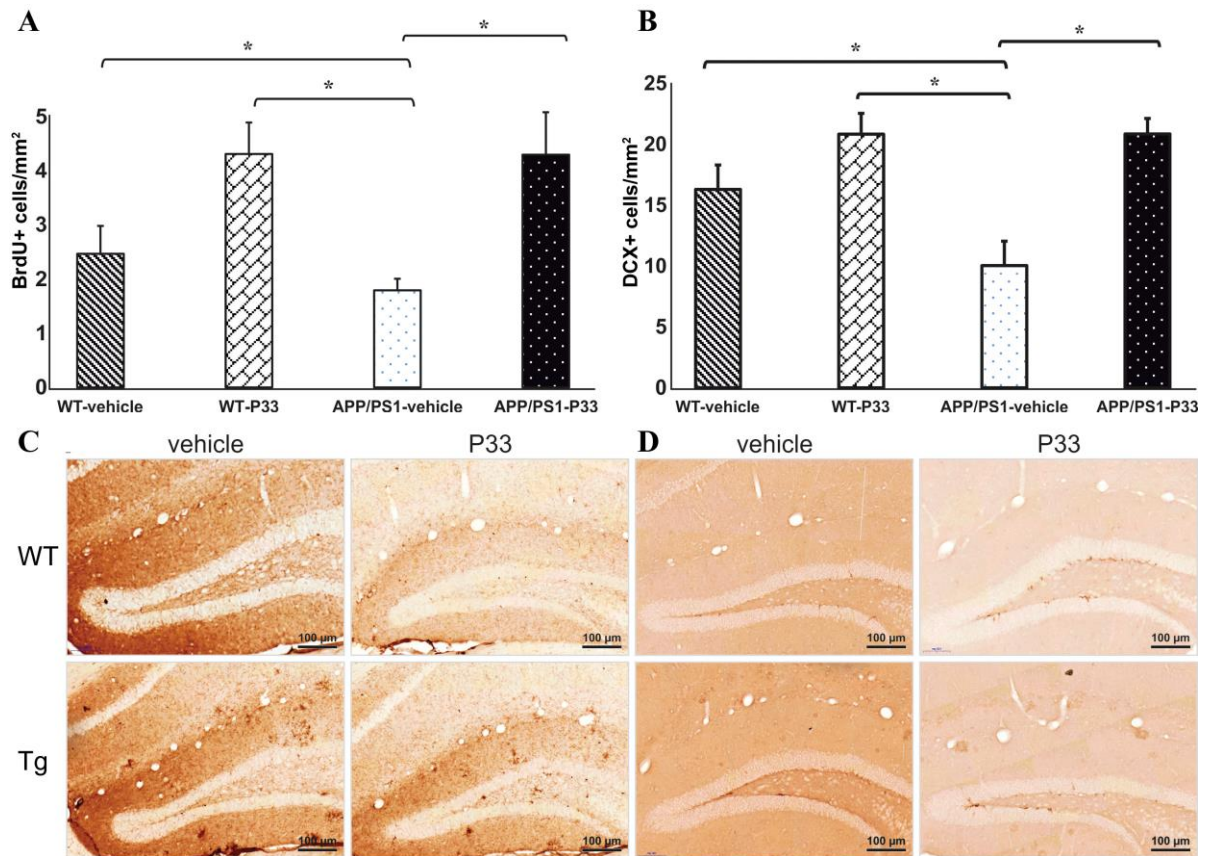


Figure 13: Quantitative results for BrdU and DCX stainings in DG of the animals. (A) Significant differences were observed among the groups in the densities of dividing cells. Decreased BrdU+ cell density was detected in the vehicle-treated APP/PS1 group compared to the WT-vehicle, the WT-P33, and the APP/PS1-P33 groups. (B) Results for DCX immunostaining. A significantly lower level of immature neuron density was detected in vehicle-treated APP/PS1 mice compared to all other groups. Data represent mean \pm S.E.M. Representative images of BrdU (C) and DCX (D) stainings. Scale bars represent 100 µm.

We also measured the density of immature cells in all animal groups. The density of DCX+ cells in vehicle-treated APP/PS1 mice was significantly lower compared to the WT-vehicle and WT-P33 groups (Figure 13B, D, one-way ANOVA $F=8.939$, $p<0.001$; Fisher's LSD *post hoc* tests: APP/PS1-vehicle *vs.* WT-vehicle $p=0.028$, *vs.* WT-P33 $p<0.001$). Treatment with P33 enhanced the density of immature cells in APP/PS1-P33 mice compared to vehicle-treated APP/PS1 controls ($p<0.001$).

4.2.5. P33 hinders inflammatory processes in the mouse brain

To examine the effect of long-term P33 administration on microglia and astrocytes, immunohistochemical stainings were performed. GFAP staining revealed that the density of hyperreactive astrocytes was higher in the whole HC and CTX of the APP/PS1-vehicle group, than in the other three groups (Figure 14A, C, one-way ANOVA $F_{3,16} = 3.343$, $p = 0.048$, Fisher's least significant difference (LSD) *post hoc* tests: APP/PS1-vehicle *vs.* WT-vehicle, WT-P33, APP/PS1-P33 $p = 0.009, 0.047, 0.039$, respectively).

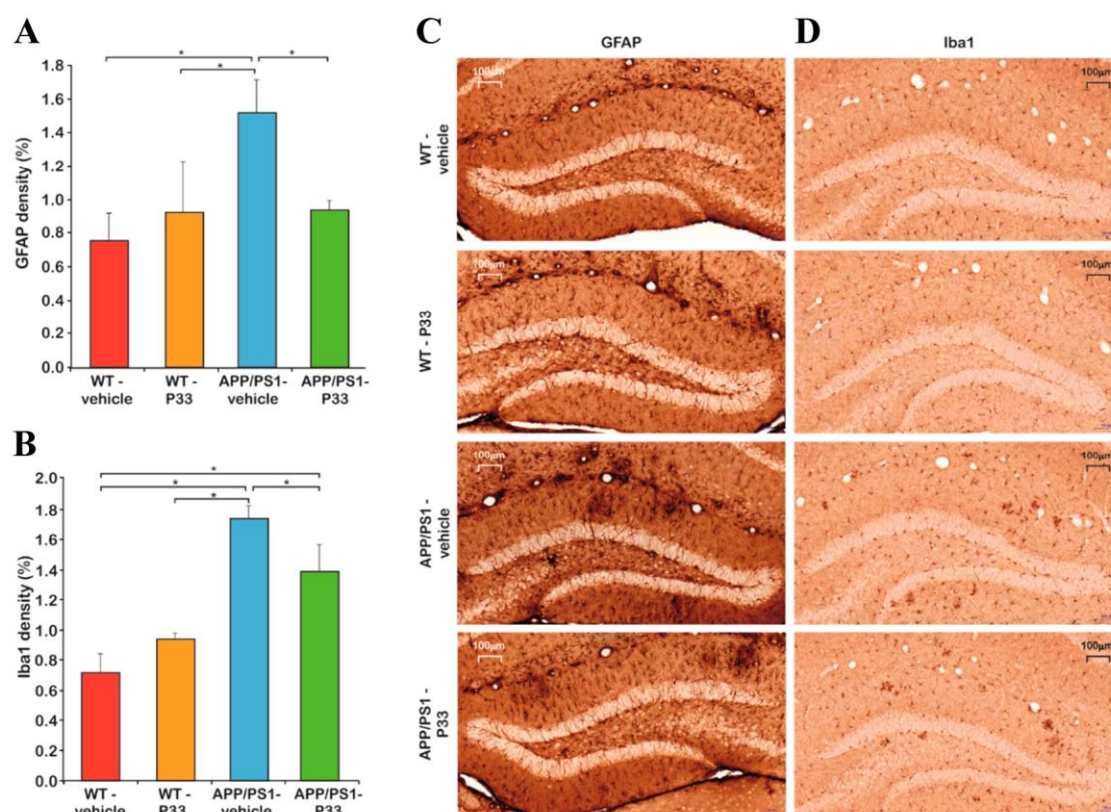


Figure 14: Quantitative results for GFAP and Iba1 stainings. **(A)** Significant differences were observed between the groups in the densities of hyperreactive astrocytes. An increased GFAP-positive cell density was detected in the APP/PS1-vehicle group compared to the WT-vehicle, the WT-P33, and the APP/PS1-P33 ones. **(B)** Results of Iba1 immunostaining. A significantly higher level of the activated microglia density was found in the APP/PS1-vehicle animals than in the other groups. Data represent mean \pm SEM. **(C)** Representative images of GFAP and Iba1 stainings. Scale bars represent 100 μ m.

Microglial density was examined by Iba1 immunostaining in HC and CTX areas. The density of Iba1-positive microglia was higher in the APP/PS1-vehicle treated mice than in the other groups (Figure 14B, D, one-way ANOVA $F_{3,16} = 6.629$, $p = 0.004$, Fisher's LSD *post hoc* tests: APP/PS1-vehicle *vs.* WT-vehicle, WT-P33, APP/PS1-P33 $p = 0.001$, 0.003 , 0.046 , respectively).

4.2.6. P33-treatment does not influence key protein levels involved in the Fe65/APP route in the transgenic mice

To determine the effect of P33 administration on the Fe65, APP, pThr⁶⁶⁸-APP levels, and C99/C83 ratio, the HC and CTX regions of the brains of nine-month-old animals were subjected to WB analyses. We found significantly elevated endogenous Fe65 concentrations in transgenic mice compared to the WT animals (Figure 15A, $H_{3,8} = 5.702$, $p = 0.022$; APP/PS1-vehicle *vs.* WT-vehicle, WT-P33 $p = 0.001$, 0.003 ; APP/PS1-P33 *vs.* WT-vehicle, WT-P33 $p \leq 0.0001$, $p = 0.002$; WT-vehicle *vs.* WT-P33 $p = 0.625$; APP/PS1-vehicle *vs.* APP/PS1-P33 $p = 0.517$), which could not be considerably changed by the treatment with P33. 6E10 recognizes only human but not mouse APP, which could also be proven by our WB studies, as no detectable amounts of APP were present in WT mice. The amount of APP in the APP/PS1 animals did not change with the P33-treatment (Figure 15B, APP/PS1-vehicle *vs.* APP/PS1-P33 $p = 0.622$).

In accordance with the literature data [132], the phosphorylation at pThr⁶⁶⁸ was found to be significantly higher in the transgenic animals than in the WT ones, while the P33-treatment had no significant effect on the pThr⁶⁶⁸-APP level (Figure 15C, $H_{3,8} = 98.096$, $p \leq 0.0001$; APP/PS1-vehicle *vs.* WT-vehicle, WT-P33 $p \leq 0.0001$, 0.0001 ; APP/PS1-P33 *vs.* WT-vehicle, WT-P33 $p \leq 0.0001$, 0.0001 ; WT-vehicle *vs.* WT-P33 $p = 0.183$; APP/PS1-vehicle *vs.* APP/PS1-P33 $p = 0.554$).

As the amyloidogenic processing is increased in the transgenic mice, an elevated C99/C83 ratio could be observed, which was not influenced by the P33 treatment considerably (Figure 15D, $H_{3,8} = 32.344$, $p \leq 0.0001$; APP/PS1-vehicle *vs.* WT-vehicle, WT-P33 $p \leq 0.0001$, 0.0001 ; APP/PS1-P33 *vs.* WT-vehicle, WT-P33 $p \leq 0.0001$, 0.0001 ; WT-vehicle *vs.* WT-P33 $p = 0.807$; APP/PS1-vehicle *vs.* APP/PS1-P33 $p = 0.926$).

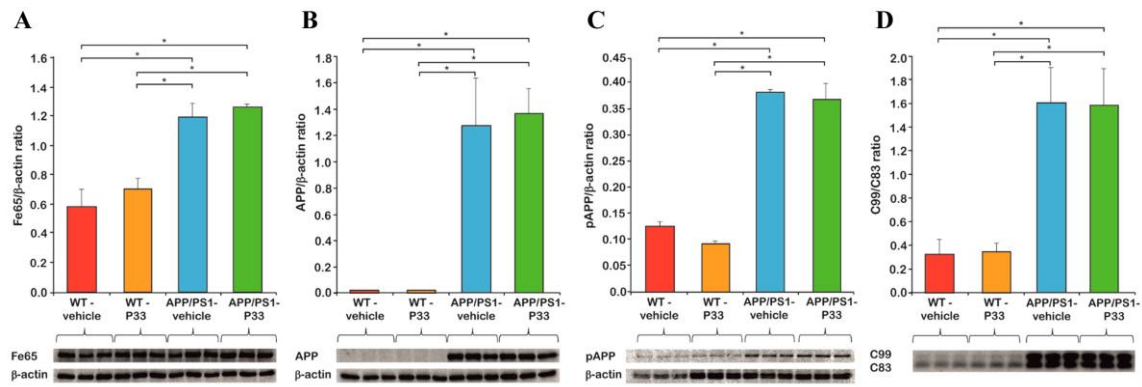


Figure 15: WB analysis of Fe65, APP, pThr⁶⁶⁸-APP levels, and C99/C83 ratio. (A) Fe65 level of the APP/PS1 mice is significantly higher than in the WT animals, which did not change upon P33-treatment (B) Human APP was observed only in transgenic mice, the level of which did not change with P33-treatment either. (C) pThr⁶⁶⁸-APP level of APP/PS1 mice is significantly higher compared to the WT animals. The P33-treatment did not alter the level of pThr⁶⁶⁸-APP (D) C99/C83 ratio of APP/PS1 transgenic mice is higher than in the WT animals, which was not affected during the P33-treatment Data represent mean \pm SEM.

4.2.7. P33 significantly reduces the amounts of both soluble and deposited A β forms in the APP/PS1 animals

We examined the amount of the soluble A β ₁₋₄₂ after the long-term injection of P33 in 9-month-old animals. The WT mice had no detectable amounts of A β ₁₋₄₂ (0 pM), proving that the 3D6 antibody supplied with the kit detects only human, not mouse A β . In the APP/PS1-vehicle group, a significantly higher A β ₁₋₄₂ concentration could be observed than in the APP/PS1-P33 group (Figure 16A, 162.70 pM, and 75.86 pM, respectively, $p < 0.0001$). The results indicate that the treatment with P33 led to a decreased level of A β ₁₋₄₂ in the APP/PS1 mice.

In order to examine the A β plaque load of both hippocampal and cortical areas, the density (%) of A β plaques was measured (Figure 16B, C). One-way ANOVA revealed a significant difference between the groups ($F_{3,16} = 48.575$, $p \leq 0.001$). Brains of WT animals were completely devoid of any A β plaque depositions. The *post hoc* analysis proved that long-term administration of the compound had significantly decreased the plaque density in APP/PS1-P33 mice compared to the APP/PS1-vehicle ($p = 0.013$).

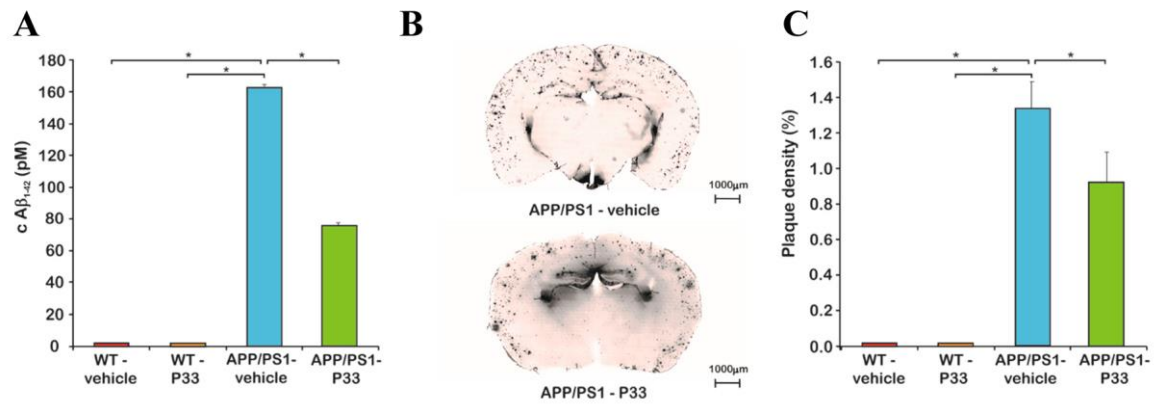


Figure 16: Measurement of Aβ₁₋₄₂ levels by ELISA, and plaque density by immunohistochemistry. **(A)** Concentration of soluble Aβ in CTX and HC: Aβ₁₋₄₂ levels of the vehicle or P33-treated WT and APP/PS1 mice measured by ELISA. No human Aβ₁₋₄₂ was detected in the WT animals. The P33-treatment reduced the Aβ₁₋₄₂ level in the transgenic mice. **(B)** Representative pictures of the 4G8 staining of amyloid plaques. **(C)** Measurements of Aβ plaque density. Aβ plaques could not be detected in WT animals. The P33-treatment influenced the plaque density considerably; the quantitative analysis revealed that chronic P33-treatment resulted in a significant decrease in the density of Aβ deposits in the APP/PS1-P33 group compared to that of the APP/PS1-vehicle animals. Data represent mean ± SEM.

5. Discussion

It is widely accepted that neurogenesis plays an important role in the development and maintenance of memory and learning functions [157-159]. Previous experiments have shown that neurogenesis declines during normal aging, as well as in neurodegenerative diseases, including AD [28, 30, 160].

Our group detected the long-term associations between neurogenesis, neuroinflammation, and AD in a transgenic mouse model of AD, using 1- to 12- and 18-month-old WT (C57BL/6J) and APP/PS1 transgenic mice. We also aimed to compare the processes of hippocampal neurogenesis and neuroinflammation in these animals, to evaluate their relationship with age and AD-like pathology.

Studies report that signs of decreased adult hippocampal neurogenesis are evident in AD, which may cause cognitive dysfunction. Mapping the molecular processes involved in altered neurogenesis would be essential to clarify whether it precedes the characteristic appearance of AD pathology or is rather a consequence of that [28, 44, 75]. To elucidate this issue, many groups have investigated the relationship between AD and neurogenesis in several FAD transgenic models, however, published studies have yielded controversial results (Table 1). Both an increase [61, 62, 161, 162] and a decrease [43, 45, 163-168] in the levels of DG markers typical of adult neurogenesis are reported for AD in this model. In Table 4, we give a representative summary of our results with young (2-3 months), adult (5-6), and old (9, 10, 12 months) mice together with those achieved by others.

In WT and Tg mice, decreasing trends in the densities of both BrdU+ and DCX+ cells were observed with aging. The densities of stem cells and immature neurons were high both in 1-month-old WT and Tg mice, which could be explained by the superior neuroplasticity of the young brain [169]. The density of BrdU+ and DCX+ cells showed a gradual decrease from 2 months of age. At older ages (9 to 12 months) significant differences were detected between the two strains in both neurogenesis markers. Similarly, other research groups reported differences in the densities of BrdU+ [43, 164] and DCX+ cells [42, 164, 166] in 9-, 10-, and 12-month-old mice, while some groups found differences already in younger animals, but surprisingly, in both directions, i.e. significantly lower, or higher than WT (2 to 6 months of age, BrdU: [42, 163, 166, 170], DCX: [42, 163]).

Markers	Age (month)							
		2	3	5	6	9	10	12
BrdU	Our study	H	H	H	L	L-S	L-S	L-S
	Ref.	L-S [163]	L-S [42, 166, 170]	L-S [166]; L [164]	NA	L-S [43, 164]	L-S [166]	NA
DCX	Our study	H	H	H	H	L-S	L-S	L
	Ref.	L-S [163]	H [166, 170]; L-S [42]	L [166]; H [164]	L-S [42]	L-S [164]	L-S [42, 166]; L [170]	L-S [42]
NeuN	Our study	NC	NC	NC	NC	NC	NC	NC
	Ref.	NA	NA	NA	NA	NA	NC [171]	NC [42]
GFAP	Our study	H	L	H	H-S	H-S	H-S	H-S
	Ref.	NA	L [42]	NA	H-S [42]	NA	H-S [42, 171]	H-S [42]
Iba1	Our study	L	H	L	H	H-S	H-S	H-S
	Ref.	NA	H [170]; L [42]	NA	H-S [42]	NA	H-S [42, 171]	H-S [42]
A β plaque	Our study	-	-	+	+	+	NA	+
	Ref.	NA	+ [85, 166]	+ [164, 166]	+ [42]	+ [43, 164]	+ [42, 166, 170, 171]	+ [42]
soluble A β	Our study	+	+	-	-	-	NA	-
	Ref.	+ [163]	NA	+ [164, 166]	NA	+ [164]	NA	NA
APP level	Our study	H	H	L	L	L	L	
	Ref.	H [163]	NA	NA	NA	NA	H [171]	
C99/C83 ratio	Our study	L	L	L	H	H	NA	H
	Ref.	NA	NA	NA	NA	NA	NA	NA

Table 4: Age-related pathological changes in APP/PS1 mice. Comparison table of our findings to literature data. L: lower than WT or low concentration; L-S: significantly lower than WT; H: higher than WT or high concentration; H-S: significantly higher than WT; NC: no change ingroup difference; -: undetectable, in our study: decreased level; +: detectable, in our study: increased level; NA: data not available.

These mixed results may result from using APP/PS1 mice with different genetic backgrounds (>10 vs. 0 generations in the C57BL/6J strain), and varying methods [43, 170]. The analysis of the data has revealed that direct comparison of our results to findings in the literature is difficult due to different experimental setups. The frequency of injections, combined with different time points for sacrificing the experimental animals (i.e., different survival times) can result in large differences and complicates comparability [42, 43, 85, 163, 164, 166, 171]. A common feature of cited articles is that the same exogenous marker, BrdU was injected intraperitoneally to detect stem cells. BrdU is a thymidine analogue that can be incorporated into DNA during the S phase of the cell cycle [151]. Regarding the dose of BrdU administered, the majority of the authors used 50 mg·kg⁻¹ [42, 43, 164, 170], while two groups

injected $100 \text{ mg}\cdot\text{kg}^{-1}$ [75, 163]. Depending on the dose of BrdU, divergent cell groups in the S phase of the cell cycle may be detected [172]. Besides dosing, the injection protocol of BrdU is also an important factor. The frequency of BrdU administration is quite diverse in the literature: some groups applied injection once a day, for 1-12 days [43, 163, 164, 166, 170] [45], while one group applied a vaccination protocol of several times a day [42]. In our experiments, mice were treated with BrdU ($100 \text{ mg}\cdot\text{kg}^{-1}$) once daily for 6 days, to label the largest possible amount of proliferating cells [173]. In addition, the timing of sacrificing the experimental animals is also important in the detection of both BrdU+ and DCX+ cells, and it varies among published studies from a few hours [75], over 1-3 days [42, 43, 164, 166] to even one month after the last BrdU injection [45, 170]. In our experiment, mice were sacrificed 14 days after the last BrdU injection. The above-mentioned factors were chosen to optimally study the long-term survival of stem cells. Proliferation can be examined within a few hours or one day after BrdU injection only while studying the long-term survival of stem cells requires a longer follow-up period [174].

Consistent with the results published by Liu *et al.* [42] and Zhang *et al.* [171], no changes were observed in the densities of mature neurons (NeuN), either in the WT or in Tg groups in our study.

In the so-called APP trafficking, which involves the expression, migration, and enzymatic processing of APP, the forming products of both the amyloidogenic and non-amyloidogenic pathways play crucial roles in neurogenesis as well. In AD, the amyloidogenic pathway predominates, which is controlled by BACE1. Enzymatic cleavage of APP by BACE1 yields C99 and A β fragments, contributing to the formation of A β plaques. APP level was found to be high in the first 4 months of life, and decreased from 5 months of age, while changes in the C99/C83 ratio followed a reverse trajectory. Demars *et al.* measured high APP protein levels in 2-month-old APP/PS1 animals [163], which agrees with our findings. Previous studies have shown that both BACE1 protein level [175] and enzymatic activity are elevated [176], and BACE1 is accumulated around plaques in AD models, independent of age [175, 177, 178]. We assume that changes in the amounts of products formed in the amyloidogenic pathway may support the hypothesis that enhanced expression and/or activity of BACE1 is likely to contribute to the cleavage of APP, resulting in reduced APP and elevated C99 levels in Tg animals.

Our assumption is further supported by the results regarding soluble A β_{1-42} , which had a high concentration in the first four months of life and started to decrease from the age of 5

months. In parallel with this finding, plaques could be detected from the age of 4 months in the brain of transgenic mice. The reduction in the level of soluble oligomeric A β ₁₋₄₂ may be explained by the fact that soluble A β ₁₋₄₂ is re-organized from the oligomeric state to form fibrillar aggregates, manifesting as plaques [179-181].

According to the literature, the appearance of plaques in APP/PS1 mice can be observed at different ages. Some groups reported that plaques were first detected in young animals of 3 [85, 166] and 4 months of age [170], accompanied by the first signs of changes in neurogenesis [85, 166, 170]. One group detected A β plaques at 6 months of age, after a detectable decline in neurogenic processes (3 months of age) [42]. Taniuchi *et al.* recognized plaques earlier (5 months of age) than significant abnormalities first appeared in neurogenesis (9 months of age) [164]. We detected a relatively late (8 to 9 months) onset of altered neurogenesis in transgenic animals, while A β plaques could be identified as early as 4 months of age. Therefore, our results support the hypothesis of early plaque formation, appearing before the onset of decline in neurogenesis.

Accumulation of A β plaques induces inflammatory responses. Activated microglia and astrocytes play an important role in the clearance step of A β phagocytosis [28, 85, 182-184]. We have demonstrated that the densities of GFAP+ (at 6 to 12 months of age) and Iba1+ (at 7 to 18 months) cells were significantly increased in Tg animals compared to WT controls. An increase in the intensity of neuroinflammation became significant after the observed shift in APP trafficking and processing, as well as after the onset of plaque formation. Based on our findings, intensified inflammatory processes could be responsible for the decline in neurogenesis.

The latest results in AD research concerned the role of key players different from A β or tau in the pathomechanism of the disease. Regulated intramembrane proteolysis of APP involves many putative proteinaceous targets to be studied and subjected to drug design. We aimed to find new sequences based on the common PXP motif, which might be able to modify the action of the WW domain-bearing Fe65, whereby an advantageous effect on the disease pathology could be achieved. Our model of choice was the APP/PS1 transgenic mouse, which, as we tested, overexpresses its own endogenous Fe65 (mFe65), presumably as a result of a feedback effect of the human APP (hAPP) overexpression. This result is not surprising and it also bears an analogy with human AD symptoms. In another hAPP-overexpressing mouse model [59], hAPP overexpression was shown to produce elevated mFe65 levels [185], while *post-mortem* analysis of human sporadic AD brain samples revealed that, in the

hippocampal areas, an increase in Fe65 immunoreactivity was associated with the severity of the disease [186]. These findings strengthen our hypothesis that the pathogenic overexpression of Fe65 might serve as a starting point to find new therapeutic ways for curing AD and that the APP/PS1 transgenic model can be applied to study molecules for that purpose.

Targeting WW domains represented in several proteins involved in AD raises the question of specificity. To address this, we searched for sequences of protein molecules in protein databases which bear WW domains and are also involved in AD pathology. Besides Fe65, we identified another one, Pin1, which participates in the tau pathology, as is able to restore the microtubule binding affinity of tau [136] by binding to its phospho-Thr⁶⁶⁸ P motif. Our newly designed pentapeptide, P33, was hypothesized to interact with the WW domains of both Fe65 and Pin1, thereby directly influencing the pathomechanism of AD through both A β and tau pathologies.

Chemical synthesis of the discrete WW domains of the relevant proteins enabled the application of in vitro methods, via which the binding affinity of P33 could be determined. Our ITC measurements confirmed the binding of P33 to the Fe65-WW with a low micromolar K_d , which falls in the range generally observed in similar experiments. Interactions between certain WW domains and proline-rich sequences possessed dissociation constants ranging from high nM to low mM values [187, 188]. On the other hand, no detectable binding to the Pin1-WW could be observed.

The results verify the selective binding of P33 to Fe65 and, therefore, we can assume that the mechanism is related to APP processing, but the tau pathology remains unaffected. The selectivity of the binding can be explained with the differences in the respective structures of the WW domains; according to a generally accepted classification, Fe65-WW belongs to Group II, the members of which recognize the PPLP motif preferentially, while Pin1-WW is in Group IV, and is, therefore, supposed to interact mostly with a (phospho-S/phospho-T) P unit of a proline-rich sequence [189].

Our results unequivocally confirmed the advantageous effect of the P33-treatment on the memory, learning ability, neurogenesis and neuroinflammation in the applied transgenic animal model. P33-treatment significantly increased the densities of BrdU+ and DCX+ cells in the transgenic mouse model. Interestingly, a similar, but insignificant change was observed in the number of BrdU+ cells in WT animals as well, suggesting that P33 may enhance cell division under physiological conditions too. Moreover, P33-treatment

significantly decreased the density of inflammatory markers (GFAP, Iba1) in 9-month-old APP/PS1 mice.

We could also detect decreased levels of density of A β plaques, soluble and aggregated A β in the P33-treated transgenic animals. Soluble A β aggregates are considered to be trigger signals to induce dendritic spine loss and synapse dysfunction at the early stage of AD, correlating with learning impairments and memory deficits [190, 191]. Recently, the synaptic protection and repair became important in AD research as key processes to ameliorate cognitive functions. In our experiments, the positive effects of P33 were demonstrated on dendritic spines and postsynaptic proteins (PSD95, SYN), together with the spatial learning and memory performances.

In order to explain the observed beneficial effects, we attempted to identify the key step in the mechanism, in which P33 should influence the action of Fe65 in the downstream processes. A series of WB studies proved that neither an alteration in the APP expression nor its pThr⁶⁶⁸-induced binding to Fe65, and a hypothesized shift in the ratio of the amyloidogenic/non-amyloidogenic processing pathways could not be held responsible for the effects exerted by P33. Therefore, we put forth that P33 acts simply by binding to the WW domain of the Fe65, consequently hindering its further interaction with other members of the pathophysiological processes. According to literature data, this “blockade” might take effect through an alteration of the bioactive conformation of Fe65. Cao *et al.* [192] proposed that Fe65 possesses an inactive closed conformation, in which the WW domain binds to the PTB2 domain. APP and a certain membrane-associated factor together are able to open the inactive form of Fe65, whereby the latter can be activated. Feilen *et al.* [120] showed that Fe65 not only adopts a closed conformation but that, in the absence of AICD, it also tends to form a homodimer through the APP-binding site. They also found that the PTB2 domain is not able to bind its own WW domain and the AICD simultaneously, since its interaction with the AICD weakens the binding to the WW, resulting in a partial opening of the inactive form [120, 192]. APP and other membrane-associated factors (e.g., PIP2) together at the cell membrane induce the dissociation of the homodimer and the opening of Fe65 simultaneously, with the formation of an Fe65–APP complex [120].

However, the influence of this activation mechanism on AD pathology is still debated in the literature. To our best knowledge, the observed biological effects of Fe65 could mainly be explained by the altered expression of the protein, not by the structural changes in the bioactive conformation; however, the results are highly contradictory.

Accordingly, in some animal models, the absence of Fe65 (Fe65 KO mice [130]) or in other cases the overexpression of Fe65 (Fe65/APP mice [110, 118]) resulted in decreased amyloid levels. In our paradigm, the Fe65 levels of the mice were proven to be identical in the P33- and the vehicle-treated transgenic animal groups; therefore, we hypothesize that the observed significant decrease in amyloid level is due to changes in the Fe65 conformation, initiated by the interaction of P33 with the WW domain of the protein. The resulting P33-Fe65 complex may decrease the quantity of the Fe65/APP complex considerably, the formation of which was proven to be an important step in APP processing, consequently leading to decreased A β production.

In a comprehensive review, Borquez *et al.* [109] summarized the so-called Fe65-interactome and also listed the binding sites, as well as the functions, of the interacting proteins. Among these, the WW-interacting ones were also proven to contain PXP motifs, through which they are attached to Fe56. Therefore, we cannot exclude the possibility that such protein–protein interactions that may have a consequent effect on the A β production might be modulated by P33 as well. Mena, Abl kinase, and GSK-3 β are such candidates, and their roles in AD are widely studied. However, starting from the represented results, further research is needed to get a deeper insight into the mechanisms through which compounds like P33 might influence the effect of these proteins in the course of AD.

6. Conclusion

Our experiments demonstrate that neurogenesis is characterized by an age-dependent decline in both WT and APP/PS1 animals, with an additional enhancement of inflammatory processes and AD pathology in the latter. Our findings provide evidence that in Tg mice the early appearance of plaques, quantitative changes in the levels of certain products of the amyloidogenic pathway, as well as the subsequent development of neuroinflammation can contribute to the physiological decline of neurogenesis with aging. Our data support the hypothesis of other research groups, indicating that the molecular development of AD pathology is a driver of the onset of AD symptoms, as well as of the simultaneous impairment of neurogenic processes, which may manifest in decreased densities of stem cells and immature neurons [43, 164].

Since AD pathology can be detected even in young APP/PS1 animals, early and elongated neuromodulator therapy may beneficially affect the natural course of AD. In our study, early and long-lasting treatment with P33, a promising neuroprotective peptide, successfully reduced the rate of decline in neurogenesis in a mouse model of AD, whereby memory and learning disturbances, as well as the decrease in the number of dendritic spines, could be minimized. Furthermore, the P33-treatment reduced neuroinflammation and positively influenced the amyloidogenic processing of APP. Therefore, P33 is worth being further investigated as a potential drug candidate that may alleviate the pathological processes characteristic of AD.

7. Acknowledgements

I am very thankful to my supervisor, Dr. Lívía Fülöp, who allowed me to join her research group and her guidance helped me to accomplish my experimental projects and my thesis.

I would like to thank my colleagues at the Department of Medical Chemistry for their help: Dr. Ildikó Shuster, Dr. Zsolt Bozsó, Dóra Tüdös, Andrea Gyebrovszki, Zita Ibolya Papp, Szilvia Pataki, Szilvia Dénes, Lídia Nagy, Viktória Varga.

I am also grateful to my colleague and friend, Emőke Borbély for guiding, supporting, and encouraging me for many years.

I would like to thank Prof. Dr. Gábor Tóth, Prof. Dr. Tamás Martinek, and Prof. Dr. Penke Botond for allowing me to work at the Department of Medical Chemistry.

I would also like to thank Prof. Dr. László Tiszlavicz for giving me the opportunity and supporting my work at the Department of Pathology.

I would like to thank Dr. Orsolya Oláh-Németh, Dr. Sándor Turkevi-Nagy, Dr. Bence Radics, Dr. Gergely Nyári and Erika Németh for their continuous encouragement and support.

And last, but not least, I would like to express my gratitude to my husband, Imre, my family, and friends for their unconditional support, love, understanding manner, and endless encouragement.

The projects described in the thesis work were supported by the National Research, Development and Innovation Office (GINOP-2.3.2-15-2016-00060) and by the Hungarian Brain Research Program I and II (Grant No. KTIA_13_NAP-A-III/7, and 2017-1.2.1-NKP-2017-00002). The Ministry of Human Capacities, Hungary (grant 20391-3/2018/FEKUSTRAT) and the Ministry of Innovation and Technology of Hungary from the National Research, Development and Innovation Fund (TKP2021-EGA-32) is acknowledged.

8. References

1. Abubakar, M.B., et al., *Alzheimer's Disease: An Update and Insights Into Pathophysiology*. Front Aging Neurosci, 2022. **14**: p. 742408.
2. Knopman, D.S., et al., *Alzheimer disease*. Nat Rev Dis Primers, 2021. **7**(1): p. 33.
3. Andrade-Guerrero, J., et al., *Alzheimer's Disease: An Updated Overview of Its Genetics*. Int J Mol Sci, 2023. **24**(4).
4. Breijyeh, Z. and R. Karaman, *Comprehensive Review on Alzheimer's Disease: Causes and Treatment*. Molecules, 2020. **25**(24).
5. Sehar, U., et al., *Amyloid Beta in Aging and Alzheimer's Disease*. Int J Mol Sci, 2022. **23**(21).
6. Wu, T., et al., *Amyloid Cascade Hypothesis for the Treatment of Alzheimer's Disease: Progress and Challenges*. Aging Dis, 2022. **13**(6): p. 1745-1758.
7. Lazarov, O. and R.A. Marr, *Neurogenesis and Alzheimer's disease: at the crossroads*. Exp Neurol, 2010. **223**(2): p. 267-81.
8. Horgusluoglu, E., et al., *Adult neurogenesis and neurodegenerative diseases: A systems biology perspective*. Am J Med Genet B Neuropsychiatr Genet, 2017. **174**(1): p. 93-112.
9. Evin, G. and Q.X. Li, *Platelets and Alzheimer's disease: Potential of APP as a biomarker*. World J Psychiatry, 2012. **2**(6): p. 102-13.
10. Coronel, R., et al., *Role of Amyloid Precursor Protein (APP) and Its Derivatives in the Biology and Cell Fate Specification of Neural Stem Cells*. Mol Neurobiol, 2018. **55**(9): p. 7107-7117.
11. Penke, B., F. Bogar, and L. Fulop, *beta-Amyloid and the Pathomechanisms of Alzheimer's Disease: A Comprehensive View*. Molecules, 2017. **22**(10).
12. Raulin, A.C., et al., *ApoE in Alzheimer's disease: pathophysiology and therapeutic strategies*. Mol Neurodegener, 2022. **17**(1): p. 72.
13. Safieh, M., A.D. Korczyn, and D.M. Michaelson, *ApoE4: an emerging therapeutic target for Alzheimer's disease*. BMC Med, 2019. **17**(1): p. 64.
14. Long, J.M. and D.M. Holtzman, *Alzheimer Disease: An Update on Pathobiology and Treatment Strategies*. Cell, 2019. **179**(2): p. 312-339.
15. Altman, J. and G.D. Das, *Autoradiographic and histological evidence of postnatal hippocampal neurogenesis in rats*. J Comp Neurol, **1965**. **124**(3): p. 319-35.
16. Kozareva, D.A., J.F. Cryan, and Y.M. Nolan, *Born this way: Hippocampal neurogenesis across the lifespan*. Aging Cell, 2019. **18**(5): p. e13007.
17. Kempermann, G., H. Song, and F.H. Gage, *Neurogenesis in the Adult Hippocampus*. Cold Spring Harb Perspect Biol, 2015. **7**(9): p. a018812.
18. Overall, R.W., M. Paszkowski-Rogacz, and G. Kempermann, *The mammalian adult neurogenesis gene ontology (MANGO) provides a structural framework for published information on genes regulating adult hippocampal neurogenesis*. PLoS One, 2012. **7**(11): p. e48527.
19. Chen, Q., et al., *Adult neurogenesis is functionally associated with AD-like neurodegeneration*. Neurobiol Dis, 2008. **29**(2): p. 316-26.
20. Demars, M.P., et al., *Soluble amyloid precursor protein- α rescues age-linked decline in neural progenitor cell proliferation*. Neurobiol Aging, 2013. **34**(10): p. 2431-40.
21. Gage, F.H., *Adult neurogenesis in mammals*. Science, 2019. **364**(6443): p. 827-828.

22. Ming, G.L. and H. Song, *Adult neurogenesis in the mammalian central nervous system*. Annu Rev Neurosci, 2005. **28**: p. 223-50.
23. Chuang, T.T., *Neurogenesis in mouse models of Alzheimer's disease*. Biochim Biophys Acta, 2010. **1802**(10): p. 872-80.
24. Lazarov, O., et al., *When neurogenesis encounters aging and disease*. Trends Neurosci, 2010. **33**(12): p. 569-79.
25. Kempermann, G., et al., *Milestones of neuronal development in the adult hippocampus*. Trends Neurosci, 2004. **27**(8): p. 447-52.
26. Shruster, A., E. Melamed, and D. Offen, *Neurogenesis in the aged and neurodegenerative brain*. Apoptosis, 2010. **15**(11): p. 1415-21.
27. Dard, R.F., L. Dahan, and C. Rampon, *Targeting hippocampal adult neurogenesis using transcription factors to reduce Alzheimer's disease-associated memory impairments*. Hippocampus, 2019. **29**(7): p. 579-586.
28. Sung, P.S., et al., *Neuroinflammation and Neurogenesis in Alzheimer's Disease and Potential Therapeutic Approaches*. Int J Mol Sci, 2020. **21**(3).
29. Essa, H., et al., *Implication of Adult Hippocampal Neurogenesis in Alzheimer's Disease and Potential Therapeutic Approaches*. Cells, 2022. **11**(2).
30. Winner, B. and J. Winkler, *Adult neurogenesis in neurodegenerative diseases*. Cold Spring Harb Perspect Biol, 2015. **7**(4): p. a021287.
31. Mu, Y. and F.H. Gage, *Adult hippocampal neurogenesis and its role in Alzheimer's disease*. Mol Neurodegener, 2011. **6**: p. 85.
32. Hollands, C., N. Bartolotti, and O. Lazarov, *Alzheimer's Disease and Hippocampal Adult Neurogenesis; Exploring Shared Mechanisms*. Front Neurosci, 2016. **10**: p. 178.
33. Zhou, Z.-d., et al., *The roles of amyloid precursor protein (APP) in neurogenesis: Implications to pathogenesis and therapy of Alzheimer disease*. Cell Adh Migr, 2011. **5**(4): p. 280-92.
34. Bonds, J.A., et al., *Presenilin-1 Dependent Neurogenesis Regulates Hippocampal Learning and Memory*. PLoS One, 2015. **10**(6): p. e0131266.
35. Lie, D.C., et al., *Wnt signalling regulates adult hippocampal neurogenesis*. Nature, 2005. **437**(7063): p. 1370-5.
36. Zhang, Y.W., et al., *Presenilin/gamma-secretase-dependent processing of beta-amyloid precursor protein regulates EGF receptor expression*. Proc Natl Acad Sci U S A, 2007. **104**(25): p. 10613-8.
37. Romano, R. and C. Bucci, *Role of EGFR in the Nervous System*. Cells, 2020. **9**(8).
38. Lee, I.S., et al., *Amyloid- β oligomers regulate the properties of human neural stem cells through GSK-3 β signaling*. Exp Mol Med, 2013. **45**(11): p. e60.
39. Haughey, N.J., et al., *Disruption of neurogenesis by amyloid beta-peptide, and perturbed neural progenitor cell homeostasis, in models of Alzheimer's disease*. J Neurochem, 2002. **83**(6): p. 1509-24.
40. Amber, S., et al., *Amyloid-beta Induced Neurotoxicity Impairs Cognition and Adult Hippocampal Neurogenesis in a Mouse Model for Alzheimer's Disease*. Curr Alzheimer Res, 2020. **17**(11): p. 1033-1042.
41. Gadadhar, A., R. Marr, and O. Lazarov, *Presenilin-1 regulates neural progenitor cell differentiation in the adult brain*. J Neurosci, 2011. **31**(7): p. 2615-23.
42. Liu, L., et al., *Multiple inflammatory profiles of microglia and altered neuroimages in APP/PS1 transgenic AD mice*. Brain Res Bull, 2020. **156**: p. 86-104.
43. Niidome, T., et al., *Differential regulation of neurogenesis in two neurogenic regions of APP^{swe}/PS1^{dE9} transgenic mice*. Neuroreport, 2008. **19**(14): p. 1361-4.
44. Liu, H., H. Zhang, and Y. Ma, *Molecular mechanisms of altered adult hippocampal neurogenesis in Alzheimer's disease*. Mech Ageing Dev, 2021. **195**: p. 111452.

45. Verret, L., et al., *Alzheimer's-type amyloidosis in transgenic mice impairs survival of newborn neurons derived from adult hippocampal neurogenesis*. J Neurosci, 2007. **27**(25): p. 6771-80.
46. Li, H., *Application of APP/PS1 Transgenic Mouse Model for Alzheimer's Disease*, Y. Wei, Editor. 2015, Journal of Alzheimer's Disease & Parkinsonism. p. 4.
47. Borchelt, D.R., et al., *A vector for expressing foreign genes in the brains and hearts of transgenic mice*. Genet Anal, 1996. **13**(6): p. 159-63.
48. Borchelt, D.R., et al., *Familial Alzheimer's disease-linked presenilin 1 variants elevate Abeta1-42/1-40 ratio in vitro and in vivo*. Neuron, 1996. **17**(5): p. 1005-13.
49. Zhang, C., et al., *Long-lasting impairment in hippocampal neurogenesis associated with amyloid deposition in a knock-in mouse model of familial Alzheimer's disease*. Exp Neurol, 2007. **204**(1): p. 77-87.
50. Games, D., et al., *Alzheimer-type neuropathology in transgenic mice overexpressing V717F beta-amyloid precursor protein*. Nature, 1995. **373**(6514): p. 523-7.
51. Reilly, J.F., et al., *Amyloid deposition in the hippocampus and entorhinal cortex: quantitative analysis of a transgenic mouse model*. Proc Natl Acad Sci U S A, 2003. **100**(8): p. 4837-42.
52. Donovan, M.H., et al., *Decreased adult hippocampal neurogenesis in the PDAPP mouse model of Alzheimer's disease*. J Comp Neurol, 2006. **495**(1): p. 70-83.
53. Hsiao, K., et al., *Correlative memory deficits, Abeta elevation, and amyloid plaques in transgenic mice*. Science, 1996. **274**(5284): p. 99-102.
54. Frautschy, S.A., et al., *Microglial response to amyloid plaques in APPsw transgenic mice*. Am J Pathol, 1998. **152**(1): p. 307-17.
55. Krezymon, A., et al., *Modifications of hippocampal circuits and early disruption of adult neurogenesis in the tg2576 mouse model of Alzheimer's disease*. PLoS One, 2013. **8**(9): p. e76497.
56. Sturchler-Pierrat, C., et al., *Two amyloid precursor protein transgenic mouse models with Alzheimer disease-like pathology*. Proc Natl Acad Sci U S A, 1997. **94**(24): p. 13287-92.
57. Van Dam, D., et al., *Age-dependent cognitive decline in the APP23 model precedes amyloid deposition*. Eur J Neurosci, 2003. **17**(2): p. 388-96.
58. Ermini, F.V., et al., *Neurogenesis and alterations of neural stem cells in mouse models of cerebral amyloidosis*. Am J Pathol, 2008. **172**(6): p. 1520-8.
59. Mucke, L., et al., *High-level neuronal expression of abeta 1-42 in wild-type human amyloid protein precursor transgenic mice: synaptotoxicity without plaque formation*. J Neurosci, 2000. **20**(11): p. 4050-8.
60. Wright, A.L., et al., *Neuroinflammation and neuronal loss precede Aβ plaque deposition in the hAPP-J20 mouse model of Alzheimer's disease*. PLoS One, 2013. **8**(4): p. e59586.
61. López-Toledano, M.A. and M.L. Shelanski, *Increased neurogenesis in young transgenic mice overexpressing human APP(Sw, Ind)*. J Alzheimers Dis, 2007. **12**(3): p. 229-40.
62. Jin, K., et al., *Enhanced neurogenesis in Alzheimer's disease transgenic (PDGF-APP^{Sw,Ind}) mice*. Proc Natl Acad Sci U S A, 2004. **101**(36): p. 13363-7.
63. Oddo, S., et al., *Triple-transgenic model of Alzheimer's disease with plaques and tangles: intracellular Abeta and synaptic dysfunction*. Neuron, 2003. **39**(3): p. 409-21.
64. Hamilton, L.K., et al., *Aberrant Lipid Metabolism in the Forebrain Niche Suppresses Adult Neural Stem Cell Proliferation in an Animal Model of Alzheimer's Disease*. Cell Stem Cell, 2015. **17**(4): p. 397-411.

65. Valero, J., et al., *Long-term effects of an acute and systemic administration of LPS on adult neurogenesis and spatial memory*. Front Neurosci, 2014. **8**: p. 83.
66. Oakley, H., et al., *Intraneuronal beta-amyloid aggregates, neurodegeneration, and neuron loss in transgenic mice with five familial Alzheimer's disease mutations: potential factors in amyloid plaque formation*. J Neurosci, 2006. **26**(40): p. 10129-40.
67. Moon, M., M.Y. Cha, and I. Mook-Jung, *Impaired hippocampal neurogenesis and its enhancement with ghrelin in 5XFAD mice*. J Alzheimers Dis, 2014. **41**(1): p. 233-41.
68. Ziegler-Walckirch, S., et al., *Seed-induced A β deposition is modulated by microglia under environmental enrichment in a mouse model of Alzheimer's disease*. EMBO J, 2018. **37**(2): p. 167-182.
69. Jin, K., et al., *Increased hippocampal neurogenesis in Alzheimer's disease*. Proc Natl Acad Sci U S A, 2004. **101**(1): p. 343-7.
70. Nagy, Z., M.M. Esiri, and A.D. Smith, *Expression of cell division markers in the hippocampus in Alzheimer's disease and other neurodegenerative conditions*. Acta Neuropathol, 1997. **93**(3): p. 294-300.
71. Moreno-Jimenez, E.P., et al., *Adult hippocampal neurogenesis is abundant in neurologically healthy subjects and drops sharply in patients with Alzheimer's disease*. Nat Med, 2019. **25**(4): p. 554-560.
72. Tobin, M.K., et al., *Human Hippocampal Neurogenesis Persists in Aged Adults and Alzheimer's Disease Patients*. Cell Stem Cell, 2019. **24**(6): p. 974-982 e3.
73. Terreros-Roncal, J., et al., *Response to Comment on "Impact of neurodegenerative diseases on human adult hippocampal neurogenesis"*. Science, 2022. **376**(6590): p. eabn7270.
74. Moreno-Jiménez, E.P., et al., *Evidences for Adult Hippocampal Neurogenesis in Humans*. J Neurosci, 2021. **41**(12): p. 2541-2553.
75. Zeng, Q., et al., *Hippocampal neurogenesis in the APP/PS1/nestin-GFP triple transgenic mouse model of Alzheimer's disease*. Neuroscience, 2016. **314**: p. 64-74.
76. Dorey, E., et al., *Apolipoprotein E, amyloid-beta, and neuroinflammation in Alzheimer's disease*. Neurosci Bull, 2014. **30**(2): p. 317-30.
77. Cassé, F., K. Richetin, and N. Toni, *Astrocytes' Contribution to Adult Neurogenesis in Physiology and Alzheimer's Disease*. Front Cell Neurosci, 2018. **12**: p. 432.
78. Araki, T., Y. Ikegaya, and R. Koyama, *The effects of microglia- and astrocyte-derived factors on neurogenesis in health and disease*. Eur J Neurosci, 2021. **54**(5): p. 5880-5901.
79. Rao, Y.L., et al., *Hippocampus and its involvement in Alzheimer's disease: a review*. 3 Biotech, 2022. **12**(2): p. 55.
80. Kinney, J.W., et al., *Inflammation as a central mechanism in Alzheimer's disease*. Alzheimers Dement (N Y), 2018. **4**: p. 575-590.
81. Xie, J., L. Van Hoecke, and R.E. Vandenbroucke, *The Impact of Systemic Inflammation on Alzheimer's Disease Pathology*. Front Immunol, 2021. **12**: p. 796867.
82. Heneka, M.T., et al., *Neuroinflammation in Alzheimer's disease*. Lancet Neurol, 2015. **14**(4): p. 388-405.
83. Edler, M.K., I. Mhatre-Winters, and J.R. Richardson, *Microglia in Aging and Alzheimer's Disease: A Comparative Species Review*. Cells, 2021. **10**(5).
84. Gray, S.C., K.J. Kinghorn, and N.S. Woodling, *Shifting equilibriums in Alzheimer's disease: the complex roles of microglia in neuroinflammation, neuronal survival and neurogenesis*. Neural Regen Res, 2020. **15**(7): p. 1208-1219.
85. Hickman, S.E., E.K. Allison, and J. El Khoury, *Microglial dysfunction and defective beta-amyloid clearance pathways in aging Alzheimer's disease mice*. J Neurosci, 2008. **28**(33): p. 8354-60.

86. Verkhatsky, A., et al., *Astrocytes in Alzheimer's disease*. Neurotherapeutics, 2010. **7**(4): p. 399-412.
87. Meraz-Ríos, M.A., et al., *Inflammatory process in Alzheimer's Disease*. Front Integr Neurosci, 2013. **7**: p. 59.
88. Ourdev, D., et al., *The Effect of $A\beta_{1-42}$ Oligomers on APP Processing and $A\beta_{1-40}$ Generation in Cultured U-373 Astrocytes*. Neurodegener Dis, 2015. **15**(6): p. 361-8.
89. Goetzl, E.J., et al., *Cargo proteins of plasma astrocyte-derived exosomes in Alzheimer's disease*. FASEB J, 2016. **30**(11): p. 3853-3859.
90. Lian, H., et al., *Astrocyte-Microglia Cross Talk through Complement Activation Modulates Amyloid Pathology in Mouse Models of Alzheimer's Disease*. J Neurosci, 2016. **36**(2): p. 577-89.
91. Owen, J.B., et al., *Oxidative modification to LDL receptor-related protein 1 in hippocampus from subjects with Alzheimer disease: implications for $A\beta$ accumulation in AD brain*. Free Radic Biol Med, 2010. **49**(11): p. 1798-803.
92. Jaynes, B. and J. Provas, *Evidence for altered LRP/RAGE expression in Alzheimer lesion pathogenesis*. Curr Alzheimer Res, 2008. **5**(5): p. 432-7.
93. Heneka, M.T., D.T. Golenbock, and E. Latz, *Innate immunity in Alzheimer's disease*. Nat Immunol, 2015. **16**(3): p. 229-36.
94. Perez-Dominguez, M., et al., *The detrimental effects of lipopolysaccharide-induced neuroinflammation on adult hippocampal neurogenesis depend on the duration of the pro-inflammatory response*. Neural Regen Res, 2019. **14**(5): p. 817-825.
95. Ekdahl, C.T., et al., *Inflammation is detrimental for neurogenesis in adult brain*. Proc Natl Acad Sci U S A, 2003. **100**(23): p. 13632-7.
96. Monje, M.L., H. Toda, and T.D. Palmer, *Inflammatory blockade restores adult hippocampal neurogenesis*. Science, 2003. **302**(5651): p. 1760-5.
97. Mishra, S.K., et al., *Intracerebroventricular streptozotocin impairs adult neurogenesis and cognitive functions via regulating neuroinflammation and insulin signaling in adult rats*. Neurochem Int, 2018. **113**: p. 56-68.
98. Zhang, W.J., et al., *Impairment of hippocampal neurogenesis in streptozotocin-treated diabetic rats*. Acta Neurol Scand, 2008. **117**(3): p. 205-10.
99. Bassani, T.B., et al., *Effects of curcumin on short-term spatial and recognition memory, adult neurogenesis and neuroinflammation in a streptozotocin-induced rat model of dementia of Alzheimer's type*. Behav Brain Res, 2017. **335**: p. 41-54.
100. Belyaev, N.D., et al., *The transcriptionally active amyloid precursor protein (APP) intracellular domain is preferentially produced from the 695 isoform of APP in a β -secretase-dependent pathway*. J Biol Chem, 2010. **285**(53): p. 41443-54.
101. Goodger, Z.V., et al., *Nuclear signaling by the APP intracellular domain occurs predominantly through the amyloidogenic processing pathway*. J Cell Sci, 2009. **122**(Pt 20): p. 3703-14.
102. Borg, J.-P., et al., *The X11a protein slows cellular amyloid precursor protein processing and reduces $A\beta_{40}$ and $A\beta_{42}$ secretion*. J. Biol. Chem., 1998. **273**(24): p. 14761-14766.
103. Dunning, C.J.R., et al., *Multisite tyrosine phosphorylation of the N-terminus of Mint1/X11a by Src kinase regulates the trafficking of amyloid precursor protein*. J. Neurochem., 2016. **137**(4): p. 518-527.
104. Miller, C.C.J., et al., *The X11 proteins, $A\beta$ production and Alzheimer's disease*. Trends Neurosci., 2006. **29**(5): p. 280-285.
105. Tamayev, R., D. Zhou, and L. D'Adamio, *The interactome of the amyloid β precursor protein family members is shaped by phosphorylation of their intracellular domains*. Mol. Neurodegener., 2009. **4**: p. No pp. given.

106. Hoe, H.S., et al., *DAB1 and Reelin effects on amyloid precursor protein and ApoE receptor 2 trafficking and processing*. J Biol Chem, 2006. **281**(46): p. 35176-85.
107. Russo, C., et al., *Signal Transduction through Tyrosine-phosphorylated C-terminal Fragments of Amyloid Precursor Protein via an Enhanced Interaction with Shc/Grb2 Adaptor Proteins in Reactive Astrocytes of Alzheimer's Disease Brain*. J. Biol. Chem., 2002. **277**(38): p. 35282-35288.
108. Tarr, P.E., et al., *Tyrosine phosphorylation of the β -amyloid precursor protein cytoplasmic tail promotes interaction with Shc*. J. Biol. Chem., 2002. **277**(19): p. 16798-16804.
109. Borquez, D.A. and C. Gonzalez-Billault, *The amyloid precursor protein intracellular domain-Fe65 multiprotein complexes: a challenge to the amyloid hypothesis for Alzheimer's disease?* Int. J. Alzheimer's Dis., 2012: p. 353145, 10 pp.
110. Bukhari, H., et al., *Small things matter: Implications of APP intracellular domain AICD nuclear signaling in the progression and pathogenesis of Alzheimer's disease*. Prog. Neurobiol. (Oxford, U. K.), 2017. **156**: p. 189-213.
111. Chang, K.-A., et al., *Phosphorylation of amyloid precursor protein (APP) at Thr668 regulates the nuclear translocation of the APP intracellular domain and induces neurodegeneration*. Mol. Cell. Biol., 2006. **26**(11): p. 4327-4338.
112. Ando, K., et al., *Phosphorylation-dependent regulation of the interaction of amyloid precursor protein with Fe65 affects the production of β -amyloid*. J. Biol. Chem., 2001. **276**(43): p. 40353-40361.
113. Penke, B., et al., *Key Peptides and Proteins in Alzheimer's Disease*. Curr Protein Pept Sci, 2019. **20**(6): p. 577-599.
114. McLoughlin, D.M. and C.C.J. Miller, *The FE65 proteins and Alzheimer's disease*. J. Neurosci. Res., 2008. **86**(4): p. 744-754.
115. Sabo, S.L., et al., *The Alzheimer amyloid precursor protein (APP) and FE65, an APP-binding protein, regulate cell movement*. J. Cell Biol., 2001. **153**(7): p. 1403-1414.
116. Sabo, S.L., et al., *The amyloid precursor protein and its regulatory protein, FE65, in growth cones and synapses in vitro and in vivo*. J. Neurosci., 2003. **23**(13): p. 5407-5415.
117. Minopoli, G., et al., *Fe65 matters: New light on an old molecule*. IUBMB Life, 2012. **64**(12): p. 936-942.
118. Santiard-Baron, D., et al., *Expression of human FE65 in amyloid precursor protein transgenic mice is associated with a reduction in β -amyloid load*. J. Neurochem., 2005. **93**(2): p. 330-338.
119. Coronel, R., et al., *Physiological effects of amyloid precursor protein and its derivatives on neural stem cell biology and signaling pathways involved*. Neural Regen Res, 2019. **14**(10): p. 1661-1671.
120. Feilen, L.P., et al., *Fe65-PTB2 Dimerization Mimics Fe65-APP Interaction*. Front Mol Neurosci, 2017. **10**: p. 140.
121. Lazarov, O. and M.P. Demars, *All in the family: how the APPs regulate neurogenesis*. Front. Neurog., 2012. **6**(June): p. 81.
122. Beckett, C., et al., *Nuclear signalling by membrane protein intracellular domains: the AICD enigma*. Cell Signal, 2012. **24**(2): p. 402-409.
123. Li Puma, D.D., R. Piacentini, and C. Grassi, *Does Impairment of Adult Neurogenesis Contribute to Pathophysiology of Alzheimer's Disease? A Still Open Question*. Front Mol Neurosci, 2020. **13**: p. 578211.
124. Chang, Y., et al., *Generation of the β -Amyloid Peptide and the Amyloid Precursor Protein C-terminal Fragment γ Are Potentiated by FE65L1*. J. Biol. Chem., 2003. **278**(51): p. 51100-51107.

125. Guenette, S.Y., et al., *hFE65L influences amyloid precursor protein maturation and secretion*. J. Neurochem., **1999**. **73**(3): p. 985-993.
126. Sabo, S.L., et al., *Regulation of β -amyloid secretion by FE65, an amyloid protein precursor-binding protein*. J. Biol. Chem., 1999. **274**(12): p. 7952-7957.
127. Tanahashi, H. and T. Tabira, *Characterization of an amyloid precursor protein-binding protein Fe65L2 and its novel isoforms lacking phosphotyrosine-interaction domains*. Biochem. J., 2002. **367**(3): p. 687-695.
128. Xie, Z., et al., *RNA Interference Silencing of the Adaptor Molecules ShcC and Fe65 Differentially Affect Amyloid Precursor Protein Processing and A β Generation*. J. Biol. Chem., 2007. **282**(7): p. 4318-4325.
129. Suh, J., et al., *FE65 proteins regulate NMDA receptor activation-induced amyloid precursor protein processing*. J. Neurochem., 2011. **119**(1 & 2): p. 377-388.
130. Guenette, S., et al., *Essential roles for the FE65 amyloid precursor protein-interacting proteins in brain development*. EMBO J., 2006. **25**(2): p. 420-431.
131. Wang, B., et al., *Isoform-specific knockout of FE65 leads to impaired learning and memory*. J Neurosci Res, 2004. **75**(1): p. 12-24.
132. Lee, M.-S., et al., *APP processing is regulated by cytoplasmic phosphorylation*. J. Cell Biol., 2003. **163**(1): p. 83-95.
133. Ghosal, K., A. Stathopoulos, and S.W. Pimplikar, *APP intracellular domain impairs adult neurogenesis in transgenic mice by inducing neuroinflammation*. PLoS One, 2010. **5**(7): p. No pp. given.
134. Ma, Q.H., et al., *A TAG1-APP signalling pathway through Fe65 negatively modulates neurogenesis*. Nat Cell Biol, 2008. **10**(3): p. 283-94.
135. Macias, M.J., et al., *Structure of the WW domain of a kinase-associated protein complexed with a proline-rich peptide*. Nature (London), 1996. **382**(6592): p. 646-649.
136. Sudol, M., K. Sliwa, and T. Russo, *Functions of WW domains in the nucleus*. FEBS Lett., 2001. **490**(3): p. 190-195.
137. Staub, O. and D. Rotin, *WW domains*. Structure (London), 1996. **4**(5): p. 495-499.
138. Sudol, M., et al., *Characterization of a novel protein-binding module - the WW domain*. FEBS Lett., 1995. **369**(1): p. 67-71.
139. Kato, Y., et al., *Determinants of ligand specificity in groups I and IV WW domains as studied by surface plasmon resonance and model building*. J. Biol. Chem., 2002. **277**(12): p. 10173-10177.
140. Lambrechts, A., et al., *cAMP-dependent protein kinase phosphorylation of EVL, a Mena/VASP relative, regulates its interaction with actin and SH3 domains*. J. Biol. Chem., 2000. **275**(46): p. 36143-36151.
141. Masin, M., et al., *Fe65 Interacts with P2X2 Subunits at Excitatory Synapses and Modulates Receptor Function*. J. Biol. Chem., 2006. **281**(7): p. 4100-4108.
142. Meiyappan, M., G. Birrane, and J.A.A. Ladias, *Structural Basis for Polyproline Recognition by the FE65 WW Domain*. J. Mol. Biol., 2007. **372**(4): p. 970-980.
143. Telese, F., et al., *Transcription regulation by the adaptor protein Fe65 and the nucleosome assembly factor SET*. EMBO Rep., 2005. **6**(1): p. 77-82.
144. Ermekova, K.S., et al., *The WW domain of neural protein FE65 interacts with proline-rich motifs in Mena, the mammalian homolog of Drosophila enabled*. J. Biol. Chem., 1997. **272**(52): p. 32869-32877.
145. Vargas, L.M., et al., *Amyloid- β oligomers synaptotoxicity: The emerging role of EphA4/c-Abl signaling in Alzheimer's disease*. Biochim. Biophys. Acta, Mol. Basis Dis., 2018. **1864**(4_Part_A): p. 1148-1159.

146. Lu, K.P. and X.Z. Zhou, *The prolyl isomerase PIN1: a pivotal new twist in phosphorylation signalling and disease*. Nat Rev Mol Cell Biol, 2007. **8**(11): p. 904-16.
147. Pastorino, L., et al., *The prolyl isomerase Pin1 regulates amyloid precursor protein processing and amyloid- β production*. Nature (London, U. K.), 2006. **440**(7083): p. 528-534.
148. Liou, Y.-C., et al., *Role of the prolyl isomerase Pin1 in protecting against age-dependent neurodegeneration*. Nature (London, U. K.), 2003. **424**(6948): p. 556-561.
149. Maudsley, S. and M.P. Mattson, *Protein twists and turns in Alzheimer disease*. Nat. Med. (N. Y., NY, U. S.), 2006. **12**(4): p. 392-393.
150. Borbély, E., et al., *Simultaneous changes of spatial memory and spine density after intrahippocampal administration of fibrillar $\alpha\beta 1-42$ to the rat brain*. Biomed Res Int, 2014. **2014**: p. 345305.
151. von Bohlen Und Halbach, O., *Immunohistological markers for staging neurogenesis in adult hippocampus*. Cell Tissue Res, 2007. **329**(3): p. 409-20.
152. Brinkmalm, G., et al., *Soluble amyloid precursor protein α and β in CSF in Alzheimer's disease*. Brain Res, 2013. **1513**: p. 117-26.
153. Gabelle, A., et al., *Correlations between soluble α/β forms of amyloid precursor protein and A β 38, 40, and 42 in human cerebrospinal fluid*. Brain Res, 2010. **1357**: p. 175-83.
154. Perneczky, R., P. Alexopoulos, and A. Kurz, *Soluble amyloid precursor proteins and secretases as Alzheimer's disease biomarkers*. Trends Mol Med, 2014. **20**(1): p. 8-15.
155. Shankar, G.M., et al., *Amyloid- β protein dimers isolated directly from Alzheimer's brains impair synaptic plasticity and memory*. Nat. Med. (N. Y., NY, U. S.), 2008. **14**(8): p. 837-842.
156. Vanderstichele, H., et al., *Standardization of measurement of beta-amyloid(1-42) in cerebrospinal fluid and plasma*. Amyloid, 2000. **7**(4): p. 245-58.
157. Deng, W., J.B. Aimone, and F.H. Gage, *New neurons and new memories: how does adult hippocampal neurogenesis affect learning and memory?* Nat Rev Neurosci, 2010. **11**(5): p. 339-50.
158. Abbott, L.C. and F. Nigussie, *Adult neurogenesis in the mammalian dentate gyrus*. Anat Histol Embryol, 2020. **49**(1): p. 3-16.
159. Epp, J.R., C. Chow, and L.A. Galea, *Hippocampus-dependent learning influences hippocampal neurogenesis*. Front Neurosci, 2013. **7**: p. 57.
160. Beckervordersandforth, R. and C. Rolando, *Untangling human neurogenesis to understand and counteract brain disorders*. Curr Opin Pharmacol, 2019. **50**: p. 67-73.
161. Yu, Y., et al., *Increased hippocampal neurogenesis in the progressive stage of Alzheimer's disease phenotype in an APP/PS1 double transgenic mouse model*. Hippocampus, 2009. **19**(12): p. 1247-53.
162. Chevallier, N.L., et al., *Perturbed neurogenesis in the adult hippocampus associated with presenilin-1 A246E mutation*. Am J Pathol, 2005. **167**(1): p. 151-9.
163. Demars, M., et al., *Impaired neurogenesis is an early event in the etiology of familial Alzheimer's disease in transgenic mice*. J Neurosci Res, 2010. **88**(10): p. 2103-17.
164. Taniuchi, N., et al., *Decreased proliferation of hippocampal progenitor cells in APP^{swe}/PS1^{dE9} transgenic mice*. Neuroreport, 2007. **18**(17): p. 1801-5.
165. Gan, L., et al., *Neurogenic responses to amyloid-beta plaques in the brain of Alzheimer's disease-like transgenic (pPDGF-APP^{Sw},Ind) mice*. Neurobiol Dis, 2008. **29**(1): p. 71-80.

166. Hamilton, A. and C. Holscher, *The effect of ageing on neurogenesis and oxidative stress in the APP^{sw}/PS1^{deltaE9} mouse model of Alzheimer's disease*. Brain Res., 2012. **1449**: p. 83-93.
167. Hu, Y.S., et al., *Complex environment experience rescues impaired neurogenesis, enhances synaptic plasticity, and attenuates neuropathology in familial Alzheimer's disease-linked APP^{sw}/PS1^{DeltaE9} mice*. Faseb j, 2010. **24**(6): p. 1667-81.
168. Dong, H., et al., *Modulation of hippocampal cell proliferation, memory, and amyloid plaque deposition in APP^{sw} (Tg2576) mutant mice by isolation stress*. Neuroscience, 2004. **127**(3): p. 601-9.
169. He, J. and F.T. Crews, *Neurogenesis decreases during brain maturation from adolescence to adulthood*. Pharmacol Biochem Behav, 2007. **86**(2): p. 327-33.
170. Unger, M.S., et al., *Early Changes in Hippocampal Neurogenesis in Transgenic Mouse Models for Alzheimer's Disease*. Mol Neurobiol, 2016. **53**(8): p. 5796-806.
171. Zhang, J., et al., *Long-term treadmill exercise attenuates A β burdens and astrocyte activation in APP/PS1 mouse model of Alzheimer's disease*. Neurosci Lett, 2018. **666**: p. 70-77.
172. Mandyam, C.D., G.C. Harburg, and A.J. Eisch, *Determination of key aspects of precursor cell proliferation, cell cycle length and kinetics in the adult mouse subgranular zone*. Neuroscience, 2007. **146**(1): p. 108-22.
173. Wojtowicz, J.M. and N. Kee, *BrdU assay for neurogenesis in rodents*. Nat Protoc, 2006. **1**(3): p. 1399-405.
174. Kuipers, S.D., J.E. Schroeder, and A. Trentani, *Changes in hippocampal neurogenesis throughout early development*. Neurobiol Aging, 2015. **36**(1): p. 365-79.
175. Zhang, X.M., et al., *Beta-secretase-1 elevation in transgenic mouse models of Alzheimer's disease is associated with synaptic/axonal pathology and amyloidogenesis: implications for neuritic plaque development*. Eur J Neurosci, 2009. **30**(12): p. 2271-83.
176. Fukumoto, H., et al., *Beta-secretase activity increases with aging in human, monkey, and mouse brain*. Am J Pathol, 2004. **164**(2): p. 719-25.
177. Luo, G., et al., *Deposition of BACE-1 Protein in the Brains of APP/PS1 Double Transgenic Mice*. Biomed Res Int, 2016. **2016**: p. 8380618.
178. Kandalepas, P.C., et al., *The Alzheimer's β -secretase BACE1 localizes to normal presynaptic terminals and to dystrophic presynaptic terminals surrounding amyloid plaques*. Acta Neuropathol, 2013. **126**(3): p. 329-52.
179. Koffie, R.M., et al., *Oligomeric amyloid beta associates with postsynaptic densities and correlates with excitatory synapse loss near senile plaques*. Proc Natl Acad Sci U S A, 2009. **106**(10): p. 4012-7.
180. Viola, K.L. and W.L. Klein, *Amyloid β oligomers in Alzheimer's disease pathogenesis, treatment, and diagnosis*. Acta Neuropathol, 2015. **129**(2): p. 183-206.
181. Ashe, K.H., *Learning and memory in transgenic mice modeling Alzheimer's disease*. Learn Mem, 2001. **8**(6): p. 301-8.
182. Czeh, M., P. Gressens, and A.M. Kaindl, *The yin and yang of microglia*. Dev Neurosci, 2011. **33**(3-4): p. 199-209.
183. Lee, C.Y. and G.E. Landreth, *The role of microglia in amyloid clearance from the AD brain*. J Neural Transm (Vienna), 2010. **117**(8): p. 949-60.
184. Richetin, K., et al., *Differential alteration of hippocampal function and plasticity in females and males of the APPxPS1 mouse model of Alzheimer's disease*. Neurobiol Aging, 2017. **57**: p. 220-231.

185. Baek, S.H., et al., *Exchange of N-CoR corepressor and Tip60 coactivator complexes links gene expression by NF-kappaB and beta-amyloid precursor protein*. Cell, 2002. **110**(1): p. 55-67.
186. Delatour, B., et al., *FE65 in Alzheimer's disease: neuronal distribution and association with neurofibrillary tangles*. Am J Pathol, 2001. **158**(5): p. 1585-91.
187. Chen, D., et al., *Rational design of YAP WW1 domain-binding peptides to target TGFβ/BMP/Smad-YAP interaction in heterotopic ossification*. J. Pept. Sci., 2015. **21**(11): p. 826-832.
188. Rubini, C., et al., *Recognition of lysine-rich peptide ligands by murine cortactin SH3 domain: CD, ITC, and NMR studies*. Biopolymers, 2010. **94**(3): p. 298-306.
189. Sudol, M. and T. Hunter, *New wrinkles for an old domain*. Cell (Cambridge, Mass.), 2000. **103**(7): p. 1001-1004.
190. Lacor, P.N., et al., *Synaptic targeting by Alzheimer's-related amyloid beta oligomers*. J Neurosci, 2004. **24**(45): p. 10191-200.
191. Wei, W., et al., *Amyloid beta from axons and dendrites reduces local spine number and plasticity*. Nat Neurosci, 2010. **13**(2): p. 190-6.
192. Cao, X. and T.C. Suedhof, *Dissection of Amyloid-β Precursor Protein-dependent Transcriptional Transactivation*. J. Biol. Chem., 2004. **279**(23): p. 24601-24611.

9. Appendix

Co-author certification

I, myself as a corresponding author of the following publication declare that the authors have no conflict of interest, and Titanilla Zita Szilágyi-Szögi Ph.D. candidate had significant contribution to the jointly published research. The results discussed in her thesis were not used and not intended to be used in any other qualification process for obtaining a PhD degree.

Szeged, 2023.09.07.



author

The publication relevant to the applicant's thesis:

Examination of Longitudinal Alterations in Alzheimer's Disease-Related Neurogenesis in an APP/PS1 Transgenic Mouse Model, and the Effects of P33, a Putative Neuroprotective Agent Thereon



Article

Effects of the Pentapeptide P33 on Memory and Synaptic Plasticity in APP/PS1 Transgenic Mice: A Novel Mechanism Presenting the Protein Fe65 as a Target

Titanilla Szögi ¹ , Ildikó Schuster ¹, Emőke Borbély ¹, Andrea Gyebrovski ¹, Zsolt Bozsó ¹, János Gera ¹, Róbert Rajkó ², Miklós Sántha ³, Botond Penke ¹ and Livia Fülöp ^{1,*}

¹ Department of Medical Chemistry, Interdisciplinary Excellence Center, University of Szeged, Dóm tér 8, H-6720 Szeged, Hungary; szogititi@gmail.com (T.S.); schuster.ildiko@med.u-szeged.hu (I.S.); borbely.emoke@med.u-szeged.hu (E.B.); andrea.gyebrovski@gmail.com (A.G.); bozso.zsolt@med.u-szeged.hu (Z.B.); gera.janos1990@gmail.com (J.G.); penke.botond@med.u-szeged.hu (B.P.)

² Institute of Process Engineering, University of Szeged, Moszkvai Krt. 5-7, H-6725 Szeged, Hungary; rajko@mk.u-szeged.hu

³ Institute of Biochemistry, Biological Research Centre, Temesvári Krt. 62, H-6726 Szeged, Hungary; santha.miklos@brc.mta.hu

* Correspondence: fulop.livia@med.u-szeged.hu; Tel.: +36-62-545-698

Received: 21 May 2019; Accepted: 21 June 2019; Published: 22 June 2019



Abstract: Regulated intramembrane proteolysis (RIP) of the amyloid precursor protein (APP) leads to the formation of fragments, among which the intracellular domain of APP (AICD) was also identified to be a causative of early pathological events. AICD-counteracting proteins, such as Fe65, may serve as alternative therapeutic targets of Alzheimer's disease (AD). The detection of elevated levels of Fe65 in the brains of both human patients and APP transgenic mice may further strengthen the hypothesis that influencing the interaction between Fe65 and APP may have a beneficial effect on the course of AD. Based on a PXP motif, proven to bind to the WW domain of Fe65, a new pentapeptide was designed and tested. The impedimental effect of P33 on the production of beta amyloid (A β) (soluble fraction and aggregated plaques) and on the typical features of the AD pathology (decreased dendritic spine density, synaptic markers, elevated inflammatory reactions) was also demonstrated. Significant enhancements of both learning ability and memory function were observed in a Morris water maze paradigm. The results led us to formulate the theory that P33 acts by altering the conformation of Fe65 via binding to its WW domain, consequently hindering any interactions between Fe65 and key members involved in APP processing.

Keywords: Alzheimer's disease; amyloid beta peptide; amyloid beta precursor protein; Fe65 protein; WW domain; proline-rich peptide

1. Introduction

During the last decade, proteolytic products of the amyloid precursor protein (APP) different from beta amyloid (A β) became the targets of Alzheimer's disease (AD) research, as A β could not be proven to possess a decisive role in the AD pathomechanism. The so-called regulated intramembrane proteolysis (RIP) [1] of APP requires the concerted action of proteases (secretases), as well as many intracellular proteins that bind to the intracellular domain of APP (AICD). AICD is formed both in the amyloidogenic and non-amyloidogenic pathways, and its interactome is wide and complex (e.g., the

X11 protein family [2–5], Disabled-1 (Dab-1) [5,6], Shc-transforming protein [7,8], c-Jun N-terminal kinase-interacting proteins (JIP-1) [5], the Fe65 protein family [1,9,10], and Peptidyl-prolyl cis-trans isomerase NIMA-interacting- (Pin1 [9,11]). Interaction between AICD and these proteins can modulate A β levels, Tau phosphorylation, and transcriptional activity [9]; therefore, AICD is hypothesized to be strongly involved in the development of AD. The internalization of APP from the plasma membrane and intracellular trafficking regulate A β production [12].

The Fe65 family (Fe65, Fe65L1, and Fe65L2) plays a principal role in APP processing and trafficking, as well as in actin cytoskeleton remodeling, cell motility, neuronal growth cone formation, synapse formation, synaptic plasticity, and consequently in the learning process [13–15]. Fe65 contains three domains: two C-terminal phosphotyrosine-binding (PTB1 and PTB2) regions and an N-terminal WW domain [13,16]; all of them are highly conserved. The mouse Fe65 WW domain is identical with that of human Fe65, while the PTB2 domains differ only in one amino acid in the two species (Figure 1).

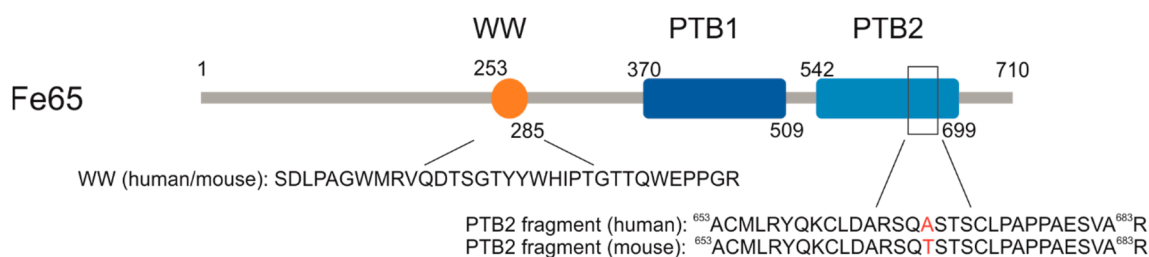


Figure 1. Human (Uniprot: O00213) and mouse (Uniprot: Q9QXJ1) domain structures of Fe65. WW (tryptophan, tryptophan) protein interaction domains are the same in human and mouse Fe65; PTB2 (phosphotyrosine-binding) domains differ only in one amino acid at position 668.

Binding of Fe65 through its PTB2 domain to APP modulates the proteolytic processing and trafficking of the latter and, consequently, A β production as well [9,13,17]. However, literary data are contradictory whether Fe65 decreases or increases the level of A β , with results seeming to vary based on the applied experimental model [9,17].

In Fe65 transfected cells (human embryonic kidney cells 293 (HEK293), human H4 neuroglioma cells (H4), and Madin–Darby Canine Kidney cells (MDCK), overexpression of Fe65 increased the production of A β [18–21]. Coincidentally, silencing the Fe65-encoding gene (*APBB1*) caused reduced levels of A β secretion in an H4 cell culture [22]. Suh et al. [23] obtained identical results in a primary cortical neuron culture. Furthermore, in two Fe65/Fe65L1 knock-out (KO) mouse strains (Tg2576 and 129SvEv Bradley), the lack of Fe65 resulted in reduced A β levels [24,25].

In contrast, Ando and colleagues [11] found that Fe65 overexpression decreases the production of A β _{1–40} and A β _{1–42} in an HEK293 cell line transiently transfected with APP695, compared to the controls. Adjacently, it was found that a Glu⁶⁶⁸-APP mutation causes a significant increase in the levels of A β _{1–40} and A β _{1–42}, presumably due to the decreased formation of pThr⁶⁶⁸-APP. This result was confirmed by experiments in double hFe65/APP (751 isoform carrying the Swedish and London mutation) and single APP transgenic mouse strains. Resulting from Fe65 overproduction, total A β and A β _{1–42} concentrations, as well as the number of A β plaques, were reduced in double transgenic mice in comparison with single APP transgenic animals [17].

The WW domain, which is also represented in Fe65, possesses a compact, antiparallel, three-stranded β -sheet structure providing an interface for binding linear peptide motifs [26,27]. WW domains are known to interact with special protein structures, the so-called proline-rich sequences [28,29]. The K_d of this binding typically falls in the low μ M range [26,30]. This was also proven for the WW domain of Fe65, which anchors several proteins equipped with a common PXP motif [1,13,31–33], many of them having key roles in Fe65-mediated transcription mechanisms (SET [34]), kinase activation, actin polymerization (Mammalian-enabled protein (Mena [35])), and A β production (Glycogen synthase kinase 3 (GSK3 β), c-Abl kinase [36]).

As Fe65 activity bears great influence on APP processing and A β formation, the stereochemical regulation of Fe65 activity through its WW domain using proline-rich sequences might pioneer new therapeutic ways to suppress or modulate AD development. To achieve this goal, we sought to design a molecule with a specific PXP motif. The pentapeptide P33 (Figure 2), which is composed of D-amino acids, was examined in isothermal titration calorimetry (ITC) studies, and its affinity to bind to the WW domain of Fe65 (Figure 2) was determined. To verify the specificity of the stereochemical regulation of Fe65, we tested the binding of P33 to the WW domain of another protein, Pin1 (Figure 2), found to also participate in APP processing. While Pin1 has a neuroprotective effect in healthy neurons, under oxidative stress or in AD, decreased Pin1 levels shift APP processing toward the amyloidogenic pathway. Pastorino et al. [37] found decreased levels of A β in Pin1 overexpressing Chinese hamster ovarian (CHO) cells. Pin1 also modulates Tau phosphorylation [9,38]. Pin1 deficit causes Tau hyperphosphorylation [39], after which the hyperphosphorylated Tau aggregates into neurofibrillary tangles (NFTs) instead of undergoing microtubule polymerization.

Fe65-WW: Acetyl-SDLPAGWMRVQDTSGTYWHIPTGTTQWEPPGR-amide

Pin1-WW: Acetyl-EKLPPGWKRMSRSSGRVYFNFHITNASQWERPSG-amide

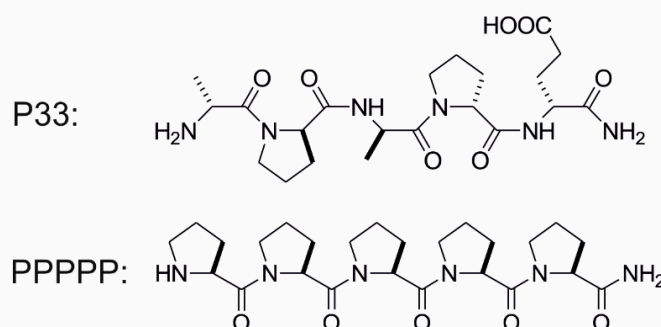


Figure 2. Sequences of the WW domains (Fe65-WW domain, Pin1-WW domain), and chemical structures of P33 and P33PPPP.

In our complex *in vivo* study, being one of the widely used animal models of familial AD [40], APP^{swe}/PS1 Δ E9 double transgenic (APP/PS1) mice were treated together with C57BL/6 wild-type (WT) mice as controls for six months with P33. We tested the effect of the pentapeptide on spatial learning and on memory with the Morris water maze (MWM), and on dendritic spine density using Golgi Cox impregnation. Synaptic function was further characterized by determining the amounts of postsynaptic density protein 95 (PSD95) and synaptophysin (SYN) with Western blots (WB). We also examined densities of the astrocytes (glial fibrillary acidic protein, GFAP), the microglia (ionized calcium-binding adapter molecule 1, Iba1), and the plaques (4G8) using immunohistochemical methods. The concentration of soluble A β was also determined with an enzyme-linked immunosorbent assay (ELISA). We also tested the effect of P33 on the Fe65, APP, pT⁶⁶⁸-APP, C83, and C99 levels of the mice. Our results suggest that elongated treatment with this pentapeptide may have beneficial effects on several biological processes (spatial learning, amyloid burden), presumably due to its influence on the Fe65 pathway.

2. Results

2.1. P33 Binds to Fe65-WW but Not to Pin1-WW *In Vitro*

Binding studies were conducted applying ITC measurements. The thermodynamical parameters of the binding interactions between P33 and the WW domain of Fe65 and Pin1 were determined in order to reveal the difference in the two WW domains in question regarding their binding with the pentapeptide. The titration of the Fe65-WW domain with P33 at 310 K resulted in the dissociation

constant $K_d = 4.68 \pm 0.04 \mu\text{M}$, calculated from the binding isotherm (Figure 3a). The stoichiometric factor $N = 1.14$ indicates an equimolar interaction and, thus, the formation of a [P33]/[Fe65-WW] complex in a 1:1 ratio.

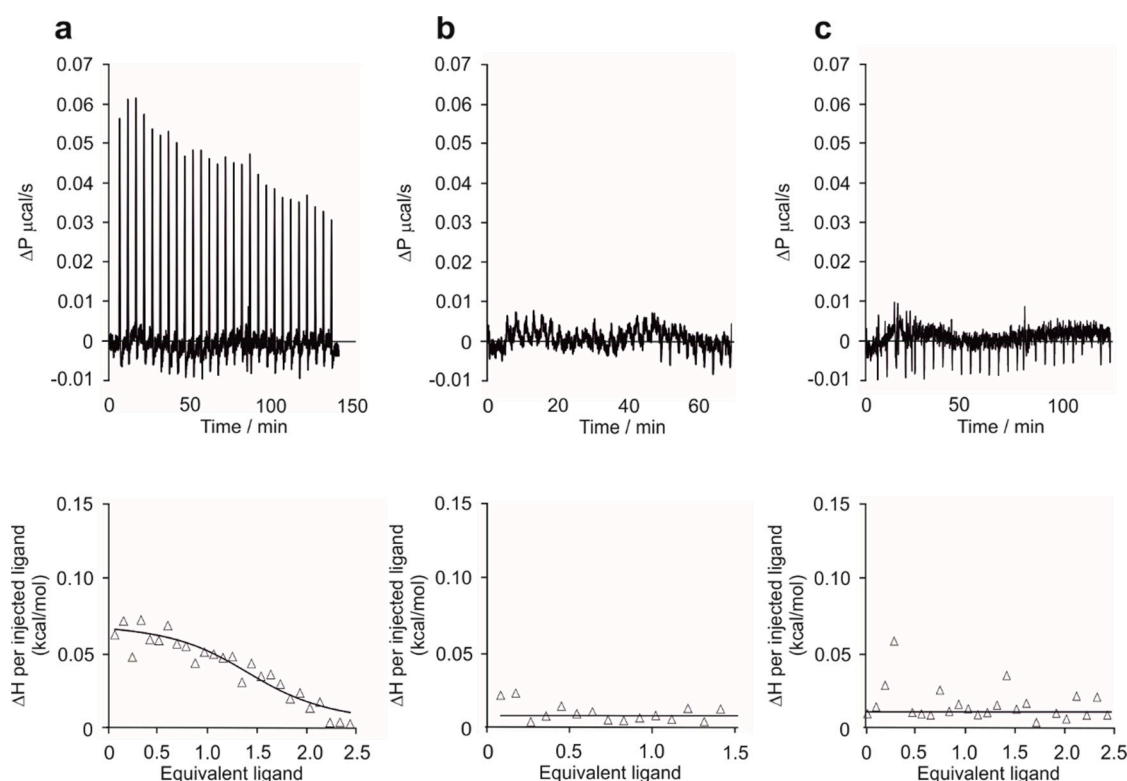


Figure 3. Isothermal titration calorimetry (ITC) measurements. Raw ITC data (top) and the integrated heat data relative to the molar ratio (bottom) in the interaction of P33 and Fe65-WW (a), PPPPP and Fe65 (b), and P33 and Pin1 (c) in phosphate-buffered saline (PBS) (pH 7.4). (a) $N = 1.14 \pm 0.01$, $\Delta H = 0.082 \pm 0.001 \text{ kcal}\cdot\text{mol}^{-1}$, $K_d = 4.68 \pm 0.04 \mu\text{M}$; (b) no binding observed; (c) no binding observed.

In a control experiment with PPPPP, no binding between the Fe65-WW and the pentapeptide could be observed at 310 K (Figure 3b), thereby proving that the unique structure of P33 is necessary for the binding interaction.

On the other hand, the titration of Pin1-WW with P33 at 310 K showed no considerable binding (Figure 3c) either. These results suggest that P33 can bind selectively to the Fe65-WW domain, which verifies the decisive role of a possible P33/Fe65-WW interaction in APP processing, instead of a Pin1-WW-involved mechanism.

2.2. P33 Treatment Does Not Influence Key Protein Levels Involved in the Fe65/APP Route in the Transgenic Mice

Three-month-old APP/PS1 double transgenic and WT mice were injected for six months with P33. To determine the effect of P33 administration on the Fe65, APP, pT⁶⁶⁸APP, C83, and C99 levels, hippocampus (HC) and cerebral cortex (CTX) regions of the brains of nine-month-old animals were subjected to WB analyses. We found significantly elevated endogenous Fe65 concentrations in transgenic mice compared to the WT animals ($H_{3,8} = 5.702$, $p = 0.022$; APP/PS1-vehicle vs. WT-vehicle, WT-P33 $p = 0.001$, 0.003 ; APP/PS1-P33 vs. WT-vehicle, WT-P33 $p \leq 0.0001$, $p = 0.002$; WT-vehicle vs. WT-P33 $p = 0.625$; APP/PS1-vehicle vs. APP/PS1-P33 $p = 0.517$), which could not be considerably changed by the treatment with P33 (Figure 4a).

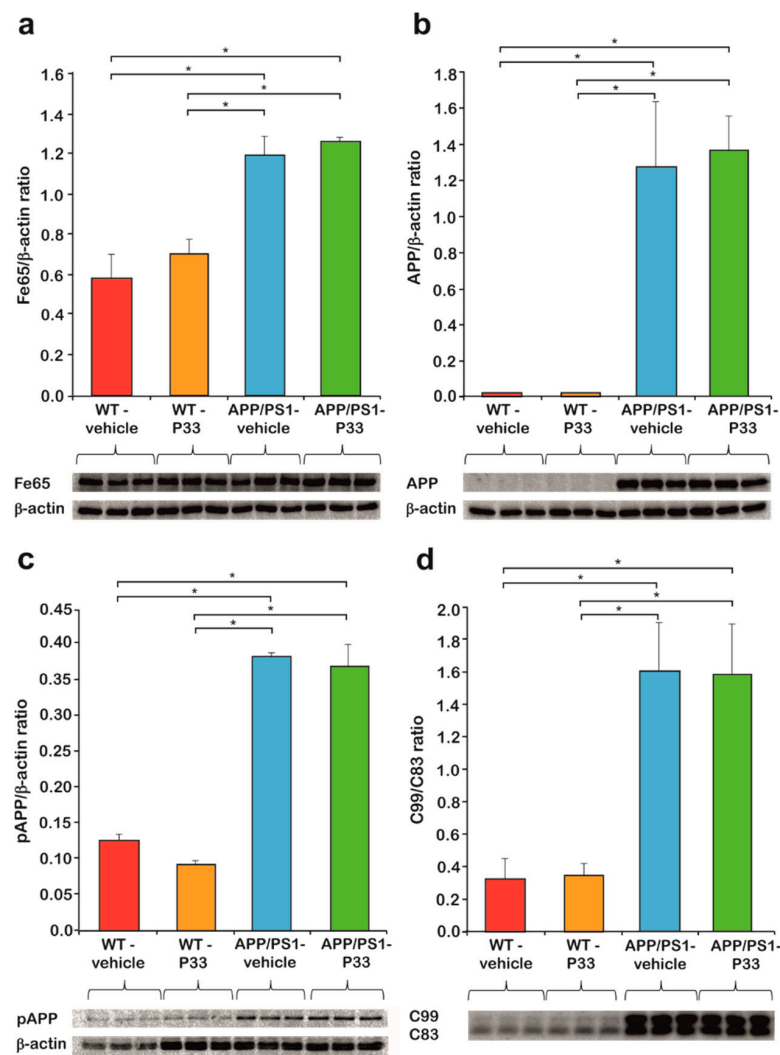


Figure 4. Western blot (WB) analysis of Fe65, amyloid precursor protein (APP), pThr⁶⁶⁸-APP, C83, and C99 levels. (a) Fe65 level of the APP/PS1 mice is significantly higher than in the wild-type (WT) animals, which did not change upon P33-treatment (* represents significant differences at the following *p*-levels: $H_{3,8} = 5.702$, $p = 0.022$; APP/PS1-vehicle vs. WT-vehicle, WT-P33 $p = 0.001$, 0.003 ; APP/PS1-P33 vs. WT-vehicle, WT-P33 $p \leq 0.0001$, $p = 0.002$; WT-vehicle vs. WT-P33 $p = 0.625$; APP/PS1-vehicle vs. APP/PS1-P33 $p = 0.517$). (b) Human APP was observed only in transgenic mice, the level of which did not change with P33-treatment either (* represents significant differences at the following *p*-levels: APP/PS1-vehicle vs. APP/PS1-P33 $p = 0.622$). (c) pThr⁶⁶⁸-APP level of APP/PS1 mice is significantly higher compared to the WT animals. The P33-treatment did not alter the level of pThr⁶⁶⁸-APP (* represents significant differences at the following *p*-levels: $H_{3,8} = 98.096$, $p \leq 0.0001$; APP/PS1-vehicle vs. WT-vehicle, WT-P33 $p \leq 0.0001$, 0.0001 ; APP/PS1-P33 vs. WT-vehicle, WT-P33 $p \leq 0.0001$, 0.0001 ; WT-vehicle vs. WT-P33 $p = 0.183$; APP/PS1-vehicle vs. APP/PS1-P33 $p = 0.554$). (d) C99/C83 ratio of APP/PS1 transgenic mice is higher than in the WT animals, which was not affected during the P33-treatment (* represents significant differences at the following *p*-levels: $H_{3,8} = 32.344$, $p \leq 0.0001$; APP/PS1-vehicle vs. WT-vehicle, WT-P33 $p \leq 0.0001$, 0.0001 ; APP/PS1-P33 vs. WT-vehicle, WT-P33 $p \leq 0.0001$, 0.0001 ; WT-vehicle vs. WT-P33 $p = 0.807$; APP/PS1-vehicle vs. APP/PS1-P33 $p = 0.926$).

Furthermore, 6E10 recognizes only human but not mouse APP, which could also be proven by our WB studies, as no detectable amounts of APP were present in WT mice. The amount of APP in the APP/PS1 animals did not change with the P33-treatment (APP/PS1-vehicle vs. APP/PS1-P33 $p = 0.622$, Figure 4b).

APP has eight phosphorylation positions in the cytoplasmic region, among which phosphorylation at T⁶⁶⁸ is held responsible for the binding of APP to Fe65, and for the consequent nuclear translocation of APP, playing a key role in the APP metabolism [18,41]. In accordance with the literature data [41], the phosphorylation at T⁶⁶⁸ was found to be significantly higher in the transgenic animals than in the WT ones, while the P33-treatment had no significant effect on the pT⁶⁶⁸-APP level ($H_{3,8} = 98.096$, $p \leq 0.0001$; APP/PS1-vehicle vs. WT-vehicle, WT-P33 $p \leq 0.0001$, 0.0001; APP/PS1-P33 vs. WT-vehicle, WT-P33 $p \leq 0.0001$, 0.0001; WT-vehicle vs. WT-P33 $p = 0.183$; APP/PS1-vehicle vs. APP/PS1-P33 $p = 0.554$, Figure 4c).

C83 is produced during the non-amyloidogenic processing of APP, while C99 is formed during the amyloidogenic pathway. The C99/C83 ratio is hypothesized, therefore, to provide information about the balance between the two pathways. As the amyloidogenic processing is increased in the transgenic mice, an elevated C99/C83 ratio could be observed, which was not influenced by the P33 treatment considerably ($H_{3,8} = 32.344$, $p \leq 0.0001$; APP/PS1-vehicle vs. WT-vehicle, WT-P33 $p \leq 0.0001$, 0.0001; APP/PS1-P33 vs. WT-vehicle, WT-P33 $p \leq 0.0001$, 0.0001; WT-vehicle vs. WT-P33 $p = 0.807$; APP/PS1-vehicle vs. APP/PS1-P33 $p = 0.926$, Figure 4d).

2.3. P33 Restores the Pathologically Reduced Spine Density and Protects the Synapses

Golgi staining was used to assess the hippocampal apical dendritic spine density of CA1 pyramidal neurons after P33 or vehicle treatment, in WT and APP/PS1 animals. During this procedure, all types of spine were analyzed. At nine months of age, there was a significant difference between the groups (one-way ANOVA; $F_{3,18} = 4.732$, $p = 0.015$). A significant reduction in the spine density could be detected in the APP/PS1-vehicle group (Figure 5a,b), compared to WT-vehicle ($p = 0.002$), and WT-P33 ($p = 0.019$) animals, while treating the APP/PS1 mice with P33 was able to normalize the diminished spine density (APP/PS1-vehicle vs. APP/PS1-P33 $p = 0.041$).

To further explore the mechanism of P33 on synapses in our AD animal model, we examined the expression of synapse associated proteins PSD95 and SYN. In SYN level, significant differences were not found between the groups (Figure 5c, $H_{3,8} = 1.573$, $p = 0.270$). The expression of PSD95 was significantly decreased in APP/PS1 vehicle-treated mice compared to the other three, which could be restored by applying P33 on APP/PS1 mice, which demonstrates the positive effect of the P33 on synapse groups (Figure 5c, $H_{3,8} = 5.473$, $p = 0.024$, APP/PS1-vehicle vs. WT-vehicle, WT-P33, APP/PS1-P33 $p = 0.026$, 0.004, 0.036, respectively).

2.4. P33 Significantly Reduces the Amounts of Both Soluble and Deposited A β Forms in the APP/PS1 Animals

The amount of soluble A β_{1-42} measured along with the plaque density provides information on the development of AD in the applied animal model. The soluble fraction of A β_{1-42} was isolated from the HC and CTX regions of the brains of nine-month-old animals, by following the method of Shankar et al. [42], and quantitatively measured with a commercially available ELISA test, which selectively recognizes human A β_{1-42} [43] and is proven to show no cross-reaction with the full-length APP. The WT mice had no detectable amounts of A β_{1-42} (0 pM), proving that the 3D6 antibody supplied with the kit detects only human, not mouse A β . In the APP/PS1-vehicle group, a significantly higher A β_{1-42} concentration could be observed than in the APP/PS1-P33 group (Figure 5d, 162.70 pM and 75.86 pM, respectively, $p < 0.0001$). The results indicate that the treatment with P33 led to a decreased level of A β_{1-42} in the APP/PS1 mice.

In order to examine the A β plaque load of both hippocampal and cortical areas, the density (%) of A β plaques was measured (Figure 5e,f). One-way ANOVA revealed a significant difference between the groups ($F_{3,16} = 48.575$, $p \leq 0.001$). Brains of WT animals were completely devoid of any A β plaque depositions. The post hoc analysis proved that long-term administration of the compound had significantly decreased the plaque density in APP/PS1-P33 mice compared to the APP/PS1-vehicle ($p = 0.013$).

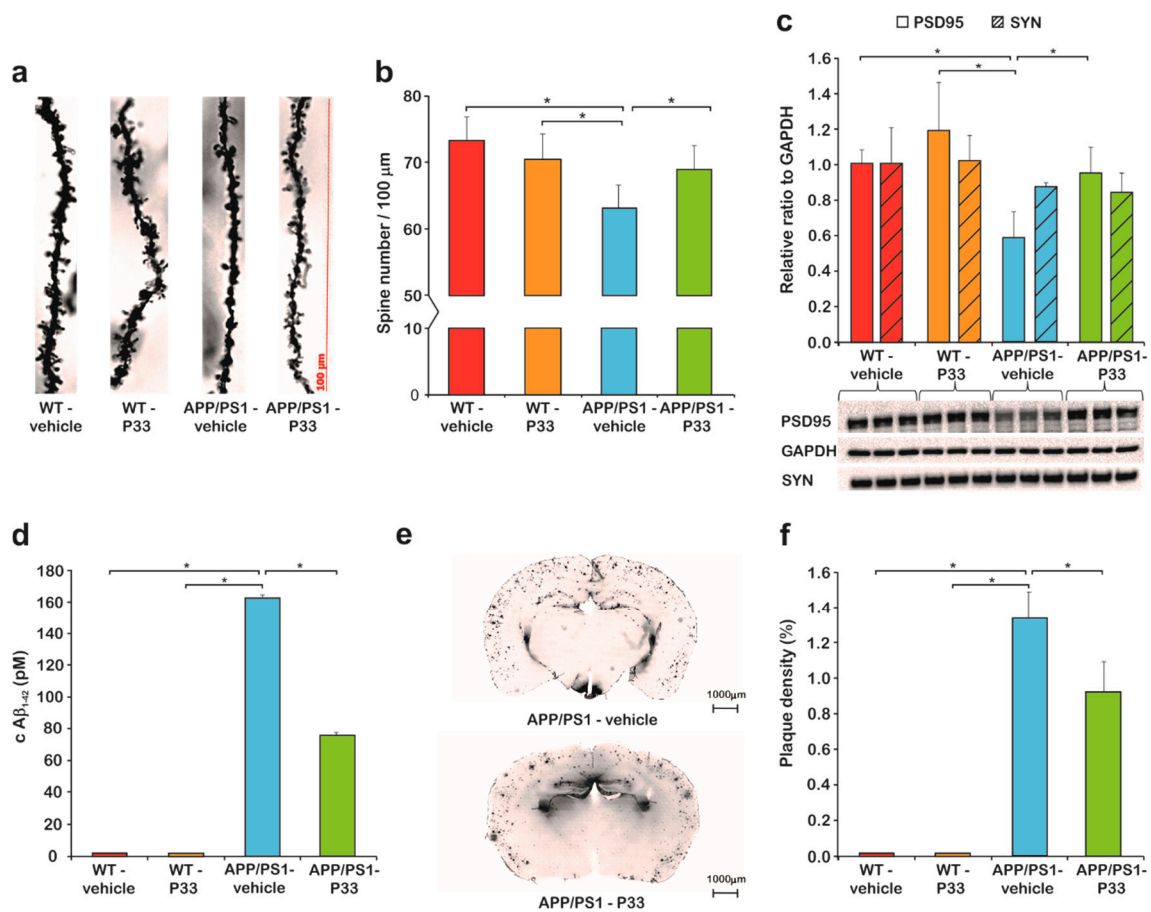


Figure 5. Histology results I. **(a)** The apical dendritic spine density in the CA1 region of the hippocampus (HC) was monitored. Representative photomicrographs of oblique dendritic segments stemming from WT-vehicle, WT-P33, APP/PS1-vehicle, and APP/PS1-P33 mice (100× magnification; scale bar: 100 μm). **(b)** Golgi staining revealed changes in the spine density after P33-treatment. Quantitative analysis of the apical dendritic spine density proved that P33 protected the synaptic terminals ($p = 0.015$). An impaired density was measured in APP/PS1-vehicle mice compared to WT-vehicle ($p = 0.002$), WT-P33 ($p = 0.019$), and APP/PS1-P33 ($p = 0.041$) animals. Bars represent the mean + standard error of the mean (SEM). * represents significant differences at the corresponding p -levels. **(c)** A significantly decreased PSD95 level was observed in APP/PS1-vehicle cohort compared to WT-vehicle, WT-P33, and APP/PS1-P33 animals (* represents significant differences at the following p -levels: $H_{3,8} = 5.473$, $p = 0.024$, APP/PS1-vehicle vs. WT-vehicle, WT-P33, APP/PS1-P33 $p = 0.026, 0.004, 0.036$). P33-treatment influenced the postsynaptic density protein 95 (PSD95) level considerably, and the statistical analysis revealed that the chronic compound treatment resulted in a significantly higher PSD95 level in APP/PS1-P33 mice compared to the APP/PS1-vehicle ones. Regarding synaptophysin (SYN) level, there is no difference between the four experimental groups ($H_{3,8} = 1.573$, $p = 0.270$). **(d)** Concentration of soluble amyloid beta (Aβ) in cerebral cortex (CTX) and HC: Aβ₁₋₄₂ level of the vehicle or P33-treated WT and APP/PS1 mice measured by ELISA. No human Aβ₁₋₄₂ was detected in the WT animals. The P33-treatment reduced the Aβ₁₋₄₂ level in the transgenic mice ($p < 0.0001$). * represents significant differences at the corresponding p -levels. **(e)** Representative pictures of the 4G8 staining of amyloid plaques. **(f)** Measurements of Aβ plaque density. Aβ plaques could not be detected in WT animals. The P33-treatment influenced the plaque density considerably; the quantitative analysis revealed that chronic P33-treatment resulted in a significant decrease in the density of Aβ deposits in the APP/PS1-P33 group compared to that of the APP/PS1-vehicle animals ($p = 0.013$). * represents significant differences at the corresponding p -levels.

2.5. P33 Hinders Inflammatory Processes in the Mouse Brain

Neuroinflammation is considered to be the result of the activation of the innate immune system in central nervous system (CNS) with a protective function against infections, injuries, and neurodegenerative processes. The inflammatory response is mediated by activated microglia and hyperreactive astrocytes. To examine the effect of long-term P33 administration on these cell types, immunohistochemical stainings were performed. GFAP staining revealed that the density of hyperreactive astrocytes was higher in the whole HC and CTX of the APP/PS1-vehicle group, than in the other three groups (Figure 6a, one-way ANOVA $F_{3,16} = 3.343$, $p = 0.048$, Fisher's least significant difference (LSD) post hoc tests: APP/PS1-vehicle vs. WT-vehicle, WT-P33, APP/PS1-P33 $p = 0.009$, 0.047, 0.039, respectively). Microglial density was examined by Iba1 immunostaining in HC and CTX areas. The density of Iba1-positive microglia was higher in the APP/PS1-vehicle treated mice than in the other groups (Figure 5b,c, one-way ANOVA $F_{3,16} = 6.629$, $p = 0.004$, Fisher's LSD post hoc tests: APP/PS1-vehicle vs. WT-vehicle, WT-P33, APP/PS1-P33 $p = 0.001$, 0.003, 0.046, respectively).

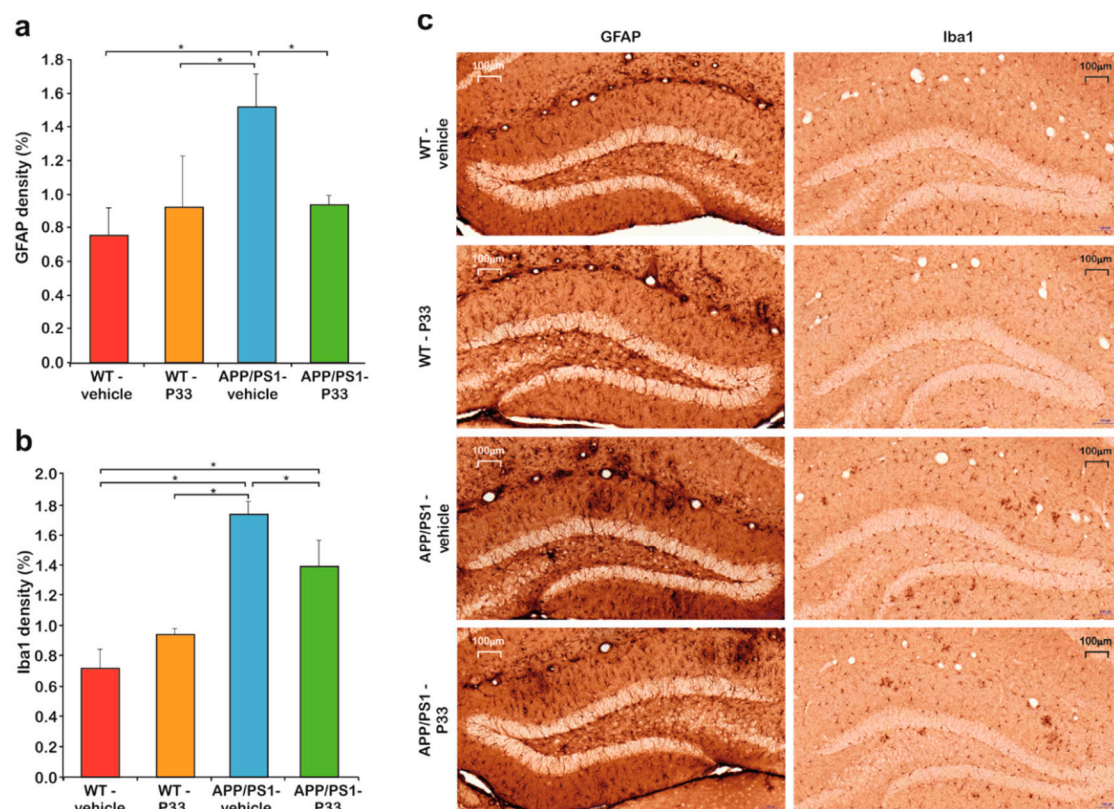


Figure 6. Histology results II. (a) Quantitative results of the glial fibrillary acidic protein (GFAP) staining. Significant differences were observed between the groups in the densities of hyperreactive astrocytes ($p = 0.048$). An increased GFAP-positive cell density was detected in the APP/PS1-vehicle group compared to the WT-vehicle ($p = 0.009$), the WT-P33 ($p = 0.047$), and the APP/PS1-P33 ($p = 0.039$) ones. * represents significant differences at the corresponding p -levels. (b) Results of the ionized calcium-binding adapter molecule 1 (Iba1) immunostaining. A significantly higher level of the activated microglia density ($p = 0.004$) was found in the APP/PS1-vehicle animals than in the other groups (WT-vehicle: $p = 0.001$, WT-P33: $p = 0.003$, APP/PS1-P33: $p = 0.046$). * represents significant differences at the corresponding p -levels. (c) Representative images of GFAP and Iba1 stainings. Scale bars represent 100 μm.

2.6. P33 Exerts a Positive Effect on the Learning Ability and Memory Functions in an MWM Paradigm

To elucidate the effects of P33 on spatial learning and memory, an MWM test was conducted for five days following the administration. Upon evaluation, we performed a mixed ANOVA in which significant differences were found between the parameters (mixed ANOVA, $F_{3,181} = 3.365$, $p = 0.030$). The post hoc analysis of the results yielded that the APP/PS1-vehicle group had a significantly bigger latency to find the platform in comparison with the other groups (WT-vehicle, $p = 0.033$; WT-P33, $p = 0.015$; APP/PS1-P33, $p = 0.006$), which confirms a learning and memory deficit in untreated transgenic mice, whereas P33 seemed to have a positive effect on their learning abilities (Figure 7a,b).

Since the measured times did not have a Gaussian distribution and because of the problems in the correct interpretation and/or determination of the probabilities of the false positive and negative decisions in cases of multiple testing, an investigation was needed to determine the differences between the groups. Figure 7a depicts the average swimming times on a bar plot. For each case, trend lines were fitted onto the average swimming times, and R^2 values of the fitted points were also calculated (Figure 7b). For the correct determination of the probability of the false positive decision error, a permutation test was applied, in which 50,000 resamples were generated by independently mixing all data related to both the mice and the days. The reciprocals of the slopes ($1/m$) of the fitted straight lines between the swimming times and the days, and swimming time data of the last days (y_{end}) were calculated and plotted onto three-dimensional (3D) distribution maps. The empirical resampled probabilities were generated for all four measured datasets (two different mice with two different treatments; calculated using the average swimming times for each) in the two-dimensional (2D) data space for getting the estimations of the probabilities of the false positive decision error; farther from the bulk of the resampled values of two variables (and closer to the origin) means a more pronounced difference from the randomness (Figure 7c). It can be concluded that WT mice results are significantly different from randomness (position of the red lines fall far from distribution of the randomly generated data), while the APP/PS1-vehicle treated mice measurements can be practically considered as a random event generation (position of the red line falls in the distribution of the randomly generated data). P33-treatment led to a significant improvement, as the randomness of the measurements was drastically decreased.

Secondly, bootstrap resampling with 50,000 iteration steps was used to generate a new dataset independently from that used for the permutation test to reveal the differences between the swimming times of the wild-type and transgenic groups. Again, the reciprocal of the slopes of the fitted straight lines ($1/m$) and swimming time data of the last day (y_{end}) were calculated and plotted onto 2D contour maps in this case. Red diamond and red dotted contour lines represent the vehicle treatments, while red circle and red continuous contour lines show the P33 treatments. The bolded continuous and dotted lines depict 90% of the generated data. Thus, the conclusion can be drawn with a probability level of 0.9. In Figure 7d (left panel), the WT groups have a high intersection area (32% and 89% of the total areas in case of vehicle and P33-treatments, respectively), which indicates that there is no significant difference in the two descriptive parameters between the groups; both were able to learn the task similarly. In the case of the APP/PS1 groups (Figure 7d, right panel), the intersection area is small (approximately 2% of the total areas of both vehicle and P33-treatments), which indicates a significant difference in the parameters between the groups, emphasizing the difference in the learning abilities of the P33-treated vs. non-treated groups. Furthermore, this visualization method demonstrates that our measurement data cannot be evaluated with classical parametric and even non-parametric test-methods, because the distributions are non-symmetrical, as the contours are not elliptical. In general, if the measured data are influenced by a systematic effect due to the learning procedure, the assumptions for the ordinary test-methods may be not fulfilled; thus, resampling methods are recommended.

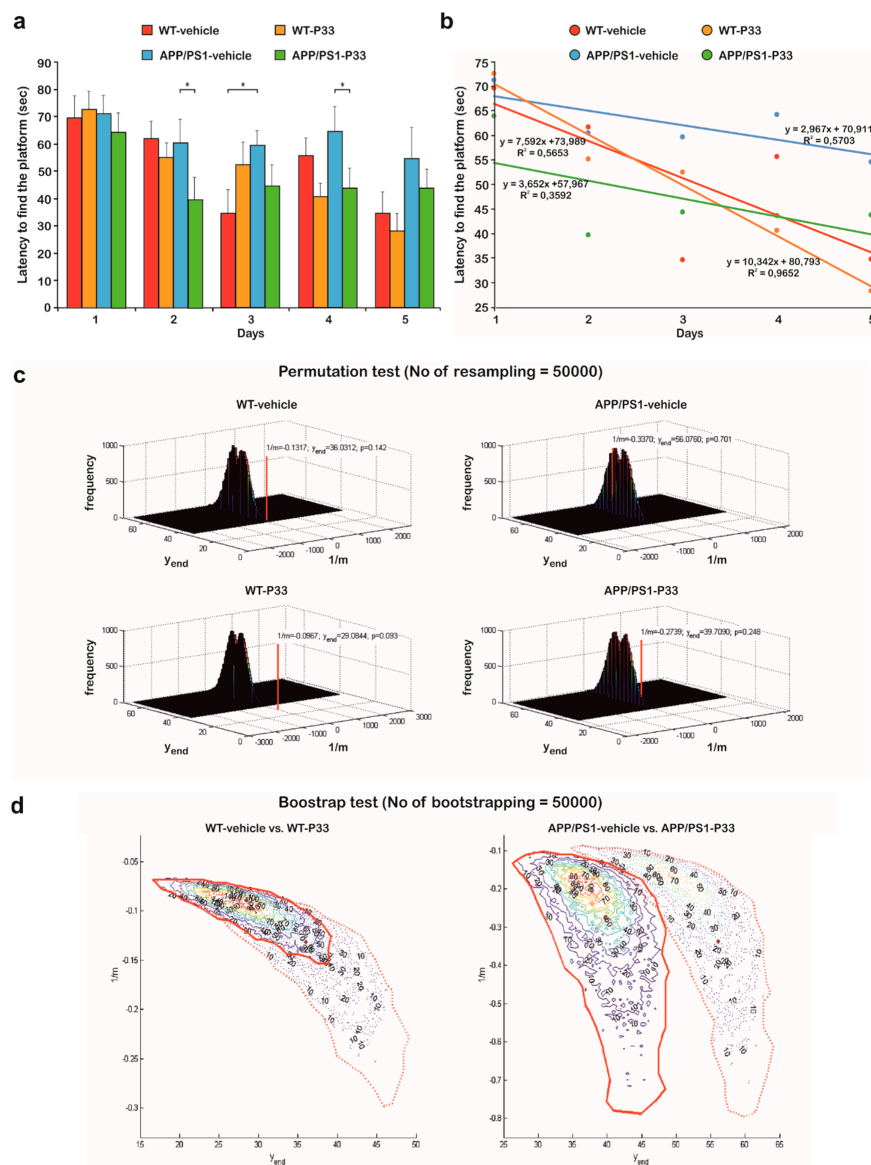


Figure 7. Statistical analysis of the behavior studies. (a) The uncertainty and the trend of every latency data versus days on a bar chart. (* represents significant differences at the following p -levels: $F_{3,181} = 3.365$, $p = 0.030$; APP/PS1 vs WT-vehicle, WT-P33, APP/PS1-P33, $p = 0.033$, 0.015 , 0.006 , respectively) (b) Former latency data to find the platform in seconds against days. For each case, trend lines were fitted onto the average swimming times. The fitted equations and the determination coefficient (R^2) values are also shown. (c) Three-dimensional (3D) distribution results of the permutation tests. WT mice results are significantly different from randomness (positions of the red lines fall far from the distribution of the randomly generated data), while the APP/PS1-vehicle treated mice measurements can be considered as a random event generation (positions of the red line fall in the distribution of the randomly generated data). P33-treatment led to a significant improvement, as the randomness of the measurements was drastically decreased. (d) Two-dimensional (2D) contour diagrams of wild-type and transgenic group data distributions based on bootstrapping. The left panel depicts that the WT groups have a high intersection area (32% and 89% of the total areas in case of vehicle and P33-treatments, respectively), indicating that there is no significant difference in the two descriptive parameters between the groups; both were able to learn the task similarly. On the right panel, in case of the APP/PS1 groups, the intersection area is small (approximately 2% of the total areas of both vehicle and P33-treatments), which indicates a significant difference in the parameters between the groups, emphasizing the difference in the learning abilities of the P33-treated vs. non-treated groups.

3. Discussion

The latest results in AD research concerned the role of key players different from A β or Tau in the pathomechanism of the disease. RIP of APP involves many putative proteinaceous targets to be studied and subjected to drug design. We aimed to find new sequences based on the common PXP motif, which might be able to modify the action of the WW domain-bearing Fe65, whereby an advantageous effect on the disease pathology could be achieved. Our model of choice was the APP/PS1 transgenic mouse, which, as we tested, overexpresses its own endogenous Fe65 (mFe65), presumably as a result of a feedback effect of the human APP (hAPP) overexpression. This result is not surprising and it also bears an analogy with human AD symptoms. In another hAPP-overexpressing mouse model [44], hAPP overexpression was shown to produce elevated mFe65 levels [45], while post mortem analysis of human sporadic AD brain samples revealed that, in the hippocampal areas, an increase in Fe65 immunoreactivity was associated with the severity of the disease [46]. These findings strengthen our hypothesis that the pathogenic overexpression of Fe65 might serve as a starting point to find new therapeutic ways for curing AD, and that the APP/PS1 transgenic model can be applied to study molecules for that purpose.

Targeting WW domains represented in several proteins involved in AD raises the question of specificity. To address this, we searched for sequences of protein molecules in protein databases which bear WW domains and are also involved in AD pathology. Besides Fe65, we identified another one, Pin1, which participates in the Tau pathology, as is able to restore the microtubule binding affinity of Tau [27] by binding to its phospho-T⁶⁶⁸P motif. Our newly designed pentapeptide, P33, was hypothesized to interact with the WW domains of both Fe65 and Pin1, thereby directly influencing the pathomechanism of AD through both A β and Tau pathologies.

Chemical synthesis of the discrete WW domains of the relevant proteins enabled the application of *in vitro* methods, via which the binding affinity of P33 could be determined. Our ITC measurements confirmed the binding of P33 to the Fe65-WW with a low micromolar K_d , which falls in the range generally observed in similar experiments. Interactions between certain WW domains and proline-rich sequences possessed dissociation constants ranging from high nM to low mM values [47,48]. On the other hand, no detectable binding to the Pin1-WW could be observed.

The results verify the selective binding of P33 to Fe65 and, therefore, we can assume that the mechanism is related to APP processing, but the Tau pathology remains unaffected. The selectivity of the binding can be explained with the differences in the respective structures of the WW domains; according to a generally accepted classification, Fe65-WW belongs to Group II, the members of which recognize the PPLP motif preferentially, while Pin1-WW is in Group IV, and is, therefore, supposed to interact mostly with a (phospho-S/phospho-T)P unit of a proline-rich sequence [49].

Our results unequivocally confirmed the advantageous effect of the P33-treatment on the memory, learning ability, and inflammatory processes in the applied transgenic animal model. Moreover, we could detect decreased amounts of both soluble and aggregated A β in the P33-treated transgenic animals. Soluble A β aggregates are considered to be trigger signals to induce dendritic spine loss and synapse dysfunction at the early stage of AD, correlating with learning impairments and memory deficits [50,51]. Recently, the synaptic protection and repair became important in AD research as key processes to ameliorate cognitive functions. In our experiments, the positive effects of P33 were demonstrated on dendritic spines and postsynaptic proteins (PSD95), together with the spatial learning and memory performances.

In order to explain the observed beneficial effects, we attempted to identify the key step in the mechanism, in which P33 should influence the action of Fe65 in the downstream processes. A series of Western blot studies proved that neither an alteration in the APP expression nor its pThr⁶⁶⁸-induced binding to Fe65, and a hypothesized shift in the ratio of the amyloidogenic/non-amyloidogenic processing pathways could not be held responsible for the effects exerted by P33. Therefore, we put forth that P33 acts simply by binding to the WW domain of the Fe65, consequently hindering its further interaction with other members of the pathophysiological processes. According to literature data, this

“blockade” might take effect through an alteration of the bioactive conformation of Fe65. Cao et al. [52] proposed that Fe65 possesses an inactive closed conformation, in which the WW domain binds to the PTB2 domain. APP and a certain membrane-associated factor together are able to open the inactive form of Fe65, whereby the latter can be activated. Feilen et al. [53] showed that Fe65 not only adopts a closed conformation, but that, in the absence of AICD, it also tends to form a homodimer through the APP-binding site. They also found that the PTB2 domain is not able to bind its own WW domain and the AICD simultaneously, since its interaction with the AICD weakens the binding to the WW, resulting in a partial opening of the inactive form [52,53]. APP and other membrane-associated factors (e.g., PIP2) together at the cell membrane induce the dissociation of the homodimer and the opening of Fe65 simultaneously, with the formation of an Fe65–APP complex [53].

However, the influence of this activation mechanism on AD pathology is still debated in the literature. To our best knowledge, the observed biological effects of Fe65 could mainly be explained by the altered expression of the protein, not by the structural changes in the bioactive conformation; however, the results are highly contradictory. Accordingly, in some animal models, the absence of Fe65 (Fe65 KO mice [24]) or in other cases the overexpression of Fe65 (Fe65/APP mice [9,17]) resulted in decreased amyloid levels. In our paradigm, the Fe65 levels of the mice were proven to be identical in the P33- and the vehicle-treated transgenic animal groups; therefore, we hypothesize that the observed significant decrease in amyloid level is due to changes in the Fe65 conformation, initiated by the interaction of P33 with the WW domain of the protein. The resulting P33–Fe65 complex may decrease the quantity of the Fe65/APP complex considerably, the formation of which was proven to be an important step in APP processing, consequently leading to decreased A β production.

In a comprehensive review, Bórquez et al. [1] summarized the so-called Fe65-interactome and also listed the binding sites, as well as the functions, of the interacting proteins. Among these, the WW-interacting ones were also proven to contain PXP motifs, through which they are attached to Fe56. Therefore, we cannot exclude the possibility that such protein–protein interactions that may have a consequent effect on the A β production might be modulated by P33 as well. Mena, Abl kinase, and GSK-3 β are such candidates, and their roles in AD are widely studied. However, starting from the represented results, further research is needed to get a deeper insight into the mechanisms through which compounds like P33 might influence the effect of these proteins in the course of AD.

4. Materials and Methods

4.1. Materials

N-terminally protected amino acids were purchased from Orpegen (Heidelberg, Germany), Bachem (Bubendorf, Switzerland), and GL Biochem (Shanghai, China). *N,N'*-Dicyclohexyl-carbodiimide (DCC), 1-hydroxybenzotriazole (HOBt), 1 [bis(dimethylamino)-methylene]-1*H*-1,2,3-triazolo[4,5-*b*]pyridinium-3-oxid hexafluorophosphate (HATU), and 4-methylbenzhydrylamine hydrochloride (MBHA \times HCl) resin were purchased from GL Biochem (Shanghai, China), and Rink Amide resin was obtained from Bachem (Bubendorf, Switzerland). Solvents and *N,N* diisopropylethylamine (DIPEA) were obtained from Sigma-Aldrich (St. Louis, MO, USA). HPLC-grade trifluoroacetic acid (TFA) was ordered from Pierce (Rockford, IL, USA).

4.2. Synthesis

For the synthesis of P33 (for structure see Figure 2), standard Boc chemistry was used on an MBHA \times HCl (1.9 mmol·g^{−1}) resin, with DCC/HOBt activation. The peptide was cleaved from the resin with a cleavage cocktail containing 10 mL of HF, 0.8 mL of dimethyl-sulfide, and 0.2 mL of anisole for 1 g of peptide-resin, at 0 °C, for 45 min. The crude peptide was precipitated with diethyl-ether, dissolved in 50% acetonitrile (ACN)/H₂O and lyophilized.

Synthesis of acetyl-Fe65-WW, acetyl-Pin1-WW, and the control PPPPP (structures involved in Figure 2) was carried out on a Rink Amide AM (0.3 mmol·g^{−1}) resin using Fmoc chemistry

and activation with HATU in the presence of DIPEA. Cleavage was achieved by a treatment with TFA/H₂O/triisopropylsilane/1,4-dithio-DL-threitol/phenol (90:5:3:1:1) at room temperature (RT). TFA was removed in vacuo, the peptides were then precipitated using cold, dry diethyl-ether, dissolved in ACN/H₂O and lyophilized.

4.3. Purification

Peptides were analyzed and purified using RP-HPLC. 0.1% TFA in deionized (d.i.) water and 80% ACN, 0.1% TFA in d.i. water were used as eluent A and eluent B, respectively.

Analytical HPLC experiments were performed on a Hewlett-Packard Agilent 1100 Series HPLC apparatus using a Luna C18 column (100 Å, 5 µm, 250 × 4.60 mm, Phenomenex, Aschaffenburg, Germany), at a flow rate of 1.2 mL·min⁻¹ with a gradient of 0 to 25% B over 25 min.

Preparative chromatography was carried out on a Shimadzu HPLC instrument equipped with a Luna C18 column (100 Å, 10 µm, 250 × 21.2 mm, Phenomenex, Aschaffenburg, Germany) at a flow rate of 4 mL·min⁻¹. The gradient was 0 to 30% B over 60 min for P33, 30% to 60% B over 100 min for Fe65-WW, 20% to 60% B over 120 min for Pin1-WW, and 0 to 40% B over 80 min for PPPPP.

4.4. ITC

Isothermal titrations were performed using a Microcal VP-ITC (Malvern Instruments, Malvern, UK) microcalorimeter. Binding experiments were carried out in degassed phosphate-buffered saline (PBS) at pH 7.4. The concentrations of Fe65-WW and Pin1-WW were normalized for the peptide contents. In one titration experiment, 10-µL portions of the ligand-containing solution (P33 or PPPPP) were injected from a computer-controlled 300-µL microsyringe at intervals of 300 s into the solution of the WW domain (Fe65-WW or Pin1-WW), dissolved in the same buffer as for the ligand. The rev of the microsyringe was set to 307 rpm. Measurements were repeated twice at 310 K. The starting concentrations of Fe65-WW and Pin1-WW in the cell were 83.5 and 81.4 µM, respectively, and the concentrations of the stock solutions containing P33 or PPPPP in the syringe were 1.006 and 1.056 mM, respectively. Control experiments were performed by injecting P33 or PPPPP into the cell containing plain buffer without the WW domain, with results achieved via subtracting the dilution heats from those measured in the presence of the WW domain.

4.5. Animals

For this study, three-month-old male and female WT and APP/PS1 mice ($n = 37$) were used. Four groups were defined: WT-vehicle (physiological saline) (male $n = 4$; female $n = 6$), WT-P33 (male $n = 6$; female $n = 5$), APP/PS1-vehicle (male $n = 3$; female $n = 5$), and APP/PS1-P33 (male $n = 6$; female $n = 2$). Animals were subjected to intraperitoneal (i.p.) injections of P33 (5 mg·kg⁻¹) for five days per week, over a course of six months. The mice were kept in groups under constant temperature (23 ± 0.5 °C), lighting (12-h/12-h light/dark cycle, lights on at 7:00 a.m.), and humidity (~50%). Standard mouse chow and tap water were supplied ad libitum. All behavioral experiments were performed in the light period. Handling was done daily at the same time.

Experiments were performed in accordance with the European Communities Council Directive of 22 September 2010 (2010/63/EU on the protection of animals used for scientific purposes) and were approved by the regional Station for Animal Health and Food Control (Csongrád-county, Hungary; project identification code: XVI/1248/2017, 20th March 2017). Formal approval to conduct the experiments was obtained from the Animal Experimentation Committee of the University of Szeged (project identification code: XXVI./3644/2017, 29th November 2017).

4.6. MWM

Spatial learning and memory were analyzed in MWM. A circular pool (d = 130, h = 60 cm), filled with water (23 ± 1 °C), served as the maze bound by a black curtain with some high-contrasted distal paper cues. Additionally, some other spatial objects were visible from the pool (e.g., lamps, video

camera). The water was opalized with milk. The maze was segmented into four virtual quadrants with the platform ($d = 10$ cm) positioned in the middle of one of these (target quadrant), set 0.5 cm below the water surface. The room was illuminated by three lamps diffusely lighting all points of the maze with approximately equal intensity.

The experiment lasted for five days, and was conducted on every occasion in the light period. Mice were tested twice every day when they were allowed to swim until they found the platform. If the animal failed to find the platform within 90 s, it was guided to it or placed manually on top of it for 15 s. Four different starting points were used during the experiment; starting points were changed randomly during the tests. Trajectories of the mice were recorded with a video camera fixed on the ceiling, equipped with the software EthoVision XT8 (Noldus Information Technology, The Netherlands, 2011). The tracking system calculated the time to reach the platform, swimming speed, length of the swimming path (distance), and percentage time spent in each of the four virtual quadrants during the trials.

4.7. ELISA

Nine-month-old mice (three animals per group) were euthanized via cervical dislocation. Their brains were removed, and the tissue containing the HC and the CTX was quickly dissected and stored at -80°C until further use. The tissue was homogenized on ice, in a buffer containing 50 mM Tris-HCl, pH 7.4; 150 mM NaCl, and 1 mM EDTA, in the presence of a protease inhibitor cocktail (1:100 dilution, Sigma-Aldrich, Saint Louis, MO, USA). The homogenate was then centrifuged at $10,000\times g$ for 15 min at a temperature of 4°C , and the supernatant was collected. The pellet was suspended in a lysis buffer supplemented with the protease inhibitor cocktail, and was centrifuged again. The supernatants were pooled and centrifuged at $15,000\times g$ for 30 min at 4°C . The final supernatants were stored at 4°C for 1–2 h until use. To quantify the level of $\text{A}\beta$ in the mice, we used a sandwich ELISA Kit (Innotest Amyloid- β_{1-2}) from Innogenetics (Gent, Belgium), following the instructions of the manufacturer. The absorbance values were measured at 450 nm on a 96-well plate reader (NOVOstar OPTIMA, BMG Labtech, Offenburg, Germany).

4.8. WB

Protein samples, identically prepared as for ELISA, (20 $\mu\text{g}/\text{lane}$) were separated on a 15% SDS-polyacrylamide gel (80 V, 20 min at RT; than 130 V, 60 min at RT) or on a 4–12% NuPAGE[®] Bis-Tris Gel (Thermo Fischer Scientific, Waltham, MA, USA, 200V, 30 min at RT) and transferred to a nitrocellulose membrane (Whatman, Maidstone, UK, 450 mA, 90 min at 4°C). The membranes were washed twice with blocking solution (Tris-buffered saline (TBS) containing 0.1% Tween-20 and 5% bovine serum albumin (BSA)); then, they were incubated overnight at 4°C with the primary antibodies (1:5000, rabbit Fe65 antibody, Thermo Fisher Scientific, Waltham, MA, USA; 1:1000, mouse 6E10 antibody, BioLegend, San Diego, CA, USA; 1:2000, rabbit pT668-APP antibody, GeneTex, Irvine, CA, USA; 1:20,000, mouse β -actin antibody, Sigma-Aldrich, St. Louis, MO, USA; 1:2000, rabbit AICD antibody, Sigma-Aldrich, St. Louis, MO, USA; 1:20,000, mouse PSD95 antibody, Invitrogen, Carlsbad, CA, USA; 1:50,000, mouse synaptophysin antibody, Invitrogen, Carlsbad, CA, USA; 1:200,000, rabbit GAPDH antibody, Cell Signaling, Leiden, Netherlands) diluted in the blocking solution. Subsequently, membranes were washed three times with washing buffer (TBS containing 0.1% Tween-20), and they were incubated with the corresponding secondary antibodies (1:5000, goat anti-rabbit or rabbit anti-mouse, Immuno Reagents, Raleigh, NC, USA) for 2 h at RT. The visualization was performed with the WesternBright[™] ECL detection kit (Sycamore, Houston, TX, USA). Membranes were scanned with a Bio-Rad Molecular Imager[®] ChemiDoc[™] XRS+Imaging System (Bio-Rad Laboratories, Hercules, CA, USA) and evaluated with the Image Lab 4.0 software.

4.9. Quantification of Spine Density

Mice (three animals per group) were deeply anaesthetized using chloral-hydrate (1 mg·kg⁻¹). The brain was quickly removed from the skull and cut into blocks. For staining, an FD Rapid Golgi Stain TM Kit (FD Neuro Technologies, Consulting & Services, Inc., Columbia, MD, USA) was used as per the manufacturers' instructions. All measurements were then conducted as described previously [54,55].

4.10. Immunohistochemistry

Mice (five animals per group) were anaesthetized with chloral-hydrate (1 mg·kg⁻¹) and perfused transcardially with PBS, followed by ice-cold 4% paraformaldehyde. The brains were removed, post-fixed in the same fixative, and immersed in a 30% sucrose solution containing 0.01% sodium-azide. They were sliced up from the dorsal to the ventral part of the HC, on a freezing microtome, into 20-µm-thick coronal sections (12 sections/animal/staining). In the free-floating sections, endogenous peroxidases were quenched with 0.3% H₂O₂ in PBS. The acquired sections were then subjected to further immunohistochemical experiments. For 4G8 staining, the sections were incubated in 100% formic acid for 1 min at RT to aid in the immunohistochemical detection of amyloid plaques. The sections were subsequently rinsed four times in PBS following the pretreatments. For GFAP stainings, the sections were blocked in a mixture of 8% normal goat serum (Sigma-Aldrich, Saint Louis, MO, USA), 0.3% BSA (Sigma-Aldrich, Saint Louis, MO, USA), and 0.3% Triton X-100 (Sigma-Aldrich, Saint Louis, MO, USA) in PBS for 1 h. For DCX and Iba1 labeling, sections were blocked in 0.1% BSA and 0.3% Triton X-100 in PBS for 1 h. Sections were incubated overnight at 4 °C with primary antibodies in the following dilutions: rabbit anti-Iba1 (1:3600; Code No.: 019-19741, Wako Chemicals GmbH, Neuss, Germany), mouse anti-GFAP (1:1500; Santa Cruz Biotechnology, Inc., Dallas, TX, USA), and anti-β-amyloid antibody (1:10,000; 4G8; BioLegend, San Diego, CA, USA). The next day, the sections were rinsed three times in PBS. For GFAP staining, the sections were treated with a polymer-based horseradish peroxidase (HRP)-amplifying system (Super Sensitive™ One-Step Polymer-HRP IHC Detection System, BioGenex, Fremont, CA, USA). The assay was used in accordance with the manufacturer's instructions. For Iba1 and β-amyloid stainings, the sections were incubated with the corresponding secondary antibodies: biotinylated goat anti-rabbit (1:400; Jackson ImmunoResearch, West Grove, PA, USA) for 60 min and biotinylated goat anti-mouse (1:400; Thermo Fisher Scientific, Waltham, MA, USA) for 90 min, respectively. The sections were then rinsed three times in PBS and incubated with an avidin-biotin complex (VECTASTAIN® Elite ABC-Peroxidase Kit; Vector Laboratories, Burlingame, CA, USA) for β-amyloid staining in 1:500, for 90 min, and for Iba1 staining in 1:400, for 60 min at RT. The peroxidase immunolabeling was developed for 30 min in 0.5 M Tris-HCl buffer (pH 7.7) with 3,3'-diaminobenzidine (DAB, 10 mM, Sigma-Aldrich, Saint Louis, MO, USA) at RT. Sections were mounted with dibutyl phthalate xylene (DPX, Sigma-Aldrich, Saint Louis, MO, USA) onto slides and cover-slipped.

4.11. Quantification of the Immunohistochemical Data

Slides were scanned by a digital slide scanner (Mirax Midi, 3DHistech Ltd., Budapest, Hungary), equipped with a Panoramic Viewer 1.15.4, CaseViewer 2.1 program and a QuantCenter, HistoQuant module (3DHistech Ltd., Budapest, Hungary). For quantification, all of the sections were analyzed. The HC and the CTX were manually outlined as the regions of interest (ROI). Antibody-positive cell types from the ROIs were counted and quantified. The percentile densities of microglia (Iba1+), astrocytes (GFAP+), and Aβ plaques were quantified by the quantification software. The cell density was represented as a percentage.

4.12. Statistical Analysis

Behavioral data were analyzed by mixed ANOVA, followed by Fisher's LSD post hoc tests for multiple comparisons. The classical and modified ANOVA data evaluation methods applied for

the raw measurements could detect only some significant effects without explaining their positions. Convenient post hoc analysis methods, like Student's *t*-statistics, need a Gaussian distribution of the analysis data. Additionally, only the probability of the false positive decision error can be set up, and the probability of the false negative decision error remains unknown. Therefore, we developed and used nonparametric statistics. The one-response variable data (swimming times) were used to generate a two-variable model: (1) the reciprocal of the slope of the fitted straight line between the swimming time and the days (its negative values close to zero indicate an improvement in the memory and learning functions of the mice from day to day); (2) swimming time data of the last day (closeness to zero indicates an effective learning process). The two variables were combined, and evaluating them together gave more reliable multiple statistical results. For the correct estimation and use of the probability of the false positive decision error, a permutation test was applied, while, for the correct estimation and use of the probability of the false negative decision error, we used bootstrap resampling. In the case of both resampling methods, 50,000 resamples were generated independently, using an in-house developed Matlab script. The detailed explanations of the mathematical statistical development will be published elsewhere.

The results of spine density and immunohistochemistry experiments were calculated with one-way ANOVA followed by Fisher's LSD post hoc tests. The WB and ELISA data did not follow normal (Gaussian) distribution; they were, therefore, analyzed with Kruskal–Wallis nonparametric tests, followed by Mann–Whitney U tests for multiple comparisons. Data were analyzed with SPSS (IBM SPSS Statistics 24), and were expressed as the mean \pm standard error of the mean (SEM). Statistical significance was set at $p \leq 0.05$.

5. Conclusions

In the present study, a novel compound is described, which was proven to significantly decrease the level of A β (soluble A β_{1-42} and amyloid plaques) in APP/PS1 mice. As a consequence, treatment with P33 reduced memory deficit and the activation of microglia and astrocytes. It also enhanced the dendritic spine densities in the transgenic animals. We hypothesize that the beneficial effects of P33 can be explained by its binding to the Fe65 protein, the overexpression of which is characteristic for AD patients, as well as for transgenic APP-overexpressing animal models. Therefore, the compound could serve as a starting point for the development of a drug family, which exerts its effect based presumably on a novel mechanism of action, focused on the modulation of the Fe65-dependent APP processing in a favorable manner.

Author Contributions: Conceptualization, L.F. and B.P.; methodology, T.S., I.S., E.B., A.G., Z.B., and M.S.; software, J.G. and R.R.; formal analysis, E.B., J.G., R.R., and L.F.; investigation, T.S., I.S., E.B., and A.G.; resources, B.P. and L.F.; data curation, T.S., I.S., E.B., J.G., and R.R.; writing—original draft preparation, T.S. and I.S.; writing—review and editing, L.F.; visualization, I.S., J.G., and R.R.; supervision, L.F.; funding acquisition, B.P. and L.F.

Funding: This project was supported by the National Research, Development and Innovation Office (GINOP-2.3.2-15-2016-00060) and by the Hungarian Brain Research Program I and II (Grant No. KTIA_13_NAP-A-III/7, and 2017-1.2.1-NKP-2017-00002). The Ministry of Human Capacities, Hungary (grant 20391-3/2018/FEKUSTRAT) is also acknowledged.

Acknowledgments: The authors thank Szabina Furdan for her technical assistance.

Conflicts of Interest: The authors declare no conflicts of interest. The funders had no role in the design of the study; in the collection, analyses, or interpretation of data; in the writing of the manuscript, or in the decision to publish the results.

Abbreviations

RIP	regulated intramembrane proteolysis
APP	amyloid precursor protein
AICD	intracellular domain of APP
AD	Alzheimer's disease

A β	beta amyloid
HEK293	human embryonic kidney cells 293
H4	human H4 neuroglioma cells
MDCK	Madin–Darby Canine Kidney cells
ITC	isothermal titration calorimetry
APP/PS1	APP ^{swe} /PS1 Δ E9 double transgenic
WT	C57BL/6 wild type
MWM	Morris water maze
GFAP	glial fibrillary acidic protein
Iba1	ionized calcium-binding adapter molecule 1
DCC	<i>N,N'</i> -dicyclohexyl-carbodiimide
HOBt	1-hydroxybenzotriazole
HATU	1-[bis(dimethylamino)-methylene]-1H-1,2,3-triazolo[4,5-b]pyridinium-3-oxid hexafluorophosphate
MBHA x HCl	4-methylbenz-hydryl-amine hydrochloride
DIPEA	<i>N,N</i> -diisopropylethylamine
TFA	trifluoroacetic acid
ACN	acetonitrile
RT	room temperature
HC	hippocampus
CTX	cerebral cortex
WB	Western blot
TBS	Tris-buffered saline
BSA	bovine serum albumin
DAB	3,3'-diaminobenzidine
DPX	dibutyl phthalate xylene
ROI	regions of interest
CNS	central nervous system
mFe65	mouse Fe65
hAPP	human APP
ELISA	enzyme-linked immunosorbent assay
PSD95	postsynaptic density protein 95
SYN	synaptophysin
NFT	neurofibrillary tangles

References

1. Borquez, D.A.; Gonzalez-Billault, C. The amyloid precursor protein intracellular domain-Fe65 multiprotein complexes: A challenge to the amyloid hypothesis for Alzheimer's disease? *Int. J. Alzheimer's Dis.* **2012**, 353145, 10. [[CrossRef](#)] [[PubMed](#)]
2. Borg, J.-P.; Yang, Y.; De Taddeo-Borg, M.; Margolis, B.; Turner, R.S. The X11 α protein slows cellular amyloid precursor protein processing and reduces A β 40 and A β 42 secretion. *J. Biol. Chem.* **1998**, 273, 14761–14766. [[CrossRef](#)] [[PubMed](#)]
3. Dunning, C.J.R.; Black, H.L.; Andrews, K.L.; Davenport, E.C.; Conboy, M.; Chawla, S.; Dowle, A.A.; Ashford, D.; Thomas, J.R.; Evans, G.J.O. Multisite tyrosine phosphorylation of the N-terminus of Mint1/X11 α by Src kinase regulates the trafficking of amyloid precursor protein. *J. Neurochem.* **2016**, 137, 518–527. [[CrossRef](#)] [[PubMed](#)]
4. Miller, C.C.J.; McLoughlin, D.M.; Lau, K.-F.; Tennant, M.E.; Rogelj, B. The X11 proteins, A β production and Alzheimer's disease. *Trends Neurosci.* **2006**, 29, 280–285. [[CrossRef](#)] [[PubMed](#)]
5. Tamayev, R.; Zhou, D.; D'Adamio, L. The interactome of the amyloid β precursor protein family members is shaped by phosphorylation of their intracellular domains. *Mol. Neurodegener.* **2009**, 4, 28. [[CrossRef](#)] [[PubMed](#)]

6. Hoe, H.-S.; Tran, T.S.; Matsuoka, Y.; Howell, B.W.; Rebeck, G.W. DAB1 and Reelin Effects on Amyloid Precursor Protein and ApoE Receptor 2 Trafficking and Processing. *J. Biol. Chem.* **2006**, *281*, 35176–35185. [[CrossRef](#)] [[PubMed](#)]
7. Russo, C.; Dolcini, V.; Salis, S.; Venezia, V.; Zambrano, N.; Russo, T.; Schettini, G. Signal Transduction through Tyrosine-phosphorylated C-terminal Fragments of Amyloid Precursor Protein via an Enhanced Interaction with Shc/Grb2 Adaptor Proteins in Reactive Astrocytes of Alzheimer's Disease Brain. *J. Biol. Chem.* **2002**, *277*, 35282–35288. [[CrossRef](#)]
8. Tarr, P.E.; Roncarati, R.; Pelicci, G.; Pelicci, P.G.; D'Adamio, L. Tyrosine phosphorylation of the β -amyloid precursor protein cytoplasmic tail promotes interaction with Shc. *J. Biol. Chem.* **2002**, *277*, 16798–16804. [[CrossRef](#)]
9. Bukhari, H.; Glotzbach, A.; Kolbe, K.; Leonhardt, G.; Loosse, C.; Mueller, T. Small things matter: Implications of APP intracellular domain AICD nuclear signaling in the progression and pathogenesis of Alzheimer's disease. *Prog. Neurobiol.* **2017**, *156*, 189–213. [[CrossRef](#)]
10. Chang, K.-A.; Kim, H.-S.; Ha, T.-Y.; Ha, J.-W.; Shin, K.Y.; Jeong, Y.H.; Lee, J.-P.; Park, C.-H.; Kim, S.; Baik, T.-K.; et al. Phosphorylation of amyloid precursor protein (APP) at Thr668 regulates the nuclear translocation of the APP intracellular domain and induces neurodegeneration. *Mol. Cell. Biol.* **2006**, *26*, 4327–4338. [[CrossRef](#)]
11. Ando, K.; Iijima, K.-I.; Elliott, J.I.; Kirino, Y.; Suzuki, T. Phosphorylation-dependent regulation of the interaction of amyloid precursor protein with Fe65 affects the production of β -amyloid. *J. Biol. Chem.* **2001**, *276*, 40353–40361. [[CrossRef](#)] [[PubMed](#)]
12. Penke, B.; Bogar, F.; Paragi, G.; Gera, J.; Fulop, L. Key Peptides and Proteins in Alzheimer's Disease. *Curr. Protein Pept. Sci.* **2019**, *20*, 577–599. [[CrossRef](#)] [[PubMed](#)]
13. McLoughlin, D.M.; Miller, C.C.J. The FE65 proteins and Alzheimer's disease. *J. Neurosci. Res.* **2008**, *86*, 744–754. [[CrossRef](#)] [[PubMed](#)]
14. Sabo, S.L.; Ikin, A.F.; Buxbaum, J.D.; Greengard, P. The Alzheimer amyloid precursor protein (APP) and FE65, an APP-binding protein, regulate cell movement. *J. Cell Biol.* **2001**, *153*, 1403–1414. [[CrossRef](#)] [[PubMed](#)]
15. Sabo, S.L.; Ikin, A.F.; Buxbaum, J.D.; Greengard, P. The amyloid precursor protein and its regulatory protein, FE65, in growth cones and synapses in vitro and in vivo. *J. Neurosci.* **2003**, *23*, 5407–5415. [[CrossRef](#)] [[PubMed](#)]
16. Minopoli, G.; Gargiulo, A.; Parisi, S.; Russo, T. Fe65 matters: New light on an old molecule. *IUBMB Life* **2012**, *64*, 936–942. [[CrossRef](#)] [[PubMed](#)]
17. Santiard-Baron, D.; Langui, D.; Delehedde, M.; Delatour, B.; Schombert, B.; Touchet, N.; Tremp, G.; Paul, M.-F.; Blanchard, V.; Sergeant, N.; et al. Expression of human FE65 in amyloid precursor protein transgenic mice is associated with a reduction in β -amyloid load. *J. Neurochem.* **2005**, *93*, 330–338. [[CrossRef](#)] [[PubMed](#)]
18. Chang, Y.; Tesco, G.; Jeong, W.J.; Lindsley, L.; Eckman, E.A.; Eckman, C.B.; Tanzi, R.E.; Guenette, S.Y. Generation of the β -Amyloid Peptide and the Amyloid Precursor Protein C-terminal Fragment γ Are Potentiated by FE65L1. *J. Biol. Chem.* **2003**, *278*, 51100–51107. [[CrossRef](#)]
19. Guenette, S.Y.; Chen, J.; Ferland, A.; Haass, C.; Capell, A.; Tanzi, R.E. hFE65L influences amyloid precursor protein maturation and secretion. *J. Neurochem.* **1999**, *73*, 985–993. [[CrossRef](#)]
20. Sabo, S.L.; Lanier, L.M.; Ikin, A.F.; Khorkova, O.; Sahasrabudhe, S.; Greengard, P.; Buxbaum, J.D. Regulation of β -amyloid secretion by FE65, an amyloid protein precursor-binding protein. *J. Biol. Chem.* **1999**, *274*, 7952–7957. [[CrossRef](#)]
21. Tanahashi, H.; Tabira, T. Characterization of an amyloid precursor protein-binding protein Fe65L2 and its novel isoforms lacking phosphotyrosine-interaction domains. *Biochem. J.* **2002**, *367*, 687–695. [[CrossRef](#)] [[PubMed](#)]
22. Xie, Z.; Dong, Y.; Maeda, U.; Xia, W.; Tanzi, R.E. RNA Interference Silencing of the Adaptor Molecules ShcC and Fe65 Differentially Affect Amyloid Precursor Protein Processing and A β Generation. *J. Biol. Chem.* **2007**, *282*, 4318–4325. [[CrossRef](#)] [[PubMed](#)]
23. Suh, J.; Lyckman, A.; Wang, L.; Eckman, E.A.; Guenette, S.Y. FE65 proteins regulate NMDA receptor activation-induced amyloid precursor protein processing. *J. Neurochem.* **2011**, *119*, 377–388. [[CrossRef](#)] [[PubMed](#)]
24. Guenette, S.; Chang, Y.; Hiesberger, T.; Richardson, J.A.; Eckman, C.B.; Eckman, E.A.; Hammer, R.E.; Herz, J. Essential roles for the FE65 amyloid precursor protein-interacting proteins in brain development. *EMBO J.* **2006**, *25*, 420–431. [[CrossRef](#)] [[PubMed](#)]

25. Wang, B.; Hu, Q.; Hearn, M.G.; Shimizu, K.; Ware, C.B.; Liggitt, D.H.; Jin, L.-W.; Cool, B.H.; Storm, D.R.; Martin, G.M. Isoform-specific knockout of FE65 leads to impaired learning and memory. *J. Neurosci. Res.* **2004**, *75*, 12–24. [[CrossRef](#)]
26. Macias, M.J.; Hyvoenen, M.; Baraldi, E.; Schultz, J.; Sudol, M.; Saraste, M.; Oschkinat, H. Structure of the WW domain of a kinase-associated protein complexed with a proline-rich peptide. *Nature* **1996**, *382*, 646–649. [[CrossRef](#)] [[PubMed](#)]
27. Sudol, M.; Sliwa, K.; Russo, T. Functions of WW domains in the nucleus. *FEBS Lett.* **2001**, *490*, 190–195. [[CrossRef](#)]
28. Staub, O.; Rotin, D. WW domains. *Structure* **1996**, *4*, 495–499. [[CrossRef](#)]
29. Sudol, M.; Chen, H.I.; Bougeret, C.; Einbond, A.; Bork, P. Characterization of a novel protein-binding module—The WW domain. *FEBS Lett.* **1995**, *369*, 67–71. [[CrossRef](#)]
30. Kato, Y.; Ito, M.; Kawai, K.; Nagata, K.; Tanokura, M. Determinants of ligand specificity in groups I and IV WW domains as studied by surface plasmon resonance and model building. *J. Biol. Chem.* **2002**, *277*, 10173–10177. [[CrossRef](#)]
31. Lambrechts, A.; Kwiatkowski, A.V.; Lanier, L.M.; Bear, J.E.; Vandekerckhove, J.; Ampe, C.; Gertler, F.B. cAMP-dependent protein kinase phosphorylation of EVL, a Mena/VASP relative, regulates its interaction with actin and SH3 domains. *J. Biol. Chem.* **2000**, *275*, 36143–36151. [[CrossRef](#)] [[PubMed](#)]
32. Masin, M.; Kerschensteiner, D.; Duemke, K.; Rubio, M.E.; Soto, F. Fe65 Interacts with P2X2 Subunits at Excitatory Synapses and Modulates Receptor Function. *J. Biol. Chem.* **2006**, *281*, 4100–4108. [[CrossRef](#)] [[PubMed](#)]
33. Meiyappan, M.; Birrane, G.; Ladas, J.A.A. Structural Basis for Polyproline Recognition by the FE65 WW Domain. *J. Mol. Biol.* **2007**, *372*, 970–980. [[CrossRef](#)] [[PubMed](#)]
34. Telese, F.; Bruni, P.; Donizetti, A.; Gianni, D.; D'Ambrosio, C.; Scaloni, A.; Zambrano, N.; Rosenfeld, M.G.; Russo, T. Transcription regulation by the adaptor protein Fe65 and the nucleosome assembly factor SET. *EMBO Rep.* **2005**, *6*, 77–82. [[CrossRef](#)] [[PubMed](#)]
35. Ermekova, K.S.; Zambrano, N.; Linn, H.; Minopoli, G.; Gertler, F.; Russo, T.; Sudol, M. The WW domain of neural protein FE65 interacts with proline-rich motifs in Mena, the mammalian homolog of Drosophila enabled. *J. Biol. Chem.* **1997**, *272*, 32869–32877. [[CrossRef](#)]
36. Vargas, L.M.; Cerpa, W.; Munoz, F.J.; Zanlungo, S.; Alvarez, A.R. Amyloid- β oligomers synaptotoxicity: The emerging role of EphA4/c-Abl signaling in Alzheimer's disease. *Biochim. Biophys. Acta Mol. Basis Dis.* **2018**, *1864*, 1148–1159. [[CrossRef](#)]
37. Pastorino, L.; Sun, A.; Lu, P.-J.; Zhou, X.Z.; Balastik, M.; Finn, G.; Wulf, G.; Lim, J.; Li, S.-H.; Li, X.; et al. The prolyl isomerase Pin1 regulates amyloid precursor protein processing and amyloid- β production. *Nature* **2006**, *440*, 528–534. [[CrossRef](#)]
38. Liou, Y.-C.; Sun, A.; Ryo, A.; Zhou, X.Z.; Yu, Z.-X.; Huang, H.-K.; Uchida, T.; Bronson, R.; Bing, G.; Li, X.; et al. Role of the prolyl isomerase Pin1 in protecting against age-dependent neurodegeneration. *Nature* **2003**, *424*, 556–561. [[CrossRef](#)]
39. Maudsley, S.; Mattson, M.P. Protein twists and turns in Alzheimer disease. *Nat. Med.* **2006**, *12*, 392–393. [[CrossRef](#)]
40. Jankowsky, J.L.; Fadale, D.J.; Anderson, J.; Xu, G.M.; Gonzales, V.; Jenkins, N.A.; Copeland, N.G.; Lee, M.K.; Younkin, L.H.; Wagner, S.L.; et al. Mutant presenilins specifically elevate the levels of the 42 residue β -amyloid peptide in vivo: Evidence for augmentation of a 42-specific γ secretase. *Hum. Mol. Genet.* **2004**, *13*, 159–170. [[CrossRef](#)]
41. Lee, M.-S.; Kao, S.-C.; Lemere, C.A.; Xia, W.; Tseng, H.-C.; Zhou, Y.; Neve, R.; Ahljianian, M.K.; Tsai, L.-H. APP processing is regulated by cytoplasmic phosphorylation. *J. Cell Biol.* **2003**, *163*, 83–95. [[CrossRef](#)] [[PubMed](#)]
42. Shankar, G.M.; Li, S.; Mehta, T.H.; Garcia-Munoz, A.; Shepardson, N.E.; Smith, I.; Brett, F.M.; Farrell, M.A.; Rowan, M.J.; Lemere, C.A.; et al. Amyloid- β protein dimers isolated directly from Alzheimer's brains impair synaptic plasticity and memory. *Nat. Med.* **2008**, *14*, 837–842. [[CrossRef](#)] [[PubMed](#)]
43. Vanderstichele, H.; Van, K.E.; Hesse, C.; Davidsson, P.; Buyse, M.A.; Andreasen, N.; Minthon, L.; Wallin, A.; Blennow, K.; Vanmechelen, E. Standardization of measurement of β -amyloid_{1–42} in cerebrospinal fluid and plasma. *Amyloid* **2000**, *7*, 245–258. [[CrossRef](#)] [[PubMed](#)]

44. Mucke, L.; Masliah, E.; Yu, G.-Q.; Mallory, M.; Rockenstein, E.M.; Tatsuno, G.; Hu, K.; Kholodenko, D.; Johnson-Wood, K.; McConlogue, L. High-level neuronal expression of A β _{1–42} in wild-type human amyloid protein precursor transgenic mice: Synaptotoxicity without plaque formation. *J. Neurosci.* **2000**, *20*, 4050–4058. [[CrossRef](#)] [[PubMed](#)]
45. Baek, S.H.; Ohgi, K.A.; Rose, D.W.; Koo, E.H.; Glass, C.K.; Rosenfeld, M.G. Exchange of N-CoR corepressor and Tip60 coactivator complexes links gene expression by NF- κ B and β -amyloid precursor protein. *Cell* **2002**, *110*, 55–67. [[CrossRef](#)]
46. Delatour, B.; Mercken, L.; El Hachimi, K.H.; Colle, M.-A.; Pradier, L.; Duyckaerts, C. FE65 in Alzheimer's disease: Neuronal distribution and association with neurofibrillary tangles. *Am. J. Pathol.* **2001**, *158*, 1585–1591. [[CrossRef](#)]
47. Chen, D.; Liu, S.; Zhang, W.; Sun, L. Rational design of YAP WW1 domain-binding peptides to target TGF β /BMP/Smad-YAP interaction in heterotopic ossification. *J. Pept. Sci.* **2015**, *21*, 826–832. [[CrossRef](#)] [[PubMed](#)]
48. Rubini, C.; Ruzza, P.; Spaller, M.R.; Siligardi, G.; Hussain, R.; Udugamasooriya, D.G.; Bellanda, M.; Mammi, S.; Borgogno, A.; Calderan, A.; et al. Recognition of lysine-rich peptide ligands by murine cortactin SH3 domain: CD, ITC, and NMR studies. *Biopolymers* **2010**, *94*, 298–306. [[CrossRef](#)]
49. Sudol, M.; Hunter, T. New wrinkles for an old domain. *Cell* **2000**, *103*, 1001–1004. [[CrossRef](#)]
50. Lacor, P.N.; Buniel, M.C.; Chang, L.; Fernandez, S.J.; Gong, Y.; Viola, K.L.; Lambert, M.P.; Velasco, P.T.; Bigio, E.H.; Finch, C.E.; et al. Synaptic targeting by Alzheimer's-related amyloid β oligomers. *J. Neurosci.* **2004**, *24*, 10191–10200. [[CrossRef](#)]
51. Wei, W.; Nguyen, L.N.; Kessels, H.W.; Hagiwara, H.; Sisodia, S.; Malinow, R. Amyloid beta from axons and dendrites reduces local spine number and plasticity. *Nat. Neurosci.* **2010**, *13*, 190–196. [[CrossRef](#)] [[PubMed](#)]
52. Cao, X.; Suedhof, T.C. Dissection of Amyloid- β Precursor Protein-dependent Transcriptional Transactivation. *J. Biol. Chem.* **2004**, *279*, 24601–24611. [[CrossRef](#)] [[PubMed](#)]
53. Feilen, L.P.; Haubrich, K.; Stier, G.; Sinning, I.; Wild, K.; Haubrich, K.; Simon, B.; Strecker, P.; Eggert, S.; Kins, S.; et al. Fe65-PTB2 Dimerization Mimics Fe65-APP Interaction. *Front. Mol. Neurosci.* **2017**, *10*, 140. [[CrossRef](#)] [[PubMed](#)]
54. Borbely, E.; Horvath, J.; Furdan, S.; Bozso, Z.; Penke, B.; Fulop, L. Simultaneous changes of spatial memory and spine density after intrahippocampal administration of fibrillar A β _{1–42} to the rat brain. *BioMed Res. Int.* **2014**, *2014*, 345305. [[CrossRef](#)] [[PubMed](#)]
55. Nagy, D.; Kocsis, K.; Fuzik, J.; Marosi, M.; Kis, Z.; Teichberg, V.I.; Toldi, J.; Farkas, T. Kainate postconditioning restores LTP in ischemic hippocampal CA1: Onset-dependent second pathophysiological stress. *Neuropharmacology* **2011**, *61*, 1026–1032. [[CrossRef](#)] [[PubMed](#)]






© 2019 by the authors. Licensee MDPI, Basel, Switzerland. This article is an open access article distributed under the terms and conditions of the Creative Commons Attribution (CC BY) license (<http://creativecommons.org/licenses/by/4.0/>).



Article

Examination of Longitudinal Alterations in Alzheimer's Disease-Related Neurogenesis in an APP/PS1 Transgenic Mouse Model, and the Effects of P33, a Putative Neuroprotective Agent Thereon

Titanilla Szögi ^{1,†} , Emőke Borbély ^{1,†}, Ildikó Schuster ¹, Zsolt Bozsó ¹ , Miklós Sántha ², Melinda E. Tóth ², Botond Penke ¹ and Livia Fülöp ^{1,*} 

¹ Department of Medical Chemistry, University of Szeged, Dóm tér 8, H-6720 Szeged, Hungary

² Institute of Biochemistry, Biological Research Centre, Temesvári Krt. 62., H-6726 Szeged, Hungary

* Correspondence: fulop.livia@med.u-szeged.hu; Tel.: +36-62-545-698

† These authors contributed equally to this work.

Abstract: Neurogenesis plays a crucial role in cognitive processes. During aging and in Alzheimer's disease (AD), altered neurogenesis and neuroinflammation are evident both in C57BL/6J, APP_{Swe}/PS1_{ΔE9} (Tg) mice and humans. AD pathology may slow down upon drug treatment, for example, in a previous study of our group P33, a putative neuroprotective agent was found to exert advantageous effects on the elevated levels of APP, Aβ, and neuroinflammation. In the present study, we aimed to examine longitudinal alterations in neurogenesis, neuroinflammation and AD pathology in a transgenic (Tg) mouse model, and assessed the putative beneficial effects of long-term P33 treatment on AD-specific neurological alterations. Hippocampal cell proliferation and differentiation were significantly reduced between 8 and 12 months of age. Regarding neuroinflammation, significantly elevated astrogliosis and microglial activation were observed in 6- to 7-month-old Tg animals. The amounts of the molecules involved in the amyloidogenic pathway were altered from 4 months of age in Tg animals. P33-treatment led to significantly increased neurogenesis in 9-month-old animals. Our data support the hypothesis that altered neurogenesis may be a consequence of AD pathology. Based on our findings in the transgenic animal model, early pharmacological treatment before the manifestation of AD symptoms might ameliorate neurological decline.

Keywords: Alzheimer's disease; neurogenesis; neuroinflammation; P33; APP/PS1 mice



Citation: Szögi, T.; Borbély, E.; Schuster, I.; Bozsó, Z.; Sántha, M.; Tóth, M.E.; Penke, B.; Fülöp, L. Examination of Longitudinal Alterations in Alzheimer's Disease-Related Neurogenesis in an APP/PS1 Transgenic Mouse Model, and the Effects of P33, a Putative Neuroprotective Agent Thereon. *Int. J. Mol. Sci.* **2022**, *23*, 10364. <https://doi.org/10.3390/ijms231810364>

Academic Editor: Timofey S. Rozhdestvensky

Received: 25 August 2022

Accepted: 5 September 2022

Published: 8 September 2022

Publisher's Note: MDPI stays neutral with regard to jurisdictional claims in published maps and institutional affiliations.



Copyright: © 2022 by the authors. Licensee MDPI, Basel, Switzerland. This article is an open access article distributed under the terms and conditions of the Creative Commons Attribution (CC BY) license (<https://creativecommons.org/licenses/by/4.0/>).

1. Introduction

In mammals, including humans, neurogenesis occurs throughout life. In adulthood, neuronal cell formation is present in the subventricular zone (SVZ) of the lateral ventricles and in the subgranular zone (SGZ) of the dentate gyrus (DG) within the hippocampus (HC) [1]. In both neurogenic niches, new cells are formed via mitosis from neural stem cells (NSCs), generating neural progenitor cells (NPCs) [2–5]. Some of the NPCs can migrate, proliferate and differentiate into neurons or glial cells, and these new cells can integrate into the circuitry of the olfactory bulb and the granular cell layer (GCL) of the DG, but a large proportion of these cells die by apoptosis early in their life cycle. Furthermore, both intrinsic modulators (signal transduction pathways, metabolic factors, hormonal stage, epigenetic factors as well as immune and vascular systems) and extrinsic factors (stress, drug and alcohol abuse, aging, physical activity, learning and environmental enrichments) affect the proliferation, differentiation, as well as the morphological and physiological maturation, fate determination and the survival of these new cells [5–14].

Adult hippocampal neurogenesis is essential for memory and learning processes. The extent of neurogenesis declines with age, and this is also made evident in neurodegenerative disorders such as Alzheimer's disease (AD) [9,11,13,15–17]. AD is characterized

by cognitive deficits, memory loss, altered neurogenesis and neuroinflammation. The familiar form of AD (FAD) is caused by mutations in genes that encode the amyloid- β protein precursor (APP), presenilin-1 (PS1) and presenilin-2 (PS2). In AD, APP can undergo several enzymatic cleavages by secretases. The metabolites produced in the amyloidogenic pathway (such as soluble APP (sAPP) and C99, the latter including APP's intracellular domain (AICD) and amyloid- β (A β)), as well as those produced in the non-amyloidogenic pathway (sAPP α and C83, the latter including AICD and p3) have significant roles in the process of neurogenesis [9,14,17–21]. PS1 regulates the differentiation of NPCs. Furthermore, PS1 is the catalytic core of γ -secretase, which cleaves APP [9,13,14,17,18]. SAPP α is assumed to have neuroprotective effects: it presumably protects neurons, promotes neurogenesis and neurite outgrowth, thus modulating the proliferation and survival of NPCs [9,13,14,18–20,22,23]. A β may exert a negative effect on adult neurogenesis, as studies suggest a strong correlation between amyloidosis, A β deposition and impaired neurogenesis [16,18,19,22,24,25]. Declining neurogenesis may serve as a hallmark of AD pathology. It is also debated whether impaired neurogenesis is a contributing factor or a consequence of AD [26,27].

A β depositions and plaques are associated with neuroinflammation in AD. Microglia and astrocytes play a crucial role in AD pathology. In the early phase of the disease, microglia and astrocytes are activated and clustered around the plaques to promote A β clearance, thus slowing the progression of AD [13,22,28–30]. In more advanced stages, the chronic activation of microglia and astrocytes turns disadvantageous, as they lead to the constant overproduction of inflammatory mediators, resulting in prolonged neuroinflammation. Activated microglia have a negative effect on neurogenesis as well [13]. Studies showed that the induction of inflammation processes by bacterial lipopolysaccharide (LPS) reduced the amount of BrdU+ and DCX+ cells and increased the number of microglia in DG [31–33]. Others reported that intracerebroventricular (ICV) injections of streptozotocin (STZ) significantly decreased the number of BrdU+ and DCX+ cells and increased neuroinflammation in DG [34,35]. These findings support the connection between neuroinflammation and decreased neurogenesis in AD models. Microglia and astrocytes may serve as early biomarkers of AD, and the elements of the inflammatory system might serve as potential therapeutic targets against the disease [13,28–30,36].

The protein Fe65, which is also known as amyloid beta A4 precursor protein-binding family B member 1 (APBB1), belongs to a family of multidomain adaptor proteins. It plays a crucial role in APP processing and trafficking, A β production, synapse formation, synaptic plasticity and in the learning process [37–41]. Transcriptionally active AICD is produced during the amyloidogenic pathway only, and can bind to Fe65 and co-binds to Tip60, forming a protein complex [37,40,41]. The complex translocates to the nucleus, where it regulates the expression of various genes (APP, BACE1, ADAM10 and GSK3 β), and thereby inhibits proliferation [20,42–46]. In a study, overexpressed AICD bound to Fe65 negatively influenced neurogenesis in the FeC γ 25 mouse strain (which co-expressed AICD and human Fe65), and the number of BrdU+ and DCX+ cells were significantly reduced as well [47]. Another study demonstrated that TAG1, the functional ligand of APP, supported AICD release, and neurogenesis was negatively regulated by Fe65 via the TAG1-APP pathway [48]. In our previous study, the peptide P33 (synthesized in-house) was also found to bind to Fe65. We have demonstrated that P33/Fe65 binding decreased the quantity of the Fe65/APP complex, leading to altered APP processing and thereby diminished A β production. Moreover, we have revealed that P33 treatment has a favorable effect on memory functions, learning ability and ameliorates inflammatory processes in 9-month-old APP_{Swe}/PS1_{dE9} mice [49].

Several transgenic mouse strains were generated to model FAD and investigate the development of AD pathology [8,12,16,50]. Among these, the APP_{Swe}/PS1_{dE9} (APP/PS1, Tg) model is a transgenic animal strain demonstrating A β pathology with histological features similar to those found in humans [16,25,26,43,51,52]. The APP_{Swe}/PS1_{dE9} line harbors two mutations, whereby these animals overexpress the chimeric mouse/human

amyloid precursor protein (Mo/HuAPP695_{Swe}) with a Swedish mutation (K595N/M596L), and a human presenilin-1 with a deletion of exon 9 (PS1_{ΔE9}) [53,54]. Although several papers discuss the alteration of neurogenesis in the APP_{Swe}/PS1_{ΔE9} strain, to the best of our knowledge, none of these studies have examined the progression of neurogenesis and gliosis throughout the lifespan of these transgenic animals.

In our current study, APP_{Swe}/PS1_{ΔE9} transgenic and C57BL/6J control mice were examined by histological methods from 1 to 12 months and at 18 months of age. Temporal changes in hippocampal neurogenesis, regarding both proliferation and differentiation processes, followed. In parallel, the activation of microglia and astrocytes was also assessed. Besides the age-related changes in the levels of APP, the soluble oligomeric forms of Aβ₁₋₄₂, C99/C83 ratio and the density of Aβ plaques were also measured. Based on these findings, a related study using 3-month-old APP/PS1 mice was executed to examine the effects of long-term (6-month) treatment with P33 on hippocampal neurogenesis associated with APP-Aβ pathology in this AD model.

2. Results

2.1. Hippocampal Neurogenesis Is Impaired by Aging in APP/PS1 and Wild-Type Mice

To characterize the first stage of neurogenesis, we stained dividing stem cells with 5-Bromo-2'-Deoxyuridine (BrdU) [55]. In the first month of life, the number of BrdU+ cells increased in both the Tg and WT groups, while between months 2 and 7 no significant between-group differences in cell proliferation were detected. From months 8 to 12, significant reductions in the number of BrdU+ cells were revealed in APP/PS1 mice compared to age-matched WT controls (Figure 1A, independent sample *t*-test: $t_8 = 2.529$ $p = 0.039$, $t_8 = 2.961$ $p = 0.018$, $t_8 = 2.329$ $p = 0.048$, $t_8 = 2.843$ $p = 0.022$, $t_8 = 2.533$ $p = 0.044$, 8 to 12 months, respectively). At 18 months of age, no significant differences in BrdU+ cell density were detected between the groups ($t_8 = -0.545$ $p = 0.601$). Along with aging, the number of BrdU+ cells continuously declined both in APP/PS1 and WT mice. A remarkably low density of stem cells (<5 number/mm²) was detected from the eighth month of life in all age groups. For representative images, see Supplement (Figure S1A).

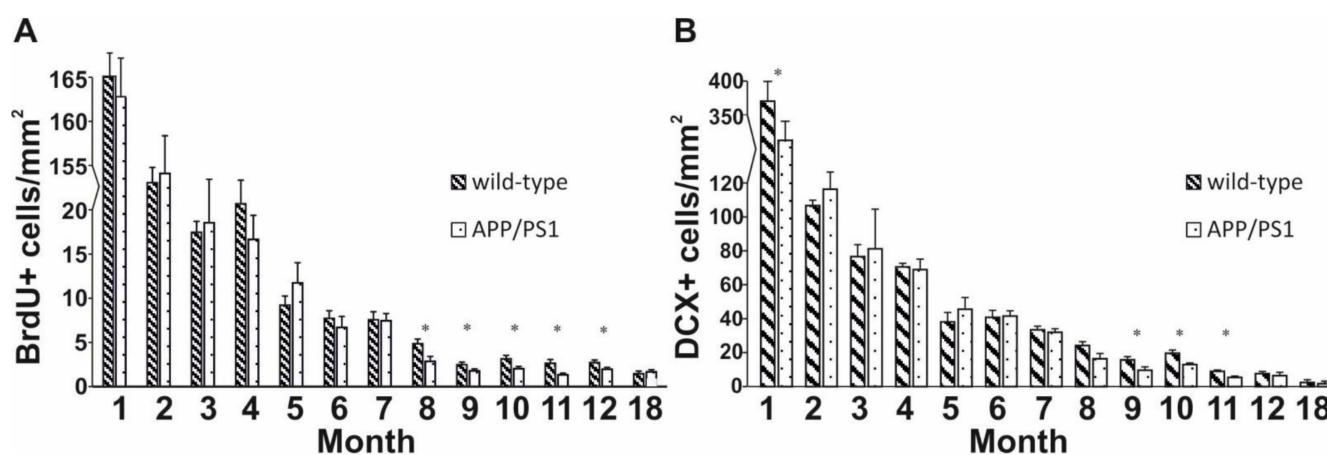


Figure 1. Quantitative results for BrdU and DCX stainings in the dentate gyrus. (A) Significant differences were observed among the groups from 8 to 12 months of age: transgenic mice had significantly fewer BrdU+ stem cells than controls. (B) DCX+ cells of the DG were analyzed in wild-type and APP/PS1 mice every month. Independent *t*-tests revealed significant differences in the 9-, 10- and 11-month-old age groups. Data represent mean \pm SEM * indicates a significant between-group difference ($p < 0.05$).

To examine the process of differentiation during adult neurogenesis, we labelled immature neurons with a doublecortin (DCX) antibody [55]. The same pattern as the one observed in the longitudinal examination of stem cells was detected: a continuous decrease

in differentiating cells was evident along with aging. In the first month of life, a prominent cell density was detected in both groups. Moreover, at 1 month of age a significant difference in the densities of immature neurons was detected between transgenic and control mice (Figure 1B, independent sample *t*-test: $t_8 = 2.330$ $p = 0.048$). However, from months 2 to 8, no significant differences were observed between the groups. In the 9- to 11-month-old age groups, a significant reduction in the densities of immature neurons was evident in transgenic mice compared to WT animals (independent sample *t*-test: $t_8 = 3.103$ $p = 0.021$, $t_8 = 3.138$ $p = 0.014$, $t_8 = 2.947$ $p = 0.022$, 9 to 11 months, respectively). Exceptionally low densities (<3 number/mm²) were detected in 12- and 18-month-old animals, but at these ages cell densities did not differ considerably between the transgenic and WT groups (independent sample *t*-test: $t_8 = 0.538$ $p = 0.610$, $t_8 = 0.511$ $p = 0.623$, 12 and 18 months, respectively). For representative images, see Supplement (Figure S1B).

The immunohistochemical analysis of neuronal nuclear marker (NeuN) did not confirm any significant differences in cell densities between Tg and WT mice at any age (Supplementary Figure S2).

2.2. Neuroinflammation Increases with Age in APP/PS1 Mice

To investigate reactive astrocytes which contribute to the neuroinflammatory cascade, we employed GFAP staining. During the first five months of life, there were no significant differences between the groups. In contrast, 6- to 12-month-old APP/PS1 mice were characterized by significantly higher GFAP+ cell densities compared to controls (Figure 2A, independent sample *t*-test: $t_8 = -2.802$ $p = 0.026$, $t_8 = -5.441$ $p < 0.001$, $t_8 = -4.554$ $p = 0.003$, $t_8 = -3.470$ $p = 0.010$, $t_8 = -3.832$ $p = 0.006$, $t_8 = -2.512$ $p = 0.040$, $t_8 = -2.626$ $p = 0.039$, 6 to 12 months, respectively). However, once again, the densities of GFAP+ cells were similar in the 18-month-old Tg and WT groups (independent sample *t*-test: $t_8 = 0.176$ $p = 0.605$). For representative images, see Supplement (Figure S3A).

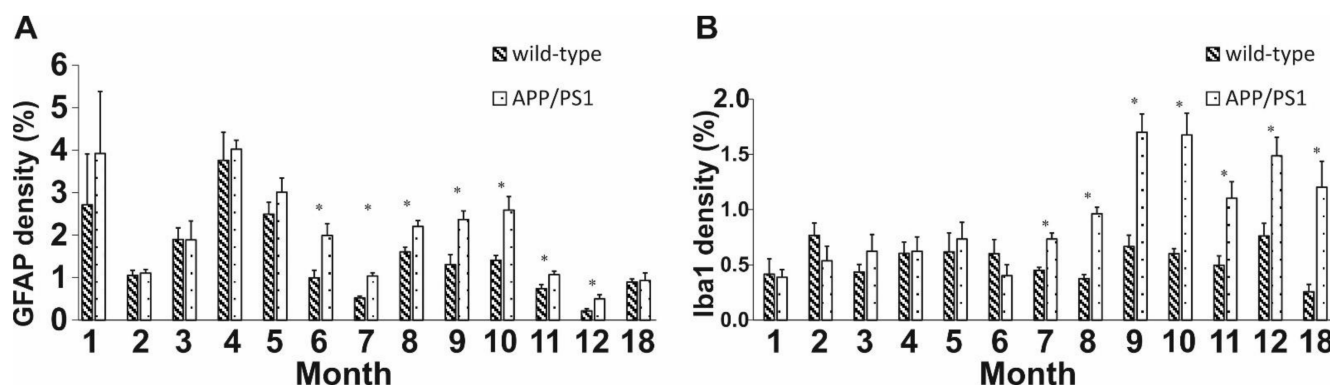


Figure 2. Quantitative results for GFAP and Iba1 stainings in DG. (A) Significant differences in the activation of reactive astrocytes were detected between 5- to 11-month-old APP/PS1 mice and age-matched controls. (B) Longitudinal alternations of microglial activation in DG. The densities of activated microglia of 7- to 18-month-old Tg mice were significantly higher compared to controls. Data represent mean \pm SEM * indicates a significant between-group difference ($p < 0.05$).

To detect activated microglia involved in A β clearance and the restoration of a normal brain environment, an Iba1 antibody was used. From 1 to 6 months of age, no differences were observed between the WT and Tg groups. However, the densities of Iba1+ cells increased drastically from 7 to 12 months and at 18 months of age in transgenic mice compared to the WT control (Figure 2B, independent sample *t*-test: $t_8 = -4.743$ $p < 0.001$, $t_8 = -8.572$ $p < 0.001$, $t_8 = -4.983$ $p = 0.002$, $t_8 = -5.315$ $p < 0.001$, $t_8 = -7.518$ $p = 0.008$, $t_8 = -3.565$ $p = 0.012$, $t_8 = 0.003$ $p = 0.013$, 7 to 12 and 18 months, respectively). For representative images, see Supplement (Figure S3B).

2.3. Age-Related Modulation of APP Processing Pathways in APP/PS1 Mice

To assess the association between neurogenesis and the development of AD, we examined the changes in APP processing pathways by analyzing the level of APP, the C99/C83 ratio by Western blot (WB), the quantity of soluble $A\beta_{1-42}$ by enzyme-linked immunosorbent assay (ELISA) and the $A\beta$ plaque density by immunohistochemical analyses.

The amount of APP may be an early biomarker of AD [23,56–58]. The APP level was elevated in Tg mice from 1 to 4 months of age, while it decreased between months 5 and 18 (one-way ANOVA $F = 18.279$, $p < 0.001$; Fisher's LSD post hoc tests: 1st month: $p_4 = 0.008$; $p_5 < 0.001$; $p_6 < 0.001$; $p_7 < 0.001$; $p_8 = 0.002$; $p_9 < 0.001$; $p_{12} < 0.001$; $p_{18} < 0.001$; second month: $p_5 < 0.001$; $p_6 < 0.001$; $p_7 < 0.001$; $p_8 < 0.001$; $p_9 < 0.001$; $p_{12} < 0.001$; $p_{18} < 0.001$; third month: $p_5 < 0.001$; $p_6 < 0.001$; $p_7 < 0.001$; $p_8 < 0.001$; $p_9 < 0.001$; $p_{12} < 0.001$; $p_{18} < 0.001$; fourth month: $p_1 = 0.008$; $p_5 < 0.001$; $p_6 < 0.001$; $p_7 < 0.001$; $p_8 < 0.001$; $p_9 < 0.001$; $p_{12} < 0.001$; $p_{18} < 0.001$) (Figure 3A).

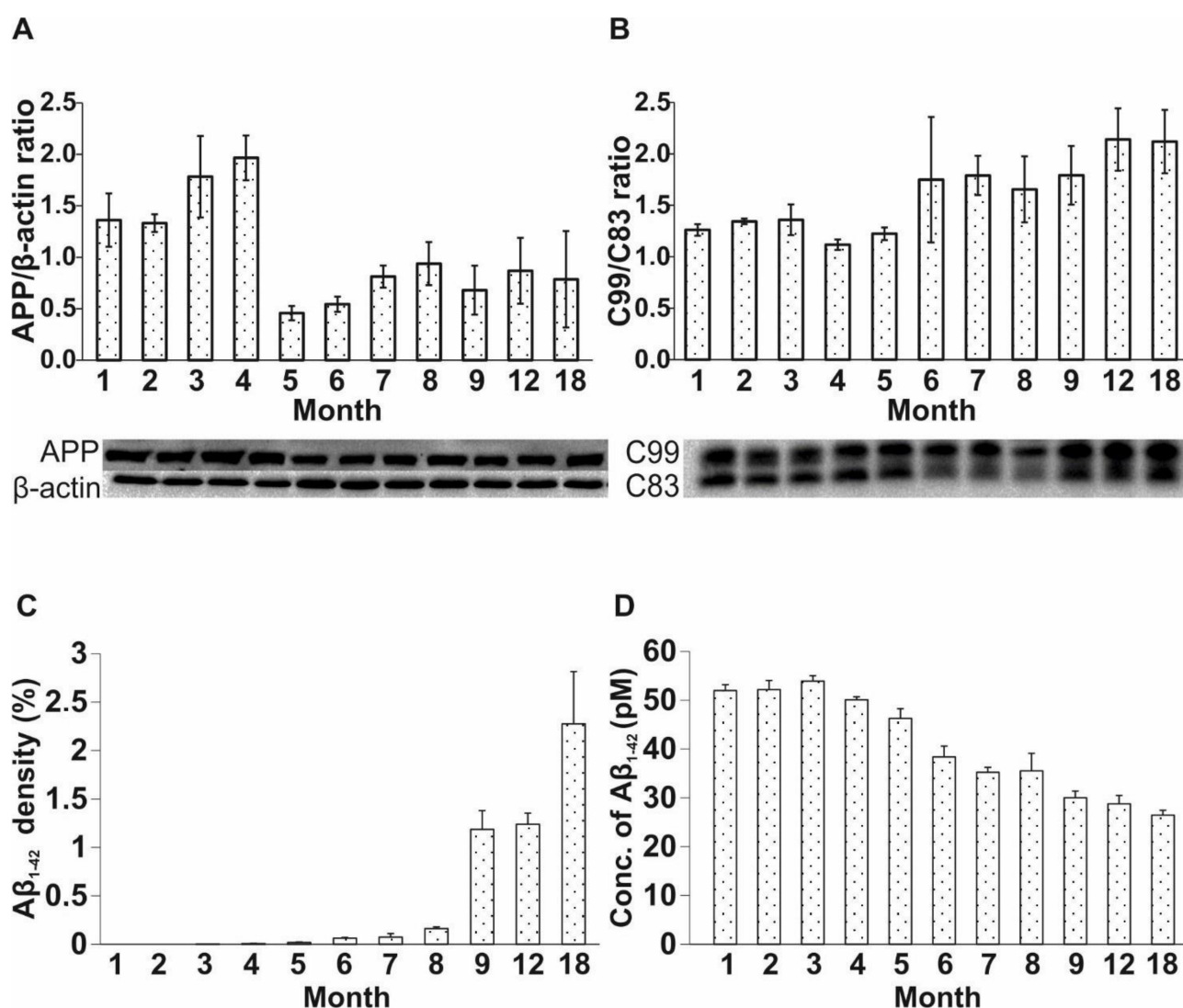


Figure 3. Measurement of APP, C99/C83 ratio by WB, soluble $A\beta_{1-42}$ by ELISA and plaque density by immunohistochemistry. (A) APP level was elevated in APP/PS1 animals from months 1 to 4, then decreased in 5- to 18-month-old mice. (B) C99/C83 ratio was elevated in Tg animals, starting from 5 months of age. (C) $A\beta$ plaques appeared in APP/PS1 mice at 4 months of age. (D) The concentration of soluble $A\beta_{1-42}$ decreased in APP/PS1 mice in the 5- to 18-month-old age groups. Data represent mean \pm SEM.

C83 is produced during the non-amyloidogenic processing of APP, while C99 is formed along the amyloidogenic pathway. Thus, the C99/C83 ratio represents the enzymatically regulated balance between these two pathways. During the first five months of age, no difference in the C99/C83 ratio was detected between the groups. From months 6 to 18, an appreciable difference in the C99/C83 ratio became evident for the APP/PS1 group, suggesting an incipient predominance of the amyloidogenic pathway from the sixth month (one-way ANOVA $F = 11.499$, $p < 0.001$; Fisher's LSD post hoc tests: first month: $p_6 < 0.001$; $p_7 < 0.001$; $p_8 = 0.013$; $p_9 < 0.001$; $p_{12} < 0.001$; $p_{18} < 0.001$; second month: $p_6 < 0.001$; $p_7 = 0.004$; $p_8 = 0.040$; $p_9 < 0.001$; $p_{12} < 0.001$; $p_{18} < 0.001$; third month: $p_6 < 0.001$; $p_7 = 0.003$; $p_8 = 0.033$; $p_9 < 0.001$; $p_{12} < 0.001$; $p_{18} < 0.001$; fourth month: $p_6 < 0.001$; $p_7 < 0.001$; $p_8 < 0.001$; $p_9 < 0.001$; $p_{12} < 0.001$; $p_{18} < 0.001$; fifth month: $p_6 < 0.001$; $p_7 < 0.001$; $p_8 = 0.003$; $p_9 < 0.001$; $p_{12} < 0.001$; $p_{18} < 0.001$) (Figure 3B).

The density of A β plaques may correlate with the development of AD in Tg mice. In our experiment, the plaques appeared in the cortical and hippocampal regions in 4-month-old APP/PS1 mice. The amount of A β plaques progressively increased with age (one-way ANOVA $F = 7.336$, $p < 0.001$; Fisher's LSD post hoc tests: first month: $p_9 = 0.015$; $p_{12} = 0.019$; $p_{18} < 0.001$; second month: $p_9 = 0.015$; $p_{12} = 0.019$; $p_{18} < 0.001$; third month: $p_9 = 0.015$; $p_{12} = 0.019$; $p_{18} < 0.001$; fourth month: $p_9 = 0.016$; $p_{12} = 0.020$; $p_{18} < 0.001$; fifth month: $p_9 = 0.017$; $p_{12} = 0.021$; $p_{18} < 0.001$; sixth month: $p_9 = 0.020$; $p_{12} = 0.025$; $p_{18} < 0.001$; seventh month: $p_9 = 0.022$; $p_{12} = 0.026$; $p_{18} < 0.001$; eighth month: $p_9 = 0.032$; $p_{12} = 0.038$; $p_{18} < 0.001$) (Figure 3C). For representative images, see Supplement (Figure S4).

In parallel with the immunohistochemical studies, we examined age-related changes in the levels of soluble A β_{1-42} in APP/PS1 mice, using a commercially available ELISA kit. Elevated levels of soluble A β_{1-42} were detected in the first 4 months of life, whereas the amount of soluble A β_{1-42} strongly decreased in 5- to 18-month-old mice (one-way ANOVA $F = 318.481$, $p < 0.001$; Fisher's LSD post hoc tests: first month: $p_3 = 0.002$; $p_5 < 0.001$; $p_6 < 0.001$; $p_7 < 0.001$; $p_8 < 0.001$; $p_9 < 0.001$; $p_{12} < 0.001$; $p_{18} < 0.001$; second month: $p_4 = 0.002$; $p_5 < 0.001$; $p_6 < 0.001$; $p_7 < 0.001$; $p_8 < 0.001$; $p_9 < 0.001$; $p_{12} < 0.001$; $p_{18} < 0.001$; third month: $p_1 = 0.002$; $p_4 < 0.001$; $p_5 < 0.001$; $p_6 < 0.001$; $p_7 < 0.001$; $p_8 < 0.001$; $p_9 < 0.001$; $p_{12} < 0.001$; $p_{18} < 0.001$; fourth month: $p_2 < 0.001$; $p_3 < 0.001$; $p_4 < 0.001$; $p_5 < 0.001$; $p_6 < 0.001$; $p_7 < 0.001$; $p_8 < 0.001$; $p_9 < 0.001$; $p_{12} < 0.001$; $p_{18} < 0.001$) (Figure 3D).

2.4. Elongated Treatment with Pentapeptide P33 Improves Neurogenesis in APP/PS1 Mice

Our previous research indicated that P33-treatment had a beneficial effect on memory, learning abilities and inflammatory processes in APP/PS1 animals [49]. Thus, in a separate experiment, we assessed the effect of elongated P33-treatment on the formation of dividing stem cells and immature neurons in APP/PS1 mice, between 3 and 9 months of age. The WT and APP/PS1 animals were divided into four groups (WT vehicle-treated (physiological saline), WT P33-treated, APP/PS1 vehicle-treated and APP/PS1 P33-treated), and the effects of 6 months of P33 treatment on neurogenesis was examined by monitoring two key markers, namely BrdU and DCX. BrdU+ cell density was found to be significantly lower in vehicle-treated APP/PS1 mice compared to the WT-vehicle and WT-P33 groups (Figure 4A, one-way ANOVA $F = 3.845$, $p = 0.026$; Fisher's LSD post hoc tests: APP/PS1-vehicle vs. WT-vehicle $p = 0.030$, vs. WT-P33 $p = 0.008$). In contrast, the density of BrdU+ cells increased in the APP/PS1-P33 group compared to the APP/PS1-vehicle control ($p = 0.009$).

We also measured the density of immature cells in all animal groups. The density of DCX+ cells in vehicle-treated APP/PS1 mice was significantly lower compared to the WT-vehicle and WT-P33 groups (Figure 4B, one-way ANOVA $F = 8.939$, $p < 0.001$; Fisher's LSD post hoc tests: APP/PS1-vehicle vs. WT-vehicle $p = 0.028$, vs. WT-P33 $p < 0.001$). Treatment with P33 enhanced the density of immature cells in APP/PS1-P33 mice compared to the vehicle-treated APP/PS1 controls ($p < 0.001$). For representative images, see Supplement (Figure S5).

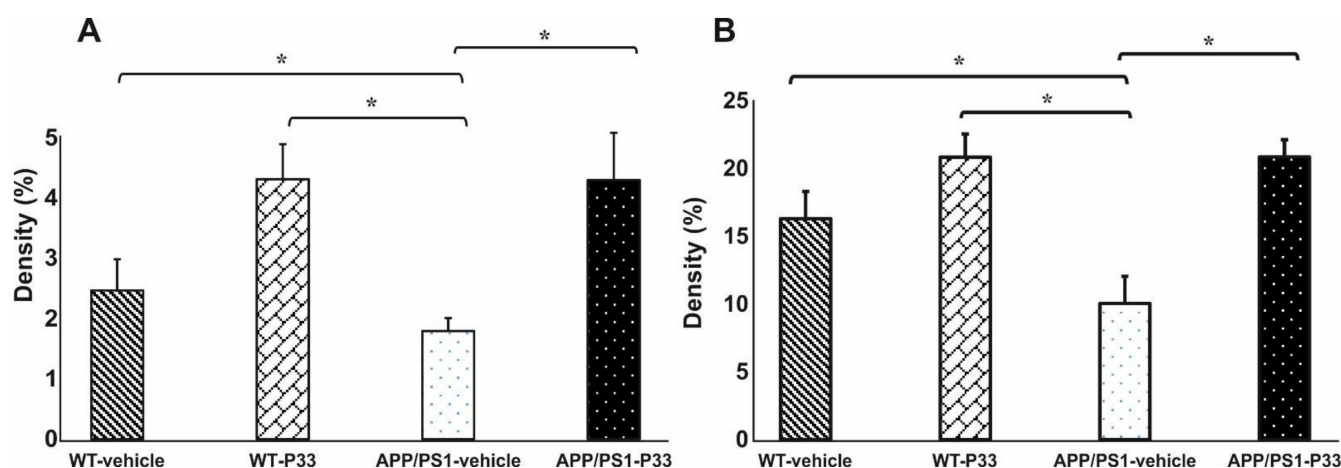


Figure 4. Quantitative results for BrdU and DCX stainings in DG of the animals. **(A)** Significant differences were observed among the groups in the densities of dividing cells ($p = 0.026$). Decreased BrdU+ cell density was detected in the vehicle-treated APP/PS1 group compared to the WT-vehicle ($p = 0.030$), the WT-P33 ($p = 0.008$) and the APP/PS1-P33 groups ($p = 0.009$). **(B)** Results for DCX immunostaining. A significantly lower level of immature neuron density ($p < 0.001$) was detected in vehicle-treated APP/PS1 mice compared to all other groups (vs. WT-vehicle: $p = 0.028$, vs. WT-P33: $p < 0.001$, vs. APP/PS1-P33: $p < 0.001$). Data represent mean \pm SEM * indicates a significant difference ($p < 0.05$).

3. Discussion

It is widely accepted that neurogenesis plays an important role in the development and maintenance of memory and learning functions [59–61]. Previous experiments have shown that neurogenesis declines during normal aging, as well as in neurodegenerative diseases, including AD [13,15,62].

To the best of our knowledge, we are the first group to study the long-term associations between neurogenesis, neuroinflammation and AD in a transgenic mouse model of AD, using 1- to 12- and 18-month-old wild-type (C57BL/6J) and APP/PS1 transgenic mice. In addition, long-term (6-month) treatment with a peptide-like neuromodulator agent (P33, designed and synthesized in-house) was tested in APP/PS1 animals, starting at 3 months of age, in order to investigate its effect on neurogenesis.

We aimed to compare the processes of hippocampal neurogenesis and neuroinflammation in C57BL/6J vs. APP/PS1 mice, to evaluate their relationship with age and AD-like pathology. Our further goal was to investigate the effect of P33 on neurogenesis in both mouse strains, as this agent has previously been demonstrated to be effective against neuroinflammation induced by A β pathology in our former study [49].

Studies report that signs of decreased adult hippocampal neurogenesis are evident in AD, which may cause cognitive dysfunction. Mapping the molecular processes involved in altered neurogenesis would be essential to clarify whether it precedes the characteristic appearance of AD pathology, or rather if it is a consequence of that [13,22,63]. To elucidate this issue, many groups have investigated the relationship between AD and neurogenesis in several FAD transgenic models; however, published studies have yielded controversial results (Table 1). Both an increase [64–67] and a decrease [25,26,52,68–72] in the levels of DG markers typical of adult neurogenesis are reported for AD. These discrepancies are likely to be explained by different experimental designs, such as utilizing different mouse models and different time scales for the examination of neurogenesis and AD, as well as a variety of selected neurogenesis markers tested.

Table 1. Age-related pathological changes in APP/PS1 mice. Comparison table of our findings to literature data. L: lower than WT or low concentration, L-S: significantly lower than WT, H: higher than WT or high concentration H-S: significantly higher than WT, NC: no change in group difference, -: disappearance, +: appearance, NA: data not available, Ref.: references.

Markers		Age (Months)																
		1	2	3	4	5	6	7	8	9	10	11	12	13	14	15	18	Ref.
BrdU	Our study	L	H	H	L	H	L	L	L-S	L-S	L-S	L-S	L-S	NA	NA	NA	H	[25,26,36,52,69,73]
	Ref.	NA	L-S [26]	L-S [36,69,73]	NA	L-S [69], L [52]	NA	NA	NA	L-S [25,52]	L-S [69]	NA	NA	NA	NA	L [69]	NA	
DCX	Our study	L-S	H	H	L	H	H	L	L	L-S	L-S	L-S	L	NA	NA	NA	L	[26,36,52,69,73]
	Ref.	NA	L-S [26]	H [69,73], L-S [36]	NA	L [69], H [52]	L-S [36]	NA	NA	L-S [52]	L-S [36,69], L [73]	NA	L-S [36]	H [73]	NA	L-S [69]	NA	
NeuN	Our study	NC	NC	NC	NC	NC	NC	NC	NC	NC	NC	NC	NC	NA	NA	NA	NC	[36,74]
	Ref.	NA	NA	NA	NA	NA	NA	NA	NA	NA	NA	NC [74]	NA	NC [36]	NA	NA	NA	
GFAP	Our study	H	H	L	H	H	H-S	H-S	H-S	H-S	H-S	H-S	H-S	NA	NA	NA	H	[36,74]
	Ref.	NA	NA	L [36]	NA	NA	H-S [36]	NA	NA	NA	H-S [36,74]	NA	H-S [36]	NA	NA	NA	NA	
Iba1	Our study	L	L	H	H	L	H	H-S	H-S	H-S	H-S	H-S	H-S	NA	NA	NA	H-S	[36,73,74]
	Ref.	NA	NA	H [73], L [36]	NA	NA	H-S [36]	NA	NA	NA	H-S [36,74]	NA	H-S [36]	NA	NA	NA	NA	
Aβ plaque	Our study	-	-	-	+	+	+	+	+	+	+	NA	NA	+	NA	NA	+	[25,29,36,52,69,73,74]
	Ref.	NA	NA	- [36], + [29], + [69]	+	[73]	+	[52,69]	+	[36]	+	[52]	NA	+	[25,52]	+	[36,69,73,74]	
soluble Aβ	Our study	+	+	+	+	-	-	-	-	-	-	NA	NA	-	NA	NA	-	[26,52,69]
	Ref.	NA	+	[26]	NA	NA	+	[52,69]	NA	+	[52]	NA	NA	NA	NA	NA	NA	
APP level	Our study	H	H	H	H	L	L	L	L	L	L	NA	NA	L	NA	NA	L	[26,74]
	Ref.	NA	H [26]	NA	NA	NA	NA	NA	NA	NA	NA	H [74]	NA	NA	NA	NA	NA	
C99/C83 ratio	Our study	L	L	L	L	L	H	H	H	H	H	NA	NA	H	NA	NA	H	

As it is seen from Table 1, our findings also contradict published experimental data in several aspects. An analysis of the literature's data has revealed that direct comparison is difficult due to different experimental setups. The frequency of injections, combined with different time points for sacrificing the experimental animals (i.e., different survival times) can result in large differences and complicates comparability [75]. A common feature of cited articles is that the same exogenous marker, BrdU, was injected intraperitoneally to detect stem cells. BrdU is a thymidine analog that can be incorporated into DNA during the S phase of cell cycle [55]. Regarding the administered dose of BrdU, the majority of the authors used 50 mg kg^{-1} [25,36,52,71,73], while two groups injected 100 mg kg^{-1} [26,63]. Depending on the dose of BrdU, divergent cell groups in the S phase of the cell cycle may be detected [76]. Besides dosing, the injection protocol of BrdU is also an important factor. The frequency of BrdU administration is quite diverse in the literature: some groups applied the injection for 1 [69], 3 [25,26,52], 5 [73] or 12 days [71] once a day, while one group applied a vaccination protocol of several times a day [36]. In our experiments, mice were treated with BrdU (100 mg kg^{-1}) once daily for 6 days, to label the largest possible amount of proliferating cells [77]. In addition, the timing of sacrificing the experimental animals also differs among published studies. Zeng et al. completed sacrificing within a few hours post-treatment [63], while others sacrificed the animals 1 to 3 days after the last BrdU injection [25,36,52,69]. Verret et al. and Unger et al. conducted extraordinarily long-term studies, and sacrificed the animals 1 month after the last BrdU administration [71,73]. In our experiment, mice were sacrificed 14 days after the last BrdU injection. The dose and injection protocol, as well as the timing of sacrificing the animals, were chosen to optimally study the long-term survival of stem cells. Proliferation can be examined within a few hours or one day after the BrdU injection only, while studying the long-term survival of stem cells requires a longer follow-up period [78].

In WT and Tg mice, decreasing trends in the densities of both BrdU+ and DCX+ cells were observed with aging. The densities of stem cells and immature neurons were high both in 1-month-old wild-type and Tg mice, which could be explained by the superior neuroplasticity of the young brain [79]. The density of BrdU+ and DCX+ cells showed a gradual decrease from 2 months of age. At older ages (8 to 12 months), significant differences were detected between the two strains in both neurogenesis markers. Similarly, other research groups also reported differences in the densities of BrdU+ [25,52] and DCX+ cells [52,69] in 9- and 10-month-old mice, while some groups also reported significant differences in young animals (2 to 5 months of age, BrdU: [26,36,69,73], DCX: [26,36]). These mixed results may result from using APP/PS1 mice with different genetic backgrounds (>10 vs. 0 generations in the C57BL/6J strain) and varying methods [25,73].

Consistent with the results published by Liu et al. [36] and Zhang et al. [74], no changes were observed in the densities of mature neurons (NeuN), either in the WT or in the Tg groups in our study.

In the so-called APP trafficking, which involves the expression, migration and enzymatic processing of APP, the forming products of both the amyloidogenic and non-amyloidogenic pathways play crucial roles in neurogenesis as well. In AD, the amyloidogenic pathway predominates, which is controlled by β -site APP cleaving enzyme 1 (BACE1). Enzymatic cleavage of APP by BACE1 yields C99 and A β fragments, contributing to the formation of A β plaques. APP level was found to be high in the first 4 months of life, and decreased from 5 months of age, while changes in the C99/C83 ratio followed a reverse trajectory. Demars et al. measured high APP protein levels in 2-month-old APP/PS1 animals [26], which agrees with our findings. Previous studies have shown that both the BACE1 protein level [80] and the enzymatic activity are elevated [81], and BACE1 is accumulated around plaques in AD models, independent of age [80,82,83]. We assume that changes in the amounts of products formed in the amyloidogenic pathway may support the hypothesis that the enhanced expression and/or activity of BACE1 is likely to contribute to the cleavage of APP, resulting in reduced APP and elevated C99 levels in Tg animals.

Our assumption is further supported by the results regarding soluble A β ₁₋₄₂, which had a high concentration in the first 4 months of life, and started to decrease from the age of 5 months. In parallel with this finding, plaques could be detected from the age of 4 months in the brain of transgenic mice. The reduction in the level of soluble oligomeric A β ₁₋₄₂ may be explained by the fact that soluble A β ₁₋₄₂ is re-organized from the oligomeric state to form fibrillar aggregates, manifesting as plaques [84–86].

According to the literature, the appearance of plaques in APP/PS1 mice can be observed at different ages. Some groups reported that plaques were first detected in young animals of 3 [29,39] and 4 months of age [73], accompanied by the first signs of changes in neurogenesis [29,69,73]. One group detected A β plaques at 6 months of age, after a detectable decline in neurogenic processes (3 months of age) [36]. Taniuchi et al. recognized plaques earlier (5 months of age) than the significant abnormalities first appeared in neurogenesis (9 months of age) [52]. We detected a relatively late (8 to 9 months) onset of altered neurogenesis in transgenic animals, while A β plaques could be identified as early as 4 months of age. Therefore, our results support the hypothesis of early plaque formation appearing before the onset of decline in neurogenesis.

Accumulation of A β plaques induces inflammatory responses. Activated microglia and astrocytes play an important role in the clearance step of A β phagocytosis [13,29,87–89]. We have demonstrated that the densities of GFAP+ (at 6 to 12 months of age) and Iba1+ (at 7 to 18 months of age) cells were significantly increased in Tg animals compared to wild-type controls. An increase in the intensity of neuroinflammation became significant after the observed shift in APP trafficking and processing, as well as after the onset of plaque formation. Based on our findings, intensified inflammatory processes could be responsible for the decline in neurogenesis.

The formation of the Fe65/APP complex strongly affects APP processing. On the other hand, the peptide P33 can bind to Fe65, and thus it has the potential to reduce the formation of the Fe65/APP complex. Consequently, it may favorably interfere with the synthesis of A β . In agreement with its advantageous biological activity, P33 was shown to significantly improve spatial memory in APP/PS1 mice, increase the number of dendritic spines and decrease the density of inflammatory markers (GFAP, Iba1) [49]. Furthermore, P33 treatment significantly reduced the density of A β plaques and the concentration of soluble A β ₁₋₄₂ [49]. In the present study, P33 treatment significantly increased the densities of BrdU+ and DCX+ cells in the transgenic mouse model. Interestingly, a similar but insignificant change was observed in the number of BrdU+ cells in WT animals as well, suggesting that P33 may enhance cell division under physiological conditions too. This positive effect may be further supported by the specific action of P33 on APP processing. As the binding of P33 to Fe65 hinders the formation of the Fe65/AICD complex, the amount of the transcriptionally active AICD form (which is typical for the amyloidogenic pathway) may be reduced, and this has a beneficial effect on the declining neurogenesis as well. We may conclude that the modulation of the formation of active AICD/Fe65 by P33 possibly reduces the inflammatory processes and thus stimulates neurogenesis.

In conclusion, our experiments demonstrate that neurogenesis is characterized by an age-dependent decline in both wild-type and APP/PS1 animals, with an additional enhancement of inflammatory processes and AD pathology in the latter. Our findings provide evidence that in Tg mice, the early appearance of plaques, quantitative changes in the levels of certain products of the amyloidogenic pathway, as well as the subsequent development of neuroinflammation may contribute to the physiological decline of neurogenesis with aging. Our data support the hypothesis of other research groups, indicating that the molecular development of AD pathology is a driver of the onset of AD symptoms, as well as of the simultaneous impairment of neurogenic processes, which may manifest in decreased densities of stem cells and immature neurons [25,52].

Since AD pathology can be detected even in young APP/PS1 animals, early and elongated neuromodulator therapy may beneficially affect the natural course of AD. In our study, early and long-lasting treatment with P33, a promising neuroprotective peptide, has

successfully reduced the rate of decline in neurogenesis in a mouse model of AD, whereby memory and learning disturbances, as well as the decrease in the number of dendritic spines could be minimized. Therefore, P33 is worth being further investigated as a potential drug candidate that may alleviate the characteristic pathological processes of AD.

4. Materials and Methods

4.1. Animals

For the longitudinal study, 1- to 12- and 18-month-old male and female WT and APP/PS1 mice ($n = 208$) were used. Thirteen groups of 5 were established (male $n = 2$, female $n = 3$). Our previous investigations have shown that the results for males and females did not differ significantly; thus, the smallest possible number of animals were chosen, and even the higher mortality of males during the long time-frame of the experiments had to be considered. Having many years of experience with APPxPS1 transgenic animals, we reckoned this group number and sex ratio routinely feasible to gain statistically evaluable results. For the P33 experiment, 3-month-old male and female WT and APP/PS1 mice were divided into four groups (5 animals each): WT vehicle-treated (physiological saline), WT P33-treated, APP/PS1 vehicle-treated and APP/PS1 P33-treated. Animals were injected with P33 intraperitoneally in a dose of 5 mg kg^{-1} for five days per week, over a course of six months, as described in [49]. APP/PS1 double transgenic mice were obtained from The Jackson Laboratory (USA), from a colony housed at the Biological Research Centre of the Hungarian Academy of Sciences, by breeding APP/PS1 males with WT females (license number: XVI./1248/2017). The mice were kept in groups under constant temperature ($23 \pm 0.5 \text{ }^{\circ}\text{C}$), lighting (12–12 h light–dark cycle, lights on at 7 a.m.), and humidity ($\sim 50\%$). Standard mouse chow and tap water were supplied *ad libitum*.

All experiments were performed in accordance with Directive 2010/63/EU of the European Parliament and of the Council of 22 September 2010 on the protection of animals used for scientific purposes, and were approved by the regional Station for Animal Health and Food Control (Csongrád County, Hungary; project identification code: I-74-16/2017, 04.07.2017). The experimental protocols were approved by the National Food Chain Safety and Animal Health Directorate of Csongrad County, Hungary (project licenses: XXVI./3642/2017, XXVI./3643/2017). Formal approval to conduct the experiments was obtained from the Animal Welfare Committee of the University of Szeged.

4.2. Immunohistochemistry

All chemicals, except the antibodies (Ab), were purchased from Sigma-Aldrich (St. Louis, MO, USA). To detect stem cells, 5 animals per group were injected intraperitoneally (i.p.) with BrdU (100 mg kg^{-1}) once a day on 6 consecutive days.

Two weeks after the last BrdU injection, mice were anesthetized with chloral hydrate (1 mg kg^{-1}) and were perfused transcardially with phosphate-buffered saline (PBS), followed by 4% paraformaldehyde (PFA). The methods for sample preparation, collection and 4G8, Iba1 and GFAP immunohistochemical stainings were identical to those previously reported [49].

For BrdU staining, the sections were incubated in 2 M HCl for 2 h at room temperature (RT) to denature DNA. Sections were blocked in a mixture of 8% normal goat serum, 0.3% bovine serum albumin (BSA) and 0.3% Triton X-100 in PBS for 1 h. For DCX labeling, sections were blocked in 0.1% BSA and 0.3% Triton X-100 in PBS for 1 h. Sections were incubated at $4 \text{ }^{\circ}\text{C}$ overnight with primary antibodies in the following dilutions: mouse anti-BrdU Ab (1:800, Santa Cruz Biotechnology, Dallas, TX, USA), goat anti-DCX Ab (1:4000, Santa Cruz Biotechnology, Dallas, TX, USA), mouse anti-NeuN Ab (1:500; Merck Millipore, Darmstadt, Germany). For BrdU and NeuN stainings, sections were treated with a polymer-based horseradish peroxidase (HRP)-amplifying system (Super Sensitive™ One-Step Polymer-HRP IHC Detection System, BioGenex, Fremont, CA, USA), according to the manufacturer's instructions. For DCX labeling, sections were incubated with a biotinylated donkey anti-goat Ab (1:1500; Jackson ImmunoResearch, West Grove, PA, USA)

for 90 min. The sections were then rinsed in PBS 3 times, and were incubated with an avidin–biotin complex (VECTASTAIN® Elite ABC-Peroxidase Kit; Vector Laboratories, Burlingame, CA, USA) for DCX staining in 1:500, for 90 min at RT. Peroxidase immunolabeling was developed in 30 min using 0.5 M Tris-HCl buffer (pH 7.7) with 3,3'-diaminobenzidine (DAB, 10 mM) at RT. Sections were mounted with dibutyl phthalate xylene (DPX) onto the slides and were coverslipped.

4.3. ELISA

WT and APP/PS1 mice (3 animals per group) were euthanized via decapitation. Their brains were removed, and the tissues containing the HC and the cerebral CTX were quickly dissected and stored at -80°C until further use. The level of $\text{A}\beta_{1-42}$ was measured by ELISA as described in [49].

4.4. WB

Animal brains were handled the same way as reported for the ELISA experiments. Quantification of APP and C99/C83 protein ratio was determined by Western blot analysis as described in [49].

4.5. Quantification of Immunohistochemistry Data

Slides were scanned by a digital slide scanner (Mirax Midi, 3DHistech Ltd., Budapest, Hungary), equipped with a Panoramic Viewer 1.15.4, a CaseViewer 2.1 program, and a QuantCenter, HistoQuant module (3DHistech Ltd., Budapest, Hungary). For quantifications, all sections derived from each animal were analyzed (12 slices per animal). In DG and HC, the regions of interest (ROI) were manually outlined. Antibody-positive cell types for all ROIs were counted and quantified. The number of stem cells (BrdU+) and neuroblasts (DCX+) were assessed at the border between GCL and the hilus. The densities (%) of neurons (NeuN+), microglia (Iba1+), astrocytes (GFAP+) and $\text{A}\beta$ plaques were calculated by the quantification software. To assess cell densities, we divided the total number of counted cells per animal with the DG/HC area, and presented the results as cells/ mm^2 (BrdU+, DCX+) or percentages (NeuN+, Iba1+, GFAP+, $\text{A}\beta$ plaques).

4.6. Statistical Analysis

The data obtained from the immunohistochemistry analyses were evaluated with Student's *t*-test for independent samples. WB and ELISA data were analyzed by one-way ANOVA followed by Fisher's LSD *post hoc* tests. Data analysis was carried out with the SPSS software (IBM SPSS Statistics 24), and the results were expressed as mean \pm (SEM). Statistical significance was set at $p \leq 0.05$.

Supplementary Materials: The following supporting information can be downloaded at: <https://www.mdpi.com/article/10.3390/ijms231810364/s1>.

Author Contributions: Conceptualization, L.F. and B.P.; methodology, T.S., E.B., I.S., Z.B., M.E.T. and M.S.; statistical analysis: E.B.; formal analysis, E.B. and L.F.; investigation, T.S., E.B., I.S. and Z.B.; resources, B.P. and L.F.; data curation, T.S., E.B. and I.S.; writing/original draft preparation, T.S. and E.B.; writing—review and editing, L.F.; visualization, E.B.; supervision, L.F.; funding acquisition, B.P. and L.F. All authors have read and agreed to the published version of the manuscript.

Funding: This project was supported by the National Research, Development and Innovation Office (GINOP-2.3.2-15-2016-00060) and by the Hungarian Brain Research Program I and II (Grant No. KTIA_13_NAP-A-III/7, and 2017-1.2.1-NKP-2017-00002). Support by the Ministry of Human Capacities, Hungary (grant 20391-3/2018/FEKUSTRAT) and the Ministry of Innovation and Technology of Hungary from the National Research, Development and Innovation Fund (TKP2021-EGA-32) is acknowledged.

Institutional Review Board Statement: The study was conducted according to the guidelines of the Declaration of Helsinki, and approved by the Institutional Review Board (or Ethics Committee) of the University of Szeged (project license: XXVI./3642/2017, XXVI./3643/2017).

Informed Consent Statement: Not applicable.

Data Availability Statement: Not applicable.

Acknowledgments: The technical assistance of Szilvia Dénes and Péter Sütő is greatly acknowledged. The authors thank Dora Bokor for proofreading the manuscript.

Conflicts of Interest: The authors declare no conflict of interest. The funders had no role in the design of the study, nor in the collection, analyses, or interpretation of data, nor in the writing of the manuscript, nor in the decision to publish the results.

Abbreviations

AD	Alzheimer's disease
AICD	APP's intracellular domain
APP	amyloid precursor protein
APP/PS1 APP _{Swe} /PS1 _{dE9}	double transgenic mice
A β	amyloid β
BrdU	5-Bromo-2'-Deoxyuridine
BSA	bovine serum albumin
CTX	cortex
DAB	3,3'-diaminobenzidine
DCX	doublecortin
DG	dentate gyrus
DPX	dibutyl phthalate xylene
ELISA	enzyme-linked immunoassay
FAD	familiar form of Alzheimer's disease
GCL	granular cell layer
GFAP	glial fibrillary acidic protein
HC	hippocampus
HRP	horseradish peroxidase
ICV	intracerebroventricular
i.p.	intraperitoneal
Iba1	ionized calcium-binding adapter molecule 1
LPS	lipopolysaccharide
NPCs	neural progenitor cells
PBS	phosphate-buffered saline
PFA	paraformaldehyde
PS1	presenilin-1
PS2	presenilin-2
ROI	regions of interest
RT	room temperature
sAPP β	soluble APP β
SEM	standard error of the mean
SGZ	subgranular zone
STZ	streptozotocin
SVZ	subventricular zone
WB	Western blot
WT C57BL/6J	wild-type mice

References

- Altman, J.; Das, G.D. Autoradiographic and histological evidence of postnatal hippocampal neurogenesis in rats. *J. Comp. Neurol.* **1965**, *124*, 319–335. [[CrossRef](#)]
- Chen, Q.; Nakajima, A.; Choi, S.H.; Xiong, X.; Sisodia, S.S.; Tang, Y.P. Adult neurogenesis is functionally associated with AD-like neurodegeneration. *Neurobiol. Dis.* **2008**, *29*, 316–326. [[CrossRef](#)] [[PubMed](#)]
- Lazarov, O.; Marr, R.A. Of mice and men: Neurogenesis, cognition and Alzheimer's disease. *Front. Aging Neurosci.* **2013**, *5*, 43. [[CrossRef](#)] [[PubMed](#)]
- Kempermann, G. Adult Neurogenesis: An Evolutionary Perspective. *Cold Spring Harb. Perspect. Biol.* **2015**, *8*, a018986. [[CrossRef](#)] [[PubMed](#)]

5. Gage, F.H. Adult neurogenesis in mammals. *Science* **2019**, *364*, 827–828. [[CrossRef](#)] [[PubMed](#)]
6. Bruel-Jungerman, E.; Davis, S.; Laroche, S. Brain plasticity mechanisms and memory: A party of four. *Neuroscientist* **2007**, *13*, 492–505. [[CrossRef](#)]
7. Ming, G.L.; Song, H. Adult neurogenesis in the mammalian central nervous system. *Annu. Rev. Neurosci.* **2005**, *28*, 223–250. [[CrossRef](#)]
8. Chuang, T.T. Neurogenesis in mouse models of Alzheimer's disease. *Biochim. Biophys. Acta* **2010**, *1802*, 872–880. [[CrossRef](#)]
9. Lazarov, O.; Mattson, M.P.; Peterson, D.A.; Pimplikar, S.W.; van Praag, H. When neurogenesis encounters aging and disease. *Trends Neurosci.* **2010**, *33*, 569–579. [[CrossRef](#)]
10. Kempermann, G.; Jessberger, S.; Steiner, B.; Kronenberg, G. Milestones of neuronal development in the adult hippocampus. *Trends Neurosci.* **2004**, *27*, 447–452. [[CrossRef](#)]
11. Shruster, A.; Melamed, E.; Offen, D. Neurogenesis in the aged and neurodegenerative brain. *Apoptosis* **2010**, *15*, 1415–1421. [[CrossRef](#)] [[PubMed](#)]
12. Dard, R.F.; Dahan, L.; Rampon, C. Targeting hippocampal adult neurogenesis using transcription factors to reduce Alzheimer's disease-associated memory impairments. *Hippocampus* **2019**, *29*, 579–586. [[CrossRef](#)]
13. Sung, P.S.; Lin, P.Y.; Liu, C.H.; Su, H.C.; Tsai, K.J. Neuroinflammation and Neurogenesis in Alzheimer's Disease and Potential Therapeutic Approaches. *Int. J. Mol. Sci.* **2020**, *21*, 701. [[CrossRef](#)] [[PubMed](#)]
14. Horgusluoglu, E.; Nudelman, K.; Nho, K.; Saykin, A.J. Adult neurogenesis and neurodegenerative diseases: A systems biology perspective. *Am. J. Med. Genet. B Neuropsychiatr. Genet.* **2017**, *174*, 93–112. [[CrossRef](#)] [[PubMed](#)]
15. Winner, B.; Winkler, J. Adult neurogenesis in neurodegenerative diseases. *Cold Spring Harb. Perspect Biol.* **2015**, *7*, a021287. [[CrossRef](#)]
16. Mu, Y.; Gage, F.H. Adult hippocampal neurogenesis and its role in Alzheimer's disease. *Mol. Neurodegener.* **2011**, *6*, 85. [[CrossRef](#)]
17. Lazarov, O.; Marr, R.A. Neurogenesis and Alzheimer's disease: At the crossroads. *Exp. Neurol.* **2010**, *223*, 267–281. [[CrossRef](#)]
18. Hollands, C.; Bartolotti, N.; Lazarov, O. Alzheimer's Disease and Hippocampal Adult Neurogenesis; Exploring Shared Mechanisms. *Front. Neurosci.* **2016**, *10*, 178. [[CrossRef](#)]
19. Zhou, Z.-d.; Chan, C.H.-s.; Ma, Q.-h.; Xu, X.-h.; Xiao, Z.-c.; Tan, E.-k. The roles of amyloid precursor protein (APP) in neurogenesis: Implications to pathogenesis and therapy of Alzheimer disease. *Cell Adh. Migr.* **2011**, *5*, 280–292. [[CrossRef](#)]
20. Coronel, R.; Bernabeu-Zornoza, A.; Palmer, C.; Muñoz-Moreno, M.; Zambrano, A.; Cano, E.; Liste, I. Role of Amyloid Precursor Protein (APP) and Its Derivatives in the Biology and Cell Fate Specification of Neural Stem Cells. *Mol. Neurobiol.* **2018**, *55*, 7107–7117. [[CrossRef](#)]
21. Zetterberg, H.; Blennow, K.; Hanse, E. Amyloid beta and APP as biomarkers for Alzheimer's disease. *Exp. Gerontol.* **2010**, *45*, 23–29. [[CrossRef](#)] [[PubMed](#)]
22. Liu, H.; Zhang, H.; Ma, Y. Molecular mechanisms of altered adult hippocampal neurogenesis in Alzheimer's disease. *Mech. Ageing Dev.* **2021**, *195*, 111452. [[CrossRef](#)] [[PubMed](#)]
23. Evin, G.; Li, Q.X. Platelets and Alzheimer's disease: Potential of APP as a biomarker. *World J. Psychiatry* **2012**, *2*, 102–113. [[CrossRef](#)] [[PubMed](#)]
24. Gadadhar, A.; Marr, R.; Lazarov, O. Presenilin-1 regulates neural progenitor cell differentiation in the adult brain. *J. Neurosci.* **2011**, *31*, 2615–2623. [[CrossRef](#)] [[PubMed](#)]
25. Niidome, T.; Taniuchi, N.; Akaike, A.; Kihara, T.; Sugimoto, H. Differential regulation of neurogenesis in two neurogenic regions of APP^{swe}/PS1^{dE9} transgenic mice. *Neuroreport* **2008**, *19*, 1361–1364. [[CrossRef](#)]
26. Demars, M.; Hu, Y.S.; Gadadhar, A.; Lazarov, O. Impaired neurogenesis is an early event in the etiology of familial Alzheimer's disease in transgenic mice. *J. Neurosci. Res.* **2010**, *88*, 2103–2117. [[CrossRef](#)]
27. Scopa, C.; Marrocco, F.; Latina, V.; Ruggeri, F.; Corvaglia, V.; La Regina, F.; Ammassari-Teule, M.; Middei, S.; Amadoro, G.; Meli, G.; et al. Impaired adult neurogenesis is an early event in Alzheimer's disease neurodegeneration, mediated by intracellular A β oligomers. *Cell Death Differ.* **2020**, *27*, 934–948. [[CrossRef](#)]
28. Gray, S.C.; Kinghorn, K.J.; Woodling, N.S. Shifting equilibriums in Alzheimer's disease: The complex roles of microglia in neuroinflammation, neuronal survival and neurogenesis. *Neural. Regen. Res.* **2020**, *15*, 1208–1219.
29. Hickman, S.E.; Allison, E.K.; El Khoury, J. Microglial dysfunction and defective beta-amyloid clearance pathways in aging Alzheimer's disease mice. *J. Neurosci.* **2008**, *28*, 8354–8360. [[CrossRef](#)]
30. Heneka, M.T.; Carson, M.J.; El Khoury, J.; Landreth, G.E.; Brosseron, F.; Feinstein, D.L.; Jacobs, A.H.; Wyss-Coray, T.; Vitorica, J.; Ransohoff, R.M.; et al. Neuroinflammation in Alzheimer's disease. *Lancet Neurol.* **2015**, *14*, 388–405. [[CrossRef](#)]
31. Ekdahl, C.T.; Claasen, J.H.; Bonde, S.; Kokaia, Z.; Lindvall, O. Inflammation is detrimental for neurogenesis in adult brain. *Proc. Natl. Acad. Sci. USA* **2003**, *100*, 13632–13637. [[CrossRef](#)] [[PubMed](#)]
32. Monje, M.L.; Toda, H.; Palmer, T.D. Inflammatory blockade restores adult hippocampal neurogenesis. *Science* **2003**, *302*, 1760–1765. [[CrossRef](#)] [[PubMed](#)]
33. Valero, J.; Mastrella, G.; Neiva, I.; Sánchez, S.; Malva, J.O. Long-term effects of an acute and systemic administration of LPS on adult neurogenesis and spatial memory. *Front. Neurosci.* **2014**, *8*, 83. [[CrossRef](#)] [[PubMed](#)]
34. Bassani, T.B.; Turnes, J.M.; Moura, E.L.R.; Bonato, J.M.; Cópola-Segovia, V.; Zanata, S.M.; Oliveira, R.M.M.W.; Vital, M.A.B.F. Effects of curcumin on short-term spatial and recognition memory, adult neurogenesis and neuroinflammation in a streptozotocin-induced rat model of dementia of Alzheimer's type. *Behav. Brain Res.* **2017**, *335*, 41–54. [[CrossRef](#)] [[PubMed](#)]

35. Mishra, S.K.; Singh, S.; Shukla, S.; Shukla, R. Intracerebroventricular streptozotocin impairs adult neurogenesis and cognitive functions via regulating neuroinflammation and insulin signaling in adult rats. *Neurochem. Int.* **2018**, *113*, 56–68. [\[CrossRef\]](#)
36. Liu, L.; Liu, Y.; Li, N.; Huang, R.; Zheng, X.; Huang, L.; Hou, S.; Yuan, Q. Multiple inflammatory profiles of microglia and altered neuroimages in APP/PS1 transgenic AD mice. *Brain Res. Bull.* **2020**, *156*, 86–104. [\[CrossRef\]](#)
37. McLoughlin, D.M.; Miller, C.C. The FE65 proteins and Alzheimer's disease. *J. Neurosci. Res.* **2008**, *86*, 744–754. [\[CrossRef\]](#)
38. Sabo, S.L.; Ikin, A.F.; Buxbaum, J.D.; Greengard, P. The Alzheimer amyloid precursor protein (APP) and FE65, an APP-binding protein, regulate cell movement. *J. Cell Biol.* **2001**, *153*, 1403–1414. [\[CrossRef\]](#)
39. Sabo, S.L.; Ikin, A.F.; Buxbaum, J.D.; Greengard, P. The amyloid precursor protein and its regulatory protein, FE65, in growth cones and synapses in vitro and in vivo. *J. Neurosci.* **2003**, *23*, 5407–5415. [\[CrossRef\]](#)
40. Santiard-Baron, D.; Langui, D.; Delehedde, M.; Delatour, B.; Schombert, B.; Touchet, N.; Tremp, G.; Paul, M.F.; Blanchard, V.; Sergeant, N.; et al. Expression of human FE65 in amyloid precursor protein transgenic mice is associated with a reduction in beta-amyloid load. *J. Neurochem.* **2005**, *93*, 330–338. [\[CrossRef\]](#)
41. Bukhari, H.; Glotzbach, A.; Kolbe, K.; Leonhardt, G.; Loosse, C.; Mueller, T. Small things matter: Implications of APP intracellular domain AICD nuclear signaling in the progression and pathogenesis of Alzheimer's disease. *Prog. Neurobiol.* **2017**, *156*, 189–213. [\[CrossRef\]](#) [\[PubMed\]](#)
42. Feilen, L.P.; Haubrich, K.; Stier, G.; Sinning, I.; Wild, K.; Haubrich, K.; Simon, B.; Strecker, P.; Eggert, S.; Kins, S.; et al. Fe65-PTB2 Dimerization Mimics Fe65-APP Interaction. *Front. Mol. Neurosci.* **2017**, *10*, 140. [\[CrossRef\]](#) [\[PubMed\]](#)
43. Lazarov, O.; Demars, M.P. All in the family: How the APPs regulate neurogenesis. *Front. Neurog.* **2012**, *6*, 81. [\[CrossRef\]](#) [\[PubMed\]](#)
44. Coronel, R.; Palmer, C.; Bernabeu-Zornoza, A.; Monteagudo, M.; Rosca, A.; Zambrano, A.; Liste, I. Physiological effects of amyloid precursor protein and its derivatives on neural stem cell biology and signaling pathways involved. *Neural Regen. Res.* **2019**, *14*, 1661–1671. [\[PubMed\]](#)
45. Beckett, C.; Nalivaeva, N.N.; Belyaev, N.D.; Turner, A.J. Nuclear signalling by membrane protein intracellular domains: The AICD enigma. *Cell Signal* **2012**, *24*, 402–409. [\[CrossRef\]](#)
46. Li Puma, D.D.; Piacentini, R.; Grassi, C. Does Impairment of Adult Neurogenesis Contribute to Pathophysiology of Alzheimer's Disease? A Still Open Question. *Front. Mol. Neurosci.* **2020**, *13*, 578211. [\[CrossRef\]](#)
47. Ghosal, K.; Stathopoulos, A.; Pimplikar, S.W. APP intracellular domain impairs adult neurogenesis in transgenic mice by inducing neuroinflammation. *PLoS ONE* **2010**, *5*, e11866. [\[CrossRef\]](#)
48. Ma, Q.H.; Futagawa, T.; Yang, W.L.; Jiang, X.D.; Zeng, L.; Takeda, Y.; Xu, R.X.; Bagnard, D.; Schachner, M.; Furley, A.J.; et al. A TAG1-APP signalling pathway through Fe65 negatively modulates neurogenesis. *Nat. Cell Biol.* **2008**, *10*, 283–294. [\[CrossRef\]](#)
49. Szögi, T.; Schuster, I.; Borbély, E.; Gyebrovcszki, A.; Bozsó, Z.; Gera, J.; Rajkó, R.; Sántha, M.; Penke, B.; Fülöp, L. Effects of the Pentapeptide P33 on Memory and Synaptic Plasticity in APP/PS1 Transgenic Mice: A Novel Mechanism Presenting the Protein Fe65 as a Target. *Int. J. Mol. Sci.* **2019**, *20*, 3050. [\[CrossRef\]](#)
50. Verret, L.; Trouche, S.; Zerwas, M.; Rampon, C. Hippocampal neurogenesis during normal and pathological aging. *Psychoneuroendocrinology* **2007**, *32* (Suppl. S1), S26–S30. [\[CrossRef\]](#)
51. Olesen, L.; Sivasaravanaparan, M.; Severino, M.; Babcock, A.A.; Bouzinova, E.V.; West, M.J.; Wiborg, O.; Finsen, B. Neuron and neuroblast numbers and cytogenesis in the dentate gyrus of aged APPswe/PS1dE9 transgenic mice: Effect of long-term treatment with paroxetine. *Neurobiol. Dis.* **2017**, *104*, 50–60. [\[CrossRef\]](#) [\[PubMed\]](#)
52. Taniuchi, N.; Niidome, T.; Goto, Y.; Akaike, A.; Kihara, T.; Sugimoto, H. Decreased proliferation of hippocampal progenitor cells in APPswe/PS1dE9 transgenic mice. *Neuroreport* **2007**, *18*, 1801–1805. [\[CrossRef\]](#) [\[PubMed\]](#)
53. Borchelt, D.R.; Davis, J.; Fischer, M.; Lee, M.K.; Slunt, H.H.; Ratovitsky, T.; Regard, J.; Copeland, N.G.; Jenkins, N.A.; Sisodia, S.S.; et al. A vector for expressing foreign genes in the brains and hearts of transgenic mice. *Genet. Anal.* **1996**, *13*, 159–163. [\[CrossRef\]](#)
54. Borchelt, D.R.; Thinakaran, G.; Eckman, C.B.; Lee, M.K.; Davenport, F.; Ratovitsky, T.; Prada, C.M.; Kim, G.; Seekins, S.; Yager, D.; et al. Familial Alzheimer's disease-linked presenilin 1 variants elevate Abeta1-42/1-40 ratio in vitro and in vivo. *Neuron* **1996**, *17*, 1005–1013. [\[CrossRef\]](#)
55. von Bohlen Und Halbach, O. Immunohistological markers for staging neurogenesis in adult hippocampus. *Cell Tissue Res.* **2007**, *329*, 409–420. [\[CrossRef\]](#)
56. Brinkmalm, G.; Brinkmalm, A.; Bourgeois, P.; Persson, R.; Hansson, O.; Portelius, E.; Mercken, M.; Andreasson, U.; Parent, S.; Lipari, F.; et al. Soluble amyloid precursor protein α and β in CSF in Alzheimer's disease. *Brain Res.* **2013**, *1513*, 117–126. [\[CrossRef\]](#)
57. Gabelle, A.; Roche, S.; Gény, C.; Bennys, K.; Labauge, P.; Tholance, Y.; Quadrio, I.; Tiers, L.; Gor, B.; Chaulet, C.; et al. Correlations between soluble α/β forms of amyloid precursor protein and A β 38, 40, and 42 in human cerebrospinal fluid. *Brain Res.* **2010**, *1357*, 175–183. [\[CrossRef\]](#)
58. Perneczky, R.; Alexopoulos, P.; Kurz, A. Soluble amyloid precursor proteins and secretases as Alzheimer's disease biomarkers. *Trends Mol. Med.* **2014**, *20*, 8–15. [\[CrossRef\]](#)
59. Deng, W.; Aimone, J.B.; Gage, F.H. New neurons and new memories: How does adult hippocampal neurogenesis affect learning and memory? *Nat. Rev. Neurosci.* **2010**, *11*, 339–350. [\[CrossRef\]](#)
60. Abbott, L.C.; Nigussie, F. Adult neurogenesis in the mammalian dentate gyrus. *Anat. Histol. Embryol.* **2020**, *49*, 3–16. [\[CrossRef\]](#)
61. Epp, J.R.; Chow, C.; Galea, L.A. Hippocampus-dependent learning influences hippocampal neurogenesis. *Front. Neurosci.* **2013**, *7*, 57. [\[CrossRef\]](#) [\[PubMed\]](#)

62. Beckervordersandforth, R.; Rolando, C. Untangling human neurogenesis to understand and counteract brain disorders. *Curr. Opin. Pharmacol.* **2019**, *50*, 67–73. [[CrossRef](#)] [[PubMed](#)]
63. Zeng, Q.; Zheng, M.; Zhang, T.; He, G. Hippocampal neurogenesis in the APP/PS1/nestin-GFP triple transgenic mouse model of Alzheimer's disease. *Neuroscience* **2016**, *314*, 64–74. [[CrossRef](#)] [[PubMed](#)]
64. Yu, Y.; He, J.; Zhang, Y.; Luo, H.; Zhu, S.; Yang, Y.; Zhao, T.; Wu, J.; Huang, Y.; Kong, J.; et al. Increased hippocampal neurogenesis in the progressive stage of Alzheimer's disease phenotype in an APP/PS1 double transgenic mouse model. *Hippocampus* **2009**, *19*, 1247–1253. [[CrossRef](#)]
65. López-Toledano, M.A.; Shelanski, M.L. Increased neurogenesis in young transgenic mice overexpressing human APP(Sw, Ind). *J. Alzheimers Dis.* **2007**, *12*, 229–240. [[CrossRef](#)]
66. Chevallier, N.L.; Soriano, S.; Kang, D.E.; Masliah, E.; Hu, G.; Koo, E.H. Perturbed neurogenesis in the adult hippocampus associated with presenilin-1 A246E mutation. *Am. J. Pathol.* **2005**, *167*, 151–159. [[CrossRef](#)]
67. Jin, K.; Galvan, V.; Xie, L.; Mao, X.O.; Gorostiza, O.F.; Bredesen, D.E.; Greenberg, D.A. Enhanced neurogenesis in Alzheimer's disease transgenic (PDGF-APP^{Sw,Ind}) mice. *Proc. Natl. Acad. Sci. USA* **2004**, *101*, 13363–13367. [[CrossRef](#)]
68. Gan, L.; Qiao, S.; Lan, X.; Chi, L.; Luo, C.; Lien, L.; Yan Liu, Q.; Liu, R. Neurogenic responses to amyloid-beta plaques in the brain of Alzheimer's disease-like transgenic (pPDGF-APP^{Sw,Ind}) mice. *Neurobiol. Dis.* **2008**, *29*, 71–80. [[CrossRef](#)]
69. Hamilton, A.; Holscher, C. The effect of ageing on neurogenesis and oxidative stress in the APP(swe)/PS1(deltaE9) mouse model of Alzheimer's disease. *Brain Res.* **2012**, *1449*, 83–93. [[CrossRef](#)] [[PubMed](#)]
70. Hu, Y.S.; Xu, P.; Pigino, G.; Brady, S.T.; Larson, J.; Lazarov, O. Complex environment experience rescues impaired neurogenesis, enhances synaptic plasticity, and attenuates neuropathology in familial Alzheimer's disease-linked APP^{swe}/PS1DeltaE9 mice. *FASEB J.* **2010**, *24*, 1667–1681. [[CrossRef](#)]
71. Verret, L.; Jankowsky, J.L.; Xu, G.M.; Borchelt, D.R.; Rampon, C. Alzheimer's-type amyloidosis in transgenic mice impairs survival of newborn neurons derived from adult hippocampal neurogenesis. *J. Neurosci.* **2007**, *27*, 6771–6780. [[CrossRef](#)] [[PubMed](#)]
72. Dong, H.; Goico, B.; Martin, M.; Csernansky, C.A.; Bertchume, A.; Csernansky, J.G. Modulation of hippocampal cell proliferation, memory, and amyloid plaque deposition in APP^{Sw} (Tg2576) mutant mice by isolation stress. *Neuroscience* **2004**, *127*, 601–609. [[CrossRef](#)] [[PubMed](#)]
73. Unger, M.S.; Marschallinger, J.; Kaindl, J.; Höfling, C.; Rossner, S.; Heneka, M.T.; Van der Linden, A.; Aigner, L. Early Changes in Hippocampal Neurogenesis in Transgenic Mouse Models for Alzheimer's Disease. *Mol. Neurobiol.* **2016**, *53*, 5796–5806. [[CrossRef](#)] [[PubMed](#)]
74. Zhang, J.; Guo, Y.; Wang, Y.; Song, L.; Zhang, R.; Du, Y. Long-term treadmill exercise attenuates A β burdens and astrocyte activation in APP/PS1 mouse model of Alzheimer's disease. *Neurosci. Lett.* **2018**, *666*, 70–77. [[CrossRef](#)] [[PubMed](#)]
75. Llorens-Martín, M.; Trejo, J.L. Multiple birthdating analyses in adult neurogenesis: A line-up of the usual suspects. *Front. Neurosci.* **2011**, *5*, 76. [[CrossRef](#)]
76. Mandyam, C.D.; Harburg, G.C.; Eisch, A.J. Determination of key aspects of precursor cell proliferation, cell cycle length and kinetics in the adult mouse subgranular zone. *Neuroscience* **2007**, *146*, 108–122. [[CrossRef](#)] [[PubMed](#)]
77. Wojtowicz, J.M.; Kee, N. BrdU assay for neurogenesis in rodents. *Nat. Protoc.* **2006**, *1*, 1399–1405. [[CrossRef](#)]
78. Kuipers, S.D.; Schroeder, J.E.; Trentani, A. Changes in hippocampal neurogenesis throughout early development. *Neurobiol. Aging* **2015**, *36*, 365–379. [[CrossRef](#)]
79. He, J.; Crews, F.T. Neurogenesis decreases during brain maturation from adolescence to adulthood. *Pharmacol. Biochem. Behav.* **2007**, *86*, 327–333. [[CrossRef](#)]
80. Zhang, X.M.; Cai, Y.; Xiong, K.; Cai, H.; Luo, X.G.; Feng, J.C.; Clough, R.W.; Struble, R.G.; Patrylo, P.R.; Yan, X.X. Beta-secretase-1 elevation in transgenic mouse models of Alzheimer's disease is associated with synaptic/axonal pathology and amyloidogenesis: Implications for neuritic plaque development. *Eur. J. Neurosci.* **2009**, *30*, 2271–2283. [[CrossRef](#)] [[PubMed](#)]
81. Fukumoto, H.; Rosene, D.L.; Moss, M.B.; Raju, S.; Hyman, B.T.; Irizarry, M.C. Beta-secretase activity increases with aging in human, monkey, and mouse brain. *Am. J. Pathol.* **2004**, *164*, 719–725. [[CrossRef](#)]
82. Luo, G.; Xu, H.; Huang, Y.; Mo, D.; Song, L.; Jia, B.; Wang, B.; Jin, Z.; Miao, Z. Deposition of BACE-1 Protein in the Brains of APP/PS1 Double Transgenic Mice. *Biomed. Res. Int.* **2016**, *2016*, 8380618. [[CrossRef](#)] [[PubMed](#)]
83. Kandalepas, P.C.; Sadleir, K.R.; Eimer, W.A.; Zhao, J.; Nicholson, D.A.; Vassar, R. The Alzheimer's β -secretase BACE1 localizes to normal presynaptic terminals and to dystrophic presynaptic terminals surrounding amyloid plaques. *Acta Neuropathol.* **2013**, *126*, 329–352. [[CrossRef](#)] [[PubMed](#)]
84. Koffie, R.M.; Meyer-Luehmann, M.; Hashimoto, T.; Adams, K.W.; Mielke, M.L.; Garcia-Alloza, M.; Micheva, K.D.; Smith, S.J.; Kim, M.L.; Lee, V.M.; et al. Oligomeric amyloid beta associates with postsynaptic densities and correlates with excitatory synapse loss near senile plaques. *Proc. Natl. Acad. Sci. USA* **2009**, *106*, 4012–4017. [[CrossRef](#)]
85. Viola, K.L.; Klein, W.L. Amyloid β oligomers in Alzheimer's disease pathogenesis, treatment, and diagnosis. *Acta Neuropathol.* **2015**, *129*, 183–206. [[CrossRef](#)]
86. Ashe, K.H. Learning and memory in transgenic mice modeling Alzheimer's disease. *Learn Mem.* **2001**, *8*, 301–308. [[CrossRef](#)]
87. Czeh, M.; Gressens, P.; Kaindl, A.M. The yin and yang of microglia. *Dev. Neurosci.* **2011**, *33*, 199–209. [[CrossRef](#)]

-
88. Richetin, K.; Petsophonsakul, P.; Roybon, L.; Guiard, B.P.; Rampon, C. Differential alteration of hippocampal function and plasticity in females and males of the APPxPS1 mouse model of Alzheimer's disease. *Neurobiol. Aging* **2017**, *57*, 220–231. [\[CrossRef\]](#)
 89. Lee, C.Y.; Landreth, G.E. The role of microglia in amyloid clearance from the AD brain. *J. Neural Transm.* **2010**, *117*, 949–960. [\[CrossRef\]](#)